ORGANIC LIGHT EMITTING DEVICE NON-EMISSIVE AREA FORMATION AND INHIBITION

KE LIN
(B. Sc, M. Eng)

A THESIS SUBMITTED
FOR THE DEGREE OF DOCTOR OF PHILOSOPY
DEPARTMENT OF ELECTRICAL ENGINEERING
NATIONAL UNIVERSITY OF SINGAPORE
2004

ACKNOWLEDGEMENT

First and foremost, I would like to extend my utmost gratitude and appreciation to my supervisors, Prof. Chua Soo Jin for his constant guidance and support through my master project, current work in Institute of Materials Research & Engineering to this PhD project for the past six years. I am deeply indebted to his infinite patience, unfaltering encouragement, deep insight and brilliant ideas.

My thanks also go to Dr. Wang Wei for his guidance and assistance in earlier stage of theoretical and experimental works. I have been very fortunate to collaborate with the following people in various aspects of my work: Dr. Zhang Keran, Mr. Ramadas Senthil Kumar, Dr. Chen Peng, Mr. Wang Weide etc. Discussions with them have been very valuable. Especially Mr. Ramadas Senthil Kumar who passed me his knowledge on thin film deposition technique without reservation. Special thanks to Ms. Lim Shuang Fang for her patient assistance in my experimental work in the beginning stage of my project.

Special thanks are extended to the following people for their kind assistance in many areas of my experimental work: Dr. Low Hong Yee, Dr. Mark Auch, Mr. He Xinbo, Ms. Jennifer Kok and Ms. Lim Li Fang.

I am also deeply grateful for the companionship of all the fellow researchers in the Opto-electronics system cluster from Institute of Materials Research and Engineering. All their names will be engraved in my memory forever. Thanks for making my stay extremely entertaining and memorable.

Most of all, I would like to express my greatest gratitude for my parents and my brother for generously giving me with all their love and support throughout all these years. Thank you for the understanding and love. Last but not the least, special thanks to my supporting and loving hubby and my little angel: Victoria Lim.

CONTENTS

SUMMARY

Organic electroluminescent (EL) devices have been studied extensively due to their commercially attractive advantages including low cost, full colour, wide angle and flexibility of large area flat panel display. However the reliability and the durability of organic or polymeric multilayer EL devices still remain as a critical issue for practical use.

In this thesis, degradation process study focused on the formation of non-emissive spots on the device active area. Cathode deterioration and polymer degradation under electrical stress have been extensively studied which contribute to the understanding of non-emissive area formation mechanism based on the device point of view.

The “dark non-emissive area” has been identified as two regions: (1) truly non-emissive region forming the core and (2) a weak emission region surrounding the core. Our studies show that due to ITO polymer interface rough and polymer material imperfection, the local shorting point causes the formation of the dark shadow center. The heating induced polymer degradation is the main reason to cause the dark shadow area growth. The ultimate failure of the device occurs when the regions of degraded polymer layer start to carbonize. Accumulations, merges and coalesces of carbonized areas lead to short and/or open circuits accompanied by device current fluctuation and final LED failure.

There are formations of ‘‘bubbles’’ at the polymer-ITO interface or polymer layer within the non-emissive area accompanied by fluctuation of device current. In this study, “Bubbles” are identified as either polymer drops or gas raised from disintegration of polymer. The growth of “bubbles” is found caused by the movability and degradation of polymer layer. High local current near dark spot center breaks conducting path, decomposes and carbonizes polymer layer.

The novel OLED structure design and suitable process technology for the effective control of non-emissive area formation and growth are proposed. A thin layer of parylene in between the ITO and the HTL layer has shown that the ITO interface became smooth, and it leads to a more uniform current flow, a larger current injection, and higher luminescence

efficiency. By inserting one more parylene layer in between the EL polymer and the cathode layer, the device cathode interface can be further stabilized, minimizing the probability of formation of the nonemissive area. Keeping the metal/polymer interface smooth by inserting a thin parylene layer, which also inhibits electrode migration and permeation of oxygen from the ITO, is one method to prolong device lifetime. The experimental results based on the designed new OLED structure prove that stabilizing and smoothing the interface is the key point to maintain uniformed current density distribution and minimize dark shadow formation in active area.

Nomenclature

η_i	Internal quantum efficiency (η_i)
T	Temperature in Kelvin
χ_c	Electron affinity of the device
μ_n	Electron mobility
μ_p	Hole mobility
N_c	Densities of states in the conduction band
N_v	Densities of states in the valence band
C_{opt}	Optical capture-emission rate
τ_n	Electron recombination lifetimes
τ_p	Hole recombination lifetimes
E_g	Energy band
R_{srh}	Shockley–Read–Hall (SRH) recombination rate
n	Electron densities
p	Hole densities
φ	Electrostatic potential
J_n	Electron current densities
J_p	Hole current densities
ϕ_n	Quasi-Fermi levels for electrons
ϕ_p	Quasi-Fermi levels for holes
V_{app}	Applied bias
E	Electric field
G	Electron - hole pair generation rate
q	Electron charge
E_g	Energy gap
T	Temperature in Kelvin
N_A^-	Ionised acceptor and donor impurity concentrations
N_D^+	Ionised acceptor and donor impurity concentrations
k	Boltzmann's constant
n_{ij}	Density of trapped electrons for the *j*th trap energy level

LIST OF FIGURES

LIST OF TABLES

LIST OF PUBLICATIONS

Journal Papers:

Shuang Fang Lim, Lin Ke, Wei Wang, Soo Jin Chua. "Correlation between dark spot growth and pinhole size in organic light-emitting diodes" Appl. Phys. Lett. Vol. 78, (13) 2116 (2001)

Karen Lin Ke, Soo Jin Chua, Shuang Fang Lim, Wei Wang "The Influence of Electrical Stress Voltage on Cathode Degradation of Organic Light Emitting Devices" J. of App. Phys. Vol. 90, (2) 976 (2001).

Lin Ke, Shuang Fang Lim, Soo Jin Chua "Organic Light Emitting Device Dark Spot Growth Behavior Analysis by Diffusion Reaction Theory" J. of Appl. Polymer Science, Part B (Polymer physics) Vol. 39, 1697, 2001

Lin Ke, Peng Chen and Soo Jin Chua "Photoluminescence Degradation in Organic Light-emitting devices" Appl. Phys. Lett., Vol 80. 697 (2002)

Lin Ke, Soo-Jin Chua, Keran Zhang, Peng Chen "Bubble formation due to electrical stressing organic light emitting devices" Appl. Phys. Lett., Vol.80, 171 (2002)

Lin Ke, Soo Jin Chua, Keran Zhang, Nikolai Yakovlev, "Degradation and Failure of Organic Light-Emitting Devices" Appl. Phys. Lett., Vol.80, 2195 (2002)

Soo-jin Chua, Lin Ke, Ramadas Senthil Kumar, Keran Zhang, "Stabilization of electrode migration in polymer electroluminescent devices" Appl. Phys.Lett. Vol 81, 1119 (2002)

Karen Ke Lin, Soo Jin Chua, Wei Wang "Degradation mechanisms in electrically stressed organic light-emitting devices" Thin Solid Films Vol. 417, 36 (2002)

Lin Ke, Keran Zhang, Yakovlev N, Soo Jin Chua. "Secondary ion mass spectroscopy study of failure mechanism in organic light emitting devices" Mat. Sci. Eng. B-Solid 97 (1): 1-4 JAN 15 2003

Lin Ke, Ramadas Senthil Kumar, Keran Zhang, Soo Jin Chua, A.T.S. Wee "Organic Light Emitting Devices Performance Improvement by Inserting Thin Parylene Layer" Syn. Met. Vol.140, 295 (2004)

Chuan Zhen Zhou, Wei Ling Wang, Karen Ke Lin, Zhi Kuan Chen, Yee Hing Laia "Poly(naphthylenethiophene)s and poly(naphthylenevinylenephenylenevinylene)s: effect of naphthalene positional isomers on the light emitting properties of their polymers" Polymer 45 2271(2004)

Chun Xiang Xu, Xiao Wei Sun, Xin Hai Zhang, Lin Ke and Soo Jin Chua "Photoluminescent properties of copper-doped zinc oxide nanowires" Nanotechnology 15, issue 7, 856 (2004)

Patent:

Karen KE Lin, Ramadas Senthil Kumar, Soo Jin Chua "Dark Spot Inhibition in Organic Light-Emitting Devices" PCT International Application No: PCT/SG02/00276 International Filing Date: 27 Nov 2002

Conference Papers:

Karen Lin Ke, Soo Jin Chua, Wei Jun Fan, "Low threshold current density and high quantum efficiency 980nm CW QW Laser" Advanced Microelectronic Processing Techniques, Proceedings of SPIE Vol. 4227 (2000)

Karen Lin Ke, Soo Jin Chua, Wei Jun Fan, "Theoretical design of low threshold current density of InAlGaAs material system" Optics and Optoelectronic Inspection and Control, SPIE Beijing Nov.8-10 (2000)

Mark Auch, Wang Wang, Jennifer Kok, Lin Ke, Ewald Guenther, Soo Jin Chua "Packaging of flexible OLED" Society for Information Display, 20th International Display Research Conference, Sep 25-28 (2000)

Karen Ke Lin, Soo Jin Chua, Shuang Fang Lim, Wei Wang, "Dependence of Dark Spot Growth on Electrical Stressing Voltage in OLED Devices" Society for Information Display, 2001 International Symposium Digest of Technical Papers Vol. XXXII, Son Jose, California June 5-7, 2001

Karen Ke Lin, , Soo Jin Chua, Wei Wang "Degradation Mechanisms in Electrical Stressed Organic LED Devices" ICMAT G11-32, P233, 2001

Siu-Yin Leo, Karen Ke Lin, Soo Jin Chua, Wang-Lin Yu "The Morphological Effects on Optical Properties of a Blue Light-Emitting Polymer" ICMAT G11-31 P232, 2001

Shuang fang Lim, Lin Ke, Wei Wang, Soo Jin Chua "Correlation Between Dark Spot Growth and Pinhole Size in Organic Light-Emitting Diodes" ICMAT G4-04 P217, 2001

Lin Ke, Soo Jin Chua, Wei Wang "Polymer UV Degradation and Recovery Investigation" Asia Display/IDW'01 Proceedings of The 21st International Display Research Conference in conjunction with The 8th International Display Workshops. Nagoya, Japan

Lin Ke, Keran Zhang, Ramadas Senthil Kumar, Soo Jin Chua, Nikolai Yakovlev "Secondary Ion Mass Spectroscopy Study of Failure Mechanism in Organic Light Emitting Devices" MRS Fall Meeting, 2001, Boston, USA

Lin Ke, Ramadas Senthil Kumar, Soo Jin Chua, "Effect of Parylene layer on the performance of OLED" Symposium G, IUMRS-ICEM2002, Xian, China.

Soo Jin Chua, Lin Ke, Ramadas Senthil Kumar and Eric Ou, "Degradation Mechanisms in OLED", Invited Paper, ASID 2002, The 7th Asian Symposium on Information Display, York Hotel, Singapore, 2-4 September. Proceedings pp183-186

CHAPTER 1 INTRODUCTION

1.1 Introduction

Have you ever wondered how a firefly glows in the dark? The little lightning bug contains reactive organic molecules that release visible light. Researchers are finding ways to copy Mother Nature, and new technology that creates light in a similar way is invading the consumer-display market. The key elements are the organic light emitting diode (OLED) and the light emitting polymer (LEP). The current 40 billion dollar display market, dominated by LCDs (standard in laptops) and cathode ray tubes (CRTs, standard in televisions), is seeing the introduction of full-color OLED and LEP-driven displays that are more efficient, brighter, and easier to manufacture. It is commonly accepted that within a decade, OLED will be widely used in hand phones, digital cameras, laptops, VCDs, DVDs, portable electronics, games, etc.

1.2 Advantages of Organic Light Emitting Device (OLED)

Compare the two most popular flat screen TV technologies: Plasma TVs and liquid crystal displays (LCDs). The plasma TVs are the current size champions. Although plasma has fast refresh rate, but suffer from burn-in produced by static images, short lifetime, heavier and thicker, high cost of fabrication etc. LCDs in various fields are catching up. But the more tempting technology is organic light emitting devices (OLEDs) which is widely believed to replace current displays commercially as well as technologically. Here below are some of its advantages.

1) Low forward-drive voltage, usually under 10V. (phosphor, plasma display, CRTs require very high driving voltage)

2) High brightness compare with plasma display and inorganic LED

3) High emission efficiency, which results in high brightness in combination with low power consumption. OLED consumes energy only when its pixels are on, while LCD would consume energy even it is not on because the backlight is always on.

4) Compact. OLED is made up of a multilayer structure, with self-luminous emission layers (< 1μm). So the device can be made very thin and light. While for LCD, it needs an extra backlight display component.

5) The emission wavelengths are tunable by incorporation of suitable fluorescent dyes in the emissive layers.

6) Wide viewing angles. There is no viewing angle dependence that is usually seen in LCD displays.

7) Fast response. It is 1000 times faster than LCD.

8) Full color, high brightness image content display can be realized. And due to the use of low temperature processing technologies, displays on plastic substrates can be realized.

1.3 Historical development of organic light emitting display

The pioneers in organic semiconductors are the 2000 Chemistry Nobel prize winners Professor Alan J. Heeger, Professor Alan G. MacDiarmid and Professor Hideki Shirakawa in 1977 with their research into the polymerization of polyacetylene. The 2000 Chemistry Nobel prize speech by Professor Bengt Nord gives a good account into the circumstances leading to the discovery of organic semiconductors. In 1962, General Electric scientist Nick Holonyak invented the Light Emitting Diode (LED)

In 1963, organic electroluminance in solids was first discovered in anthracene crystals.

In 1967, research made great progress on polymerization of acetylene.

In 1977, Alan Heeger, Alan MacDiarmid and Hideki Shirakawa discovered the way to oxidize the silver polyacetylene film using iodine vapour which resulted in conductivity similar to metal.

In 1982, Kodak achieved the first patent on OLED by using small molecule.

In 1987, Ching Tang and Steven van Slyke at Eastman Kodak formed a two-layer OLED made of nonpolymeric organic compounds. First practical OLED display structure was made. [1-3] Tang and co-workers employed a transparent hole-injecting electrode of indium tin oxide (ITO) on glass to improve the extraction of light. They sandwiched a p-type, hole-transporting molecular film of aromatic diamine and an emitting layer of the n-type, electron-transporting metal chelate tris-hydroxyquinoline aluminium (Alq3) between the ITO anode and a low work-function alloy of magnesium as the electron-injecting cathode. Both the diamine and Alq3 possess conjugated carbon bonds and were prepared using sublimation techniques available to purify small molecule compounds. The use of magnesium as the cathode was important for the same reason given for the reactive cathode mentioned earlier, namely to more closely match the p*energy band of the luminescent semiconducting material to achieve electron injection with lower applied electric fields. The use of this two-layer structure, purified materials, and properly chosen electrodes permitted OLEDs to operate at voltages below 10V for the first time. To date, OLEDs based on vacuum-sublimated small molecules follow this Kodak teaching.

In 1990, first report on electroluminance in Poly(p-phenylene vinylene) (PPV) was published.[4-8] The Cambridge group of Friend announced that they had achieved green yellow EL using the conjugated polymer poly(p-phenylene vinylene) (PPV) in a single layer device structure. PPV, with its aromatic phenyl ring and conjugated vinylene linkage, was first synthesised by Wessling at Dow in 1968, and has a p±p* electronic energy gap of about 2.5 eV. Cambridge Display Technology (CDT) was founded in 1992 to exploit a key patent from Cambridge University in light emission from conjugated polymers. CDT has been active ever since in materials and technology issues to promote the commercial development of PLEDs. As a result of this activity, chemical companies began to further explore the PPV polymer, including a synthetic chemistry group in Hoechst. This group later formed part of a spin-off company, which was to evolve into Covion Organic Semiconductors in 1999, and whose materials portfolio remains largely PPV-based.

In 1990, Prof. Michael Graetzel research group in Switzerland invented the dye solar cell.

In 1991, Heeger and co-workers at the University of California at Santa Barbara announced the electroluminescence (EL) application of a soluble derivative of PPV, namely poly[2-methoxy-5-(2¢-ethylhex-yloxy)-1,4-phenylenevinylene] or MEH-PPV.[9] MEH-PPV has a p±p* electronic energy gap of about 2.2 eV, which is red-shifted from that of PPV. Owing to its dialkoxy side chain, MEH-PPV offered the advantage of being soluble in conjugated form in organic solvents. [10,11] The Santa Barbara group also employed calcium as the reactive cathode metal for improved device efficiency. UNIAX, a commercial venture spun out of the University of California at Santa Barbara and recently acquired by DuPont, was established to develop optimal process manufacturing guidelines for the commercialisation of PLED-based devices.

In the early 1992, researchers at Dow developed a family of 9,9-dialkylfluorene homo- and copolymers that exhibit purity levels unattainable over a decade ago. Work at Dow resulted in the development of a modified Suzuki polymerisation process, [12] which provides a wide range of high-molecular-weight (50 000 to 600 000 Da), low polydispersity (<2), fluorine-based homo-polymers and copolymers in high yields and purity. This improved Suzuki coupling process has permitted the preparation of a portfolio of fluorine-containing copolymers that emit colours spanning the entire visible range. [13]

In 1997, Pioneer introduce the first commercialized product with organic semiconductors; a passive matrix display.

In 1999, Pioneer made the first multicolor product used in car stereo.

In 2000, Pioneer/Motorola successfully applied multicolor OLED display in a cell phone. The inkjet printing of copper contacts represents a further step toward an all-printed thin-film transistor technology is also demonstrated in Princeton Univ.

In 2001, Sony demonstrated 13-inch AMOLED.

In 2002, , Eastman Kodak Company and Sanyo Electric Co. showed a prototype fifteen-inch flat-panel OLED display.

At present, no one has determined, either experimentally or theoretically, an upper limit to

material and device performance that can be achieved, either in colour, efficiency, or lifetime. This is due, in part, to the incomplete understanding of the underlying principles governing PLED device performance. Nevertheless, we anticipate that the next decade will surpass the last, with new and improved results in active and passive materials development that will continue to drive this technology forward.

1.4 Review of organic-based light emitting diodes degradation research

Polymeric electroluminescent devices are now being invented and made to achieve lifetimes of several thousands of hours at room temperature, and are probably nearing to commercial appearance. Currently, the best devices reported have lifetimes at room temperature of several thousand of hours [14-17] (some devices have lifespan greater than 10 000 hrs), which is satisfactory for many applications. However, research into decay processes remains very active for several reasons: stability at elevated temperatures is still a major issue; all colours are not equally stable; and some of the device processing steps that have proven useful in extending lifetime may turn out to have unacceptable impact on cost or other performance specifications.

1.4.1 Loss of EL efficiency and increase of bias

Typical EL polymers device decay process is:

(1) Device luminance shows with an early rapid decay followed by a slower one. 50% of luminance drop occurs in a few tens of hours, with about 85% decay in 100hrs. After that, the rate of decay slows dramatically, and the device continues to emit light for nearly two thousand hours.

(2) During the whole device stressing period, device bias keeps on rising.

(3) There are lots of shorts that appear as the device is stressed and which often are the cause

of final failure.

One of the most striking of these observations was first reported by the Cambridge group [19], who found no decay in an ITO/PPV/Ca device operated for 1200hrs. Their device was subjected to a constant voltage square wave (equal excursions above and below zero), which was gradually increased in steps, from 5.5 to 6.0 and finally 6.9 V, with a final current density of 0.85 A/cm^2; thus, about 3 x 10^6 C/cm^2 of charge were passed. Although the efficiency actually increased (from 0.01 to 0.04%) it was too low to be significant for practical applications. However, the fact that such a large amount of current (which is essentially all hole current) could be passed has major implications for degradation mechanisms. These results have recently been greatly extended [20]: a similar device has now been run for more than 7000hrs at constant current (60mA/cm^2), and the luminance has not decreased (there was a gradual rise to a steady value of about 10 cd/m^2). This is a similar amount of charge (1.5 x 10^6 C/cm^2), but the light output is equivalent to running for 700hrs at 100cd/m^2 without degradation. These data suggest that neither light emission nor hole transport affect PPV over very long time. It was noted [20, 21] that the quantum yield for photodegradation (in vacuum) of a dialkoxy-PPV was about 3 x 10^{-9}. Thus, the excited state is very stable. The excited state reactivity could contribute to the EL device degradation. It is possible that the presence of charge carriers affects exciton stability. Until now, there is no direct evidence for such an interaction, and the EL data [39], , point to its absence. Other devices with greater efficiency, however, do still exhibit the slow luminance decay: for example, an ITO/PEDT-PSS/PPV/Al:Li device with initial efficiency 0.5 lm/W and luminance 100cd/m^2 decays smoothly to 50% over 3200hrs[15,16]. Similarly, an ITO/PEDT-PSS/dialkoxy-PPV/Ca device with luminance (L), of 70 cd/m^2 and similar efficiency begins to decay [14] (after rising slightly to 85cd/m^2) after 1500 hrs, reaching 60cd/m^2 at 5500hrs. At 70°C this type of device decays to 0.7L, in 600hrs, and the rate appears to be accelerating near the end. The ITO/PPV/Ca devices [16] are quite temperature insensitive: the same total absence of decay is seen at 60°C (data for 2000 hrs) and 80°C (data for 1300 hrs).

1.4.2 Photobleaching of polymer materials

Photooxidation of the conjugated polymers used for EL is generally facile [21-23], and has been shown to be singlet oxygen-mediated [21]. A kinetic characterisation of this process in thin film has recently been published by the Phillips group [24]. Substituents significantly affect the rates: cyano or trifluoromethyl [25] substitution on the vinyl positions greatly slows the process. Polymers lacking the double bond entirely (polyphenylene or polyfluorene types) are also expected to be resistant to photooxidation: a substituted poly-fluorene has been described as impervious to photooxidation [26]. However, on similar polyfluorenes we have observed decreases in PL intensity after a few J/cm of irradiation in air,. The photoreaction of vinyl-containing EL polymers results in the formation of aromatic aldehydes which are effective quenchers of PL, through a charge-transfer mechanism. Hijrhold [27] has recently reported on some phenyl-ene vinylene polymers in which the repeat unit contains a ketone in the main chain, and has found close to 0.05% EL efficiency. Thus, although there seems to be little doubt that oxidation of EL polymers is detrimental, the specific nature of the chemical defect is important, and apparently subtle changes may have quite different effects.

1.4.3 Anode reactivity

ITO is an air-stable material, and has been successfully used by electrochemists when a transparent electrode material is needed [28]. However Scott et al. [29] found by Fourier transform infrared spectroscopy (FTIR) that major changes in the ITO occurred as a consequence of operation of an ITO/MEH-PPV/Ca device (MEH-PPV=2-methoxy, 5-(2'-ethylhexoxy)-1,4-phenylene vinylene). The spectra also indicated aldehyde formation, suggesting that oxygen from the ITO may be incorporated into the polymer. This was the first indication that ITO stability might be a problem. Since then there have been a large number of reports on ITO degradation [30-33], and all long-lived PLED devices use some sort of 'buffer

layer' between the ITO and the emitting polymer. The most widely used materials for this purpose are polyaniline (Pani) [34,35] and poly(ethyl-enedioxythiophene) (PEDOT) [36,37], protons doped to provide conductivity (PEDOT is usually doped with poly(styrenesulfonic acid) (PSS).

The mechanism of the ITO degradation has not been well understood. Scott and co-workers [29,35] have shown that the loss of oxygen as the primary event, and ascribe it to an electrochemical process [36]: oxygen is pulled out of the ITO by holes in a neighbouring space charge layer. However, this mechanism should not be operative more than a few molecular layers from the electrode (and so has some difficulty in accounting for degradation throughout the film). In addition, the oxygen ion would have to be moving against the applied field gradient: even if a space charge layer does build up due to low hole mobility, the overall gradient remains in the applied direction, and hole mobilities are generally greater than electron mobilities for EL polymers [38].

Indium ions, on the other hand, would be moving with the applied field should they migrate from anode to cathode, and evidence has been reported that In can move into the polymer [39,40],. Once In has been removed, the O_2- anion will be left in a less stable state; it is at least plausible that it can then be oxidised by arriving holes to produce O_2 or O_2- anion. In view of the said, the remedy is simply to reduce the field gradient near the ITO surface, which is accomplished by a conducting polymer buffer layer.

1.4.4 Shorts

There is a type of behaviour which is quite commonly observed by many researchers: there is a great deal of 'leakage' current at voltages even well before the appearance of luminescence. Although localised differences in conductivity of the EL polymer cannot be ruled out (and indeed there is some evidence for this) [41], the most likely cause of shorting is penetration of the polymer by metallic components. The initial presence of pinholes is revealed by time-of-flight secondary-ion mass spectrometry (TOF-SIMS) experiments in which it is observed that Si in submicron-sized patches in a film (about 1400 Å thick) of a polyfluorene on a Si wafer, and similarly when the film is on IT0 [42]. The amount of In on the polymer surface (observed after dissolving away the cathode) grows with stress time. When the organic film is removed, the ITO surface is found to be damaged to an extent correlated with the amount of stress: it is depleted in In, and shows topography on the scale of hundreds of Å in some places. These observations can be accounted for by the presence of some initial distribution of pinholes, and the migration of In ions in the applied field. Pinholes or very thin spots caused by coating defects (primarily particles) will allow cathode metal to penetrate or migrate to the anode. These high-resistance paths can be burnt out by a large concentrated current flow, which heats the metal until it reacts or melts and loses contact. Reports have found that the conducting polymers lose their conductivity at about 200°C. One can expect that, as current flows through a short with the buffer present, it could cause this region to become insulating at a more modest temperature (and hence lower current), so that even the first *I*-*V* scan shows no noise. The buffer layers also doubtlessly provide some planarization of defects [43]; however, ordinary hole transport materials do not work as well. During further stress, if the field gradient is high enough, In ions move into the film, where they are reduced by passing electrons (anion radicals). Eventually, a whisker of In builds up to the cathode and a new short is formed. This type of ion migration could possibly be facilitated by the presence of morphological defects (pinholes or particles. Elimination of the problem can only come from

lowering the field gradient at the ITO, as occurs when a conducting polymer, or even a very efficient hole transport material, is placed adjacent to it. There do not appear to be any published studies in which the ITO has been carefully examined after stressing a device with such buffer layers present..

1.4.5 Cathode Oxidation

Cathode oxidation has been most thoroughly studied and understood on organic light emitting devices with Mg cathodes, because of the need to use low work function metals. Recent publications suggest that the phenomenon with Ca on polymers behave similarly. Cathode oxidation will greatly increase the driving power to maintain the same amount of luminescence. Other reports believe that cathode oxidation is the main cause of dark non-emissive area formation.

1.4.6 Dark Spot Formation

One of the most noticeable ways in which an organic LED decays is by the formation and growth of non-luminous ‘black spots’. At the initial stage, such non-emissive areas are small and have a dot-like shape. They are sometimes referred to as “dark spots’ or “black spots” due to their dot-like shape. Their further growth will gradually nibble the entire active areas and ultimately destroy entire diodes. What is daunting is the observation that dark spots were found even in “well-encapsulated” OLED devices. [43]

The electrical shorts and the metal diffusion [44-47] into polymers have been proposed as origins leading to the dark spot formation and device failure. The non-emissive spots had been attributed initially to local heating caused by short circuits, which lead to the formation of pinholes and local ablation [46] or local fusion of the polymer and metallic cathode. [43,48] Device dark spot growth is also largely attributed to the delamination between

different layers, [49,50] crystallisation of organic materials, such as emitting or hole transport (HL) materials, or the electrochemical reaction on interfaces. [51] Recent studies revealed that the nonemissive spots have domelike structures termed ‘‘bubbles’’ filled with gases mostly oxygen presumably evolved in the course of electrochemical and photoelectrochemical processes in the presence of water. [52,53] According to some recent articles [54] the bubbles originate around pinholes in metallic electrode in the presence of atmospheric humidity, degradation of organic electroluminescent materials and/or metallic cathode materials. However, an understanding of the degradation process is still far from being complete.

1.5 Motivation and objective

In summary of the above mentioned, although OLED renders many advantages, these devices still fail to achieve long term durability due to formation of non-emissive areas (dark spots). The non-emissive areas result in a decrease in device luminescence and reliability. There are many factors responsible for the reliability of the device, such as the properties of the materials, process technology, and interfaces of the layers, environmental conditions and importantly encapsulation technique, however the degradation mechanism is still remain unclear and arguable.

In this PhD project, the degradation and failure states of organic light-emitting device have been simulated and experimentally observed. The results are systematically analysed and device degradation mechanisms are proposed. Novel OLED structure design and a suitable process technology for the effective control of non-emissive area formation and its growth are proposed and demonstrated.

1.6 Outline of the thesis

One of the most noticeable ways in which an organic LED decays is by the formation and growth of non-luminous ‘black spots’. In this project, I studied various attributes of dark non-

emissive area formation and growth from the device point of view. The thesis starts with the introduction of the organic light emitting device technology and history. Chapter 2 introduces the basic operation principal of the organic light emitting device. The basic investigation tools of this study and general performance of the investigated device. Chapter 3 presents detailed simulation results on organic light emitting device or current voltage characteristics related to dark non-emissive area. Chapter 4 concentrates on the conducting luminescence polymer degradation mechanism. Device degradation mechanism is detailed elaborated and experiment results are presented in Chapter 5. Device final degradation phenomena and bubble formation mechanisms are also the subject of this chapter. In chapter 6, a useful method to study dark non-emissive area growth kinetics is invented and described. In chapter 7, a novel device structure and process technique has been proved to be helpful in reducing the dark non-emissive area formation and prolong device lifetime. An overall conclusion is provided in Chapter 8, the major contributions of this study and suggestions for future work in this area will be briefly described. Finally the references cited in this thesis are listed in the appendices which supplement the main text.

CHAPTER 2 ORGAINC LIGHT EMITTING DISPLAY

2.1 Basic principles of organic electroluminescence materials

Organic Light Emitting Displays (OLED) is a future generation technology based on Poly (phenylene vinylene) (PPV) and its soluble derivatives. Light is produced in the polymer by the fast decay of excited molecular states, the color of which depends on the energy difference between those excited states and the molecular ground level. A light-emitting device comprises a thin-film structure of one or two layers typically no more than 0.1 μm thick, sandwiched between two electrodes. Optimal device efficiency is achieved if the two electrodes are dissimilar, specifically where the respective electrode materials possess Fermi levels or electronic work functions that closely match the valence (ground) and conduction (or excited state) energy levels in the polymer. It is also necessary that one of the electrodes is transparent to the wavelength of light generated. This can be achieved with very thin metal films or more preferably the oxide of indium tin, which retains good electrical conductivity but which is transparent in layers below 0.2 μm thick. Completely packaged units have a low product profile, with device thickness between 2 and 4 mm commonly achieved, depending on the complexity of the display. OLED technologies have progressed considerably over the past 10 years. At their present stage, OLEDs are broadly comparable in brightness and efficiency to inorganic LEDs based on Group III-V elements. OLEDs are also advancing rapidly in their applicability for functional lighting in architectural applications as well as general signal.

2.1.1 The bonding of sp2-hybridised carbon

Organics electroluminescence materials are based on the unusual properties of the carbon atom: Among other configurations, it can form the so-called sp2-hybridisations where the

sp2-orbitals form a triangle within a plane and the p *z* -orbital is perpendicular to it. A σ -bond between two carbons can then be formed by formation of an orbital overlapping of two sp2-orbitals. The energy difference between the occupied binding orbital and the unoccupied anti-binding orbital is quite large and well beyond the visible spectral range. Correspondingly, longer chains of bound carbon atoms would have a large gap between the highest occupied molecular orbital (HOMO) and the lowest unoccupied molecular orbital (LUMO), leading to insulating properties.

However, in the sp2-hybridisation, the p *z* -orbital form additionally π-bonds. These bonds have much smaller energy difference between the HOMO and LUMO, leading to semiconducting properties and strong absorption in or near the visible spectral range:

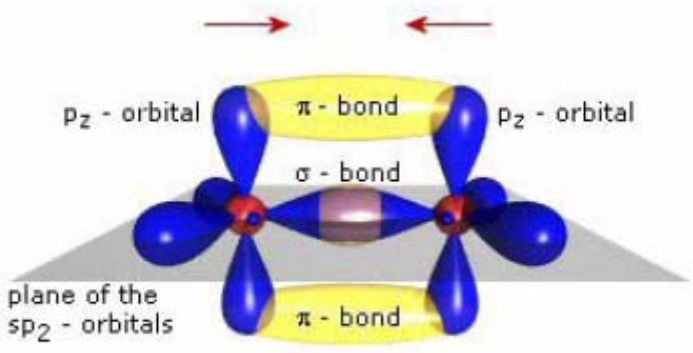

Figure 2.1 Scheme of the orbital and bond for two sp2-hybridised carbon atoms

2.1.2 Small-molecule organic electroluminescence materials

If carbon atoms form larger molecules, typically with benzene rings as the basic unit, the π-bonds become delocalized and form a π -system. The gap between occupied and empty states in these π-systems becomes smaller with increasing delocalization, leading to absorption and fluorescence in the visible. These substances can be prepared as molecular single crystals. Due to the close coupling of the π-systems of the molecules in these crystals, they show, in a purified form, remarkable transport properties, including band transport up to room

temperature with mobility of 1-10 cm^2/Vs. Most of the molecules can also be easily evaporated to form polycrystalline (hopping transport with mobility typically around 10^{-3} cm^2/Vs at 300K) or amorphous (hopping with mobility typically around 10^{-5} cm 2 /Vs at 300K) layers.

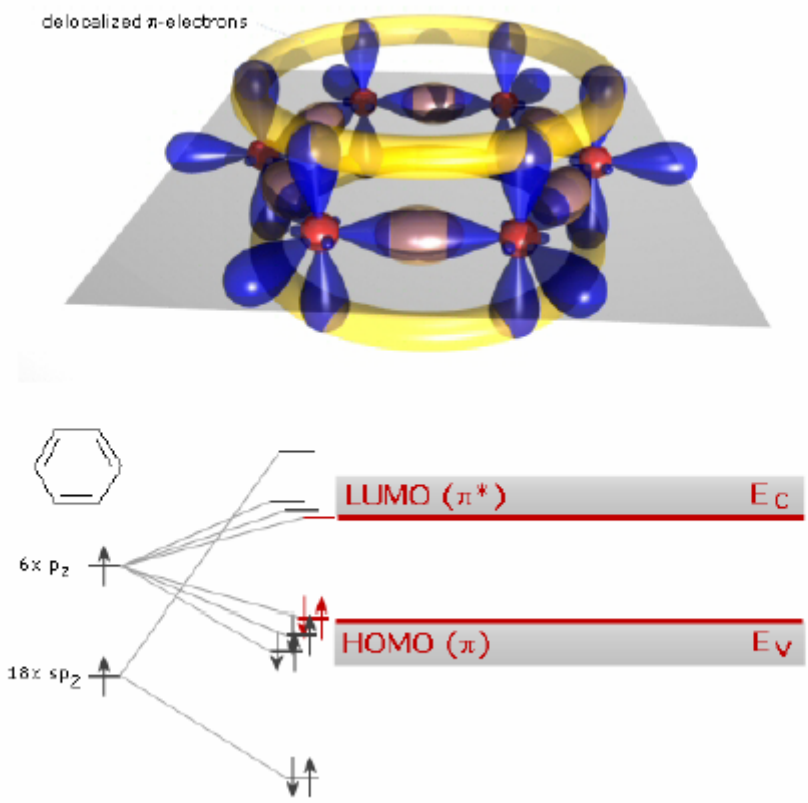

Figure 2.2 Scheme of a benzene ring (top) and the energy structure of small-molecule organics.

2.1.3 Polymer organic electroluminescence materials

If a long chain of carbon atoms is formed, the π-bonds become delocalized along the chain and form a one-dimensional electronic system. The 1D-band has a considerable band width (on the scale of an eV), i.e., we have a 1D semiconductor with a filled valence band originating from the HOMOs and an empty conduction band originating from the LUMOs. The transport properties of such polymers are usually determined by defects in the 1D-chains or by hopping from chain to chain. Therefore, the samples do not show band transport, but

thermally activated hopping. Polymer organic semiconductors are usually deposited in wet processes, like coating or doctor blading.

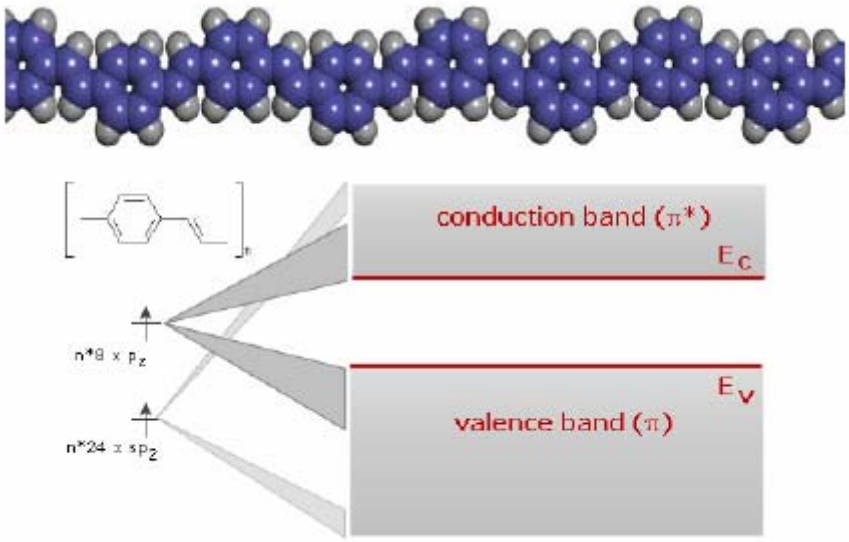

Figure 2.3 Scheme of a polymer subunit (top right) and the energy structure of polymer organics

2.1.4 Band diagram

The basic physics of a polymeric light emitting diode can be explained by a simplified scheme of energy levels. Via a metallic electrode, electrons are injected into the conduction band and holes are injected into the valence band of the polymeric semiconductor. The injected electrons and holes can drift or diffuse towards each other and finally recombine. Through this process, neutral excitations are created. These neutral excitations are bound states of an electron-hole pair, which can move along a polymer chain. Once these exited states decay into their ground state, a characteristic fluorescence may be generated. However, the exciton may be either in a singlet-state that spontaneously generates fluorescence, or in a triplet-state that due to spin selection has a very long life time and typically decays with very low quantum yield for light generation.

When a carrier is injected into an electrolminescent material, it may recombine (radiatively or

non-radiatively) or may pass through the material to the opposite electrode without recombining at all. Thus in order to increase the luminescence efficiency, equal numbers of electrons and holes need to be injected. The injection of carriers is governed by barriers formed at the anode/organic emission interface, and the organic emission layer/cathode interface, if abrupt interfaces are assumed, the hole barrier is largely determined by the difference between the work function of the electrode and the organic ionisation potential. On the other side, the electron barrier is largely determined by the difference between the organic electron affinity and the work function of the electrode. B.H. Cumpston et al. [44] reported the effect of electron barrier height on quantum efficiency of PPV-LEDs. They fabricated PPV based LEDs with an indium tin oxide (ITO) anode and cathodes with varying work functions.

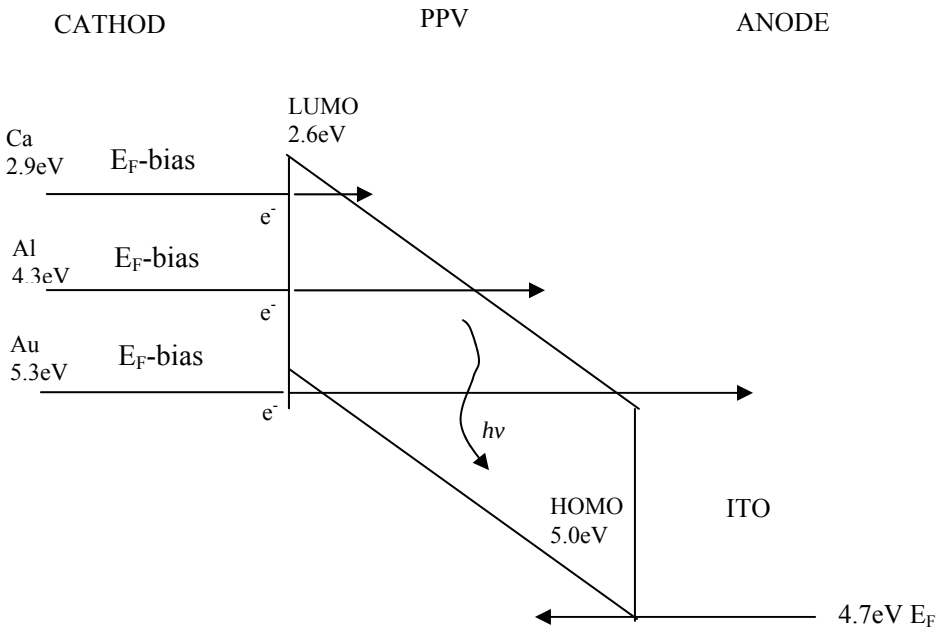

Figure 2.4: A simplified band diagram of PPV with cathodes and anodes with different work functions. This diagram assumes no interface effect between PPV and the electrodes.

The internal quantum efficiency (η_i) of the LED showed the dependence on the electron

barrier, it varied from $5x10^{-5}$% with a gold (Au) cathode, 0.002% with an aluminium (Al) cathode, and to 0.1% with a calcium (Ca) cathode. The calculated electron barrier heights between these metals and PPV are 2.7eV for Au (-5.3eV), 1.6eV for Al (-4.2eV) and 0.27eV for Ca (-2.87eV). The PPV ionisation potential is 5.1eV and the electron affinity is -2.6eV. In addition to dependence of η_i on electron barrier, Parker demonstrated η_i dependence on the hole barrier with MEH-PPV, η_i of MEH-PPV LEDs is also higher with the smaller electron and hole barriers. By reducing the hole barrier using Au (instead of ITO), it doubled η_i of MEH-PV LED with Ca cathode. In the chapter 3, I will demonstrate the relationship of the efficiency with regards to anode and cathode barriers respectively.

2.2 Process and fabrication of organic light emitting display

2.2.1 Materials

In this work, an EL copolymer of poly(*p*-phenylene vinylene) (PPV) containing phenyl and alkoxyphenyl side groups, kindly provided by Covion Organic Semiconductors GmbH (Figure 2.5), and polyethylenedioxythiophene (PEDOT), (Figure 2.6) kindly provided by Bayer AG, were used as the emitting and hole transport materials, respectively. The indium tin oxide (ITO) coated glass is from Merck Display Technology with a sheet resistance of about 30 ohms per square. The ITO thickness is about 120 nm and the glass thickness is 0.7 mm.

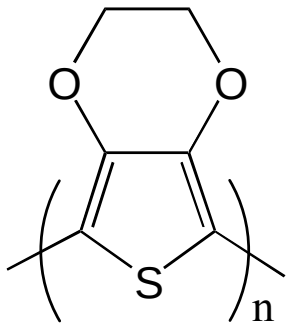

Figure 2.5: Poly(3,4-ethylenedioxythiophene) (PEDOT)

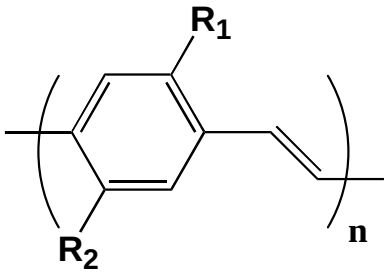

Figure 2.6: PPV derivatives containing phenyl and alkoxyphenyl side groups

Figure 2.5 shows the Poly(3,4-ethylenedioxythiophene) (PEDOT) structure and Figure 2.6 is the PPV derivatives structure which containing phenyl and alkoxyphenyl side groups Unsubstituted conjugated polymers are typically insoluble. They do not melt and cannot be evaporated. To process them into thin films, it is therefore necessary to modify e.g. by introducing alkyl (preferably branched) side chains, which render them soluble. The possible impact of such side chains on the optoelectronic performance of the conjugated back bone can be tuned by appropriate selection of the particular substitution of the PPV. In our work, we use novel poly(p-phenylene vinylenes) (PPVs) which exhibiting, to the best of our knowledge, the best performance reported up to now. The subsequent dehydrohalogenation polymerisation in tetrahydrofurane is achieved by adding potassium tert-butanolate as reagent. The actual PPV-derivative is substituted with the alkoxy side groups OR and OR' which red shift the emission relative to the unsubstituted PPV. With such polymers, large area Polymer LEDs, emissive displays, and displays on flexible substrates can be fabricated.

2.2.2 Device fabrication

Organic LEDs were prepared by first plasma treated cleaned surface of the ITO-coated glass. Then the hole transport layer (HTL) material, polyethylenedioxythiophene (PEDOT) is spin-coated on the cleaned surface of the patterned ITO glass substrate. After baking at 200^{o}C for 5 minutes to remove moisture, a toluene solution of the EL copolymer was spin-coated with a spin coater (Karl Suss RC8 Gyrset 8) with the cover down. The HTL layer was spun at a rate of 2000 rpm and an acceleration of 2000rpm per second for 20 seconds. The EL polymer layer was spun at a rate of 500 rpm and an acceleration of 400 rpm per second for 30 seconds. The polymer concentration was 5g/lit. The thickness of PEDOT and PPV-copolymer was 20 nm and 80-100 nm, respectively. Following that, a calcium (Ca, 99.5% purity) cathode was deposited on the PPV copolymer by thermal evaporation. The thickness of the Ca cathode is 5 nm, except for the Ca thickness variation experiments. To protect the Ca cathode, a 200 nm thick silver (Ag, 99.99% purity) layer was deposited. Thermal evaporation was carried out in ULVAC system evaporation chamber by ULVAC company, Japan shown in Figure 2.7 at a pressure of 2.0×10^{-6} Torr. For each device, eight separated diodes having a 2mm×2mm-size are fabricated on an ITO-coated glass substrate (50mm×50mm).

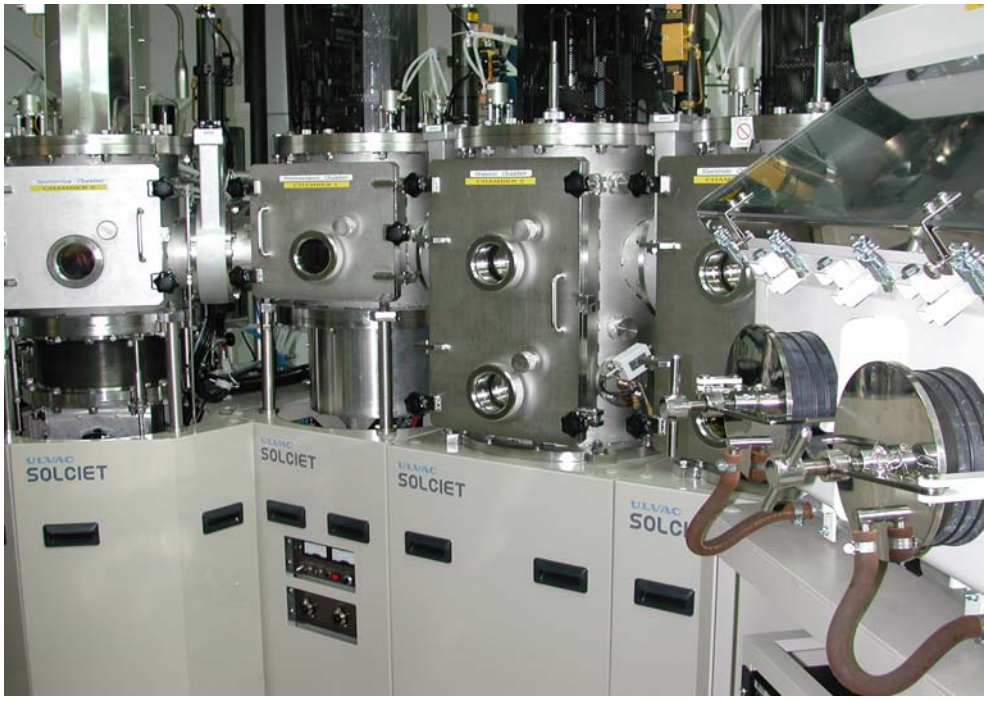

Figure 2.7: Device fabrication ULVAC system

2.2.3 Encapsulation and sealing

In order to understand the effect of oxygen or moisture on the degradation of polymer, cathode and the whole device, also to quantitatively check the encapsulation and sealing quality, some devices using in the study were encapsulated using a glass cap and then sealed with a thermal curing epoxy resin (Araldite, Ciba Speciality Chemicals) or an ultraviolet (UV) curing epoxy resin. The viscous epoxy resin was at first placed on the joining area between the glass substrate and cap in glove box. The thermal curing process was performed at an oven pre-set at 60 °C for 10 min, while the UV curing process was done with a UV source (Dymax, 2000-EC, 400W power) at room temperature for 1 min. All the encapsulation and sealing processes were completed within 15 min.

2.3 Instrumentation

2.3.1 Determination of device performance

The current-luminance-voltage (*J-L-V*) curves were measured using a computer controlled system consisting of a dynamic multimeter (Keithley DMM 2001), a source meter (Keithley 3A 2420) and eight calibrated Si photodiodes. The software was based on LabView. The current input and luminescence output measurements of the OLED were carried out by applying a voltage scan from 0 Vol. to 15 Vol. with steps either 0.2 Vol. or 0.5 Vol. Device current at normal driving condition is below 5mA. With sever degradation, the device current can reach 20mA. All measurements were performed in the glove box with water and oxygen concentrations less than 1 ppm.

2.3.2 Monitor and analysis of dark sports

In this work, the driving voltage used for powering the OLED in order to observe the dark spots was 8 volts except for experiments where the driving voltage was varied. In our experiment, the formation and evolution of dark spots were monitored in real time by an optical microscope (Olympus BX-30) with an attached CCD camera and at ambient condition (21^{o}C and 60-70% humidity). Normally, non-encapsulated devices were studied, except when sealing quality was the object of investigation. The digital optical images were analyzed using Photoshop and image analysis software. For time aging studies recording of the time began immediately when the thermal evaporation chamber was vented. The experiment setup is shown in Figure 2.8.

Figure 2.8: Dark Non-emissive area monitor system set-up.

2.3.3 Secondary ion mass spectrometry (SIMS)

The secondary ion mass spectrometry (SIMS) measurements were done in a TOF-SIMS IV instrument with time-of-flight secondary ion detection. Pulsed Ga 25 kV beam was used for analysis. Ar 3 kV beam was used for sputtering during depth profiling. In this project, SIMS is used for detecting ion migration and distribution in the device, in order to get the information of device interface and boundary movement.

2.3.4 Photoluminescence

Photoluminescence spectra (range from 300nm to 1200nm) were recorded using a cooled photomultiplier tube with lock-in detection. The emitted light was chopped at a frequency of 365Hz. A Ca-He UV laser, with peak wavelength at 325nm, was used as the excitation source. In this project, PL is used to detect polymer materials degradation.

2.3.5 X-ray Diffraction

X-ray diffraction was measured at room temperature by the Philips X'Pert system. Normally our device X-ray diffraction experiments were performed using 2θ-ω scan between 1 and 20 degrees at the scan rate of 0.001 degree per second. Polymer materials with obvious degradation will show noticeable crystallization peaks in X-ray diffraction spectra.

2.3.6 Scanning Electron Microscopy

The morphology of degraded devices was studied using scanning electron microscopy (Phillips FEG-SEM XL-30). The Scanning Electron Microscopy (SEM) observations were performed on the device cathode. In this project, SEM is used to observe the degraded surface and electrodes of the OLED.

2.3.7 Atomic Force Microscopy

An atomic force microscopy (Digital Instruments DI-3000) with the controller IIIa was used to record the surface profiles of the free surface of the solidified layers. To minimize the inelastic deformation of the sample, the tapping mode was employed in this work to attain the height, amplitude and phase images. In this project, AFM is used to observe the interfaces of organic light emitting layers.

2.3.8 Photoluminescence Quantum Efficiency (PLQE)

Photoluminescence Quantum Efficiency (PLQE) tool is widely used and is highly significant in refractive index samples, such as thin films of polymeric semiconductors. In the context of

conjugated polymers, there is great interest in establishing the absolute quantum efficiency of photoluminescence as this is considered to determine the limits to the efficiency of electroluminescent diodes. A quantitative measurement of external PL efficiency is useful for a number of other reasons. For instance, in conjunction with time-resolved photoluminescence measurements, determining the radiative and non-radiative decay constants etc.

The external radiative quantum efficiency is defined by equation:

$$\eta = \frac{\text{Number of Photons Emitted}}{\text{Number of Photons Absorbed}},$$

The standard technique for measuring PLQE involves the use of an integrating sphere. An integrating sphere is a hollow sphere which has its inner surface coated with diffusely reflecting materials (typically barium sulfate). When a light source is placed in an ideal integration sphere, the light is redistributed isotropically over the sphere interior surface regardless of the angular dependence of the emission. A baffle is also coated with barium sulfate to prevent direct illumination of the optical fiber. Figure 2.9 shows the photoluminescence quantum efficiency measurement system set-up.

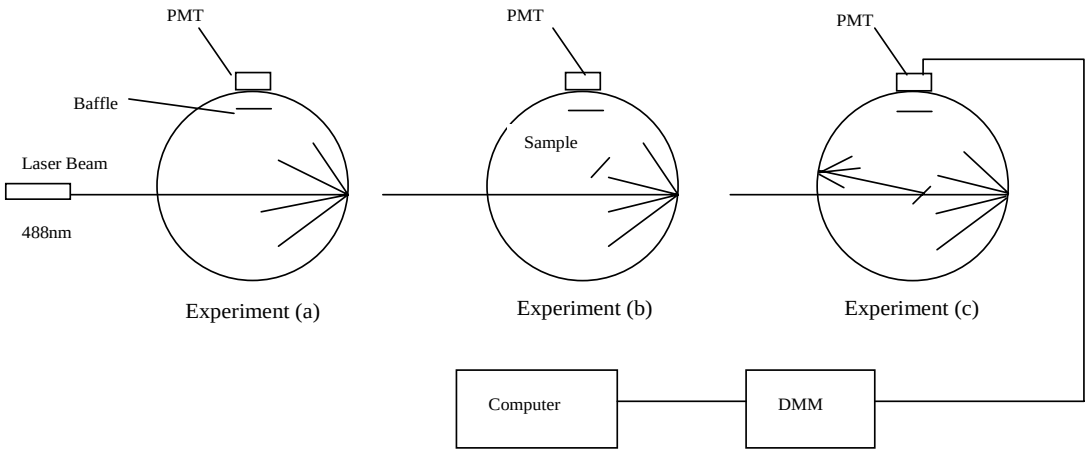

Figure 2.9: Photoluminescence quantum efficiency measurement system set-up.

In our experiment setup, photo-multiplier tube (PMT) and Integrating Sphere are purchased from Lab Sphere Com, USA. UV Laser Source of wavelength of 325nm and power of 11mW and Dynamic Multimeter are used for optical source and signal detector. Data sampling and efficiency calculation are done through programming using LabView.

Final efficiency is calculated by three measurements results. Assume A is the fraction of incident light that is directly absorbed by the sample and μ is the fraction of laser light scattered from the sphere wall that is absorbed by the sample. The first measurement is done without sample inside the integrating sphere:

$$M_1 = L_a \qquad (2.1)$$

The second measurement while sample is inside the integrating sphere but not in the laser path:

$$M_2 = L_a(1-\mu) + \eta\mu L_a \qquad (2.2)$$

The third measurement while sample is inside the integrating sphere and also inside the laser path:

$$M_3 = L_a(1-\mu)(1-A) + \mu A L_a\eta + L_a A\eta \qquad (2.3)$$

M_1, M_2 and M_3 are the total signal values for 1st, 2nd and 3rd time measurements respectively. L_a, L_b and L_c are the laser part of signal in the total signal for 1st, 2nd and 3rd time measurements respectively. Value A can be measured by spectrophotometer at the wavelength of the light source which is 325nm.

Final efficiency η are obtained by solving equations of 2.1, 2.2 and 2.3.

2.4 General performance of our device

2.4.1 J-L-V

Figure 2.10 shows a typical *J-L-V* relation measured from the devices fabricated in accordance with the procedure mentioned above. At about 3 V, the current density, *J*, starts to increase dramatically. However, the device starts to emit light at about 5.5 V. The luminescence (*L*) was about 20 cd/m^2 at 6 V and achieved 100 cd/m^2 at 7.2 V. At 8 V, the driving voltage selected for electrically stressing, the typical luminescence is about 240 cd/m^2. Figure 2.11 shows the typical efficiency curve, the maximum efficiency of our processed device is around 6 Cd/A.

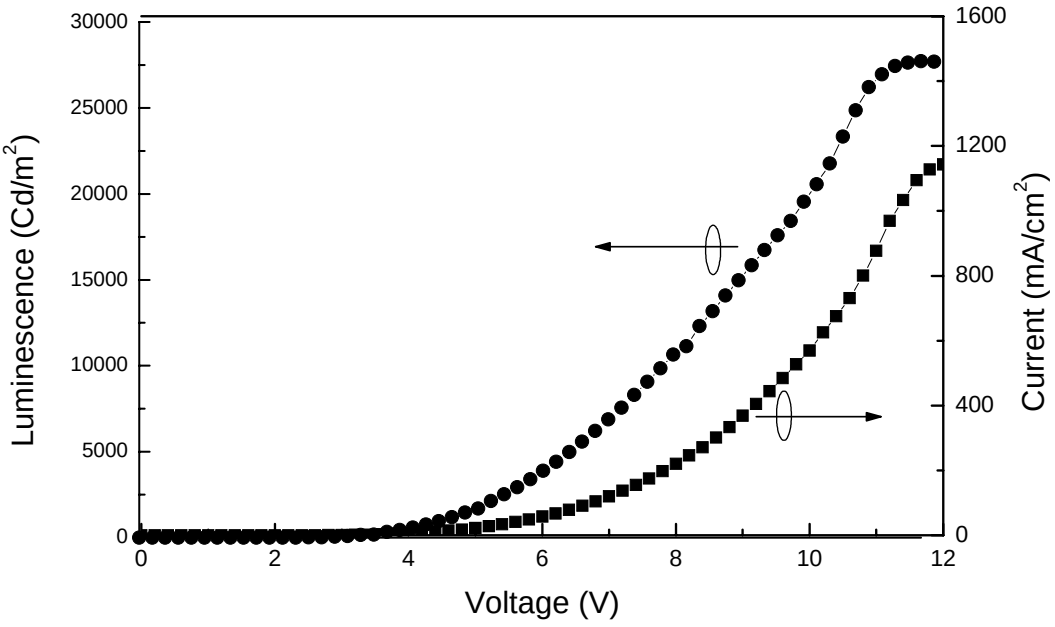

Figure 2.10: Typical device *J-L-V* curve.

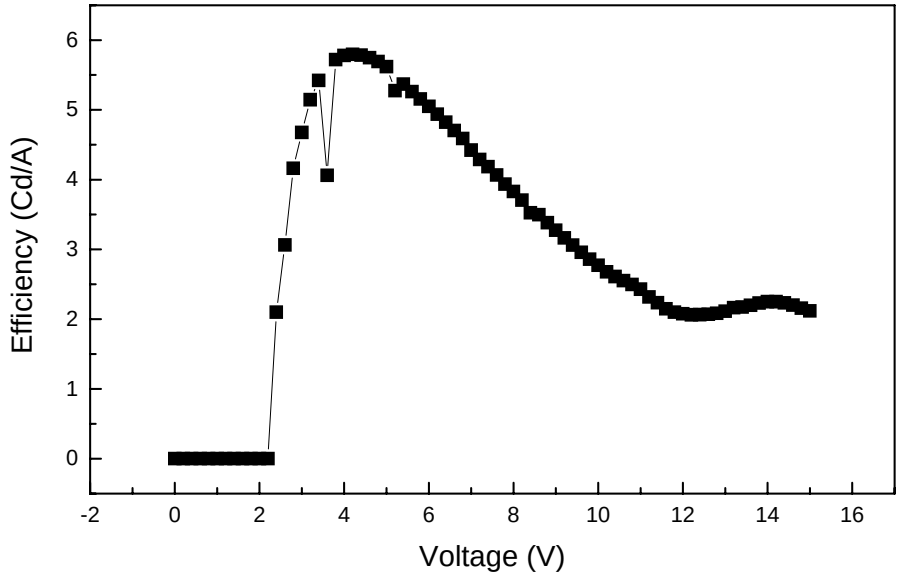

Figure 2.11: Typical device efficiency curve.

2.4.2 Lifetime

Figure 2.12 shows the typical lifetime curve of our devices without encapsulation and measurement is done in ambient condition. The voltage rises steadily starting from the very beginning of the run, indicating an increase in the dc impedance of the device. At the same time the luminous output drops, the quantum efficiency decreases. The loss in luminance occurs at a considerably faster rate than the increase in impedance and there appears to be two regimes: an initial and very rapid loss over the first several minutes, followed by a more gradual decline over tens to hundreds of hours. The general lifetime of our devices operating in inert condition can reach several thousand hours with the device driven at constant current and emitting at an initial performance of around 100cd/m^2. In the initial stage of the lifetime

test, there is a decrease in luminance followed by a slow rise to a broad plateau at around several thousand hours, after which it begins an ultimate decline in luminance.

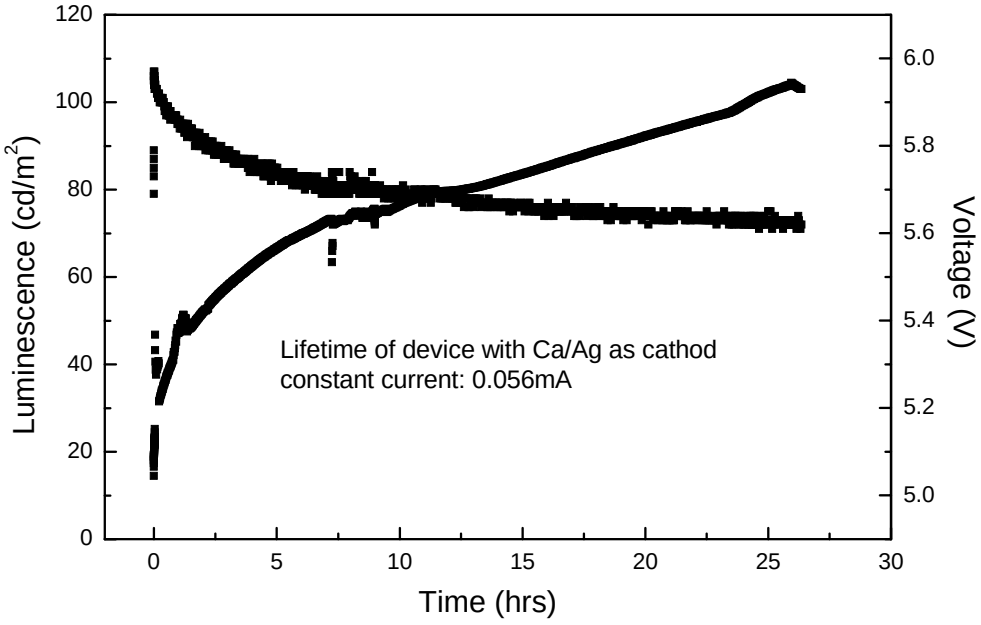

Figure 2.12: Typical device lifetime curve.

2.5 Summary

In this chapter, operation principal of organic light emitting device has been elaborated. Frequently used scientific research tools used in this work are given. The general performance of our device is also described. Start from next chapter, we will investigate the organic light emitting device degradation mechanism from different point of view based on these kind of devices.

CHAPTER 3 DEVICE PHYSICS

3.1 Introduction

It is crucial to understand the operation and degradation mechanism of OLED because they are able to facilitate better understanding of the types of mechanism that control the current flow *I* and applied bias *V,* and how those values of *I* and *V* are related to the intensity of emitted light. In this chapter, the OLED device performance using various layer parameters has been simulated although so far no single mechanism adequately describes the current–voltage characteristic over the full operational range of the OLEDs and the mechanisms are still remain disputable. In this chapter, Matlab software and SILVACO software are used to simulate the OLED's performance.

3.2 Background of modeling OLED devices

Several theoretical models for OLEDs have been proposed in the past, each consists of different assumptions to simplify the complex interplay of mechanisms involved. Due to the large variety of known OLED setups, suitable materials, and mechanisms governing their behavior, distinct models were developed to explain the experimental findings. Both injection dominated and bulk dominated mechanisms have been proposed as the rate limiting process in the current–voltage *(I*V) behavior of polymer and small molecule organic LEDs. Proposed injection dominated mechanisms are tunnelling [55,56] and thermionic emission. [57] Proposed bulk dominated mechanisms are Ohmic conduction, [58] space-charge limited current (SCLC) conduction [55,58,59] and space-charge limited conduction with an exponential distribution of traps. [70] Most of the modeling methods are borrowed from semiconductor theory and no mature and single modeling could

adequately describe the current–voltage characteristic over the full operational range of the OLEDs.

Device processes

Charge carrier in an OLED device normally goes through injection, transport, recombination, and exciton decay etc. processes. The difficulty in modelling polymer devices such as OLED is the fact that the properties of conjugated polymers are poorly known at present. Among these are electron and hole mobilities, ionization potentials, electron affinities, trap concentrations and distributions, doping levels, interfacial barriers, and recombination mechanism etc.

I. Charge injection

The injecting contacts for holes and electrons are assumed to be ohmic when the injection barrier is smaller than 0.1eV, the current is considered as space charge limited. And the barrier larger than 0.6eV, the current is considered totally barrier injection controlled. For high performance OLED devices, the current limitation due to barriers at the electrode–organic interfaces is not acceptable, therefore, the simulation is limited within the cases of small barrier height. [55,56]]

II. Carrier transport

The local electric field in the organic layers is responsible for the drift of the free charge carriers. In amorphous molecular organic solids such transport phenomena are commonly described as hopping processes. Holes are transported in the HOMOs, whereas electrons are transported in the LUMOs. [58]

In addition to the charge carrier drift parallel to the direction of the electric field, a random charge carrier movement due to thermally stimulated hopping processes with no preferential direction occurs. This is called free charge carrier diffusion.[59]

III. Charge recombination

The recombination of holes and electrons to excitons occurs due to attractive Coulombic interaction between the two different charge carrier species.

IV. Charge carrier trapping

Charge carrier traps are states with energetic positions in between the energetic levels of the HOMO and the LUMO. Trap states may have various origins, e.g., material impurities or structural disorder. The occupation of trap states, which are uncharged when empty, depends on the free charge carrier densities and the trap depth, given as the energetic distance of the trap state to the next transport site.

For shallow trap states arising from structural disorder in the organic layers, recombination of free charge carriers with trapped ones is assumed to be radiative with the same efficiency as for recombination in between free charge carriers.

V. Internal interfaces

Interfaces between two adjacent organic layers have a major influence on current flow and device efficiency. The actual processes at internal interfaces are not fully understood yet. In this simulation, a simple model of the interface processes is assumed. The organic materials

are assumed not to interact directly. This means that no particular surface state and charge transfer complex formation are considered.

VI. Singlet excitons

The recombination of holes and electrons in the organic layers results in the formation of singlet and triplet excitons in a ratio of 1:3 [57] due to spin statistics. In this simulation, excitons are supposed to be Frenkel excitons rather than charge-transfer excitons or Mott–Wannier excitons, which mean that they are spatially limited to one (excited) molecule. Efficient light emission due to radiative decay of excited molecules can only be expected from singlet excitons in non-doped OLEDs, since the diffusion length of triplet excitons is due to their long lifetime large enough to favour nonradiative recombination at the electrodes. The implementation of exciton diffusion and decay will therefore be limited to singlet excitons.

3.3. Theoretical model

The device model includes charge injection, transport, recombination, and space charge effects in the organic material. The model assumes hole injection at the left contact x = 0.1um, ITO thickness is 0.1um; electron injection at the right contact. The transport of carriers in the organic material is described by time dependent continuity equations, with a drift-diffusion form for current density, coupled to Poisson's equation. The drift diffusion method involves finding a self-consistent solution for the electron and hole densities *n* and *p* and for the electrostatic potential ψ. The three equations to be solved are discussed below.

3.3.1 The continuity equations for *n* and p

Carriers can either recombine in the organic layer, or traverse the organic layer without recombining. Maximum quantum efficiency is achieved by having all carriers recombine. Carriers which traverse the device without recombining are lost and thus lower the quantum efficiency. To determine the fraction of carriers which recombine we start with the continuity equations for electrons and holes,

$$\frac{dn}{dt} - \frac{1}{q}\frac{dJ_n}{dx} = G - R \qquad (1)$$

$$\frac{dp}{dt} + \frac{1}{q}\frac{dJ_p}{dx} = G - R \qquad (2)$$

where the electron and hole current densities are J_n and J_p , respectively, G is the electron-hole pair generation rate and q the electron charge magnitude. The recombination rate R has two contributions, the optical recombination rate R_{opt}, where C_{opt} is the optical capture-emission rate, and the Shockley–Read–Hall (SRH) recombination rate R_{srh}, where τ_n and τ_p are the electron and hole recombination lifetimes, respectively. The intrinsic charge density n_i is given by

$$n_i^2 = N_c N_v \exp(-\frac{E_g}{kT}) \qquad (3)$$

where E_g is the energy gap, N_c and N_v are the densities of states in the conduction and valence bands, respectively, T is the temperature in Kelvin and k is Boltzmann's constant.

$$R_{opt} = C_{opt}(np - n_i^2) \qquad (4)$$

$$R_{srh} = \frac{np - n_i^2}{\tau_n(p + n_i) + \tau_p(n + n_i)} \qquad (5)$$

3.3.2 Poisson's equation for the potential ψ or the electric field (ε)

$$-\frac{d\varepsilon}{dx}=\frac{d^2\psi}{dx^2}=-\frac{q}{\varepsilon}(p-n-N_A^-+N_D^+-n_{ij}) \quad (6)$$

where N_A^- and N_D^+ are the ionised acceptor and donor impurity concentrations and n_{ij} is the density of trapped electrons for the *j*th trap energy level, given in Eq. 10 below. Maxwell–Boltzmann statistics have been assumed, thus

$$n=N_C\exp[\frac{q}{k_BT}(\psi-\phi_n+\frac{\chi_c}{q})] \quad (7)$$

$$p=N_V\exp[-\frac{q}{k_BT}(\psi-\phi_p+\frac{E_g+\chi_c}{q})] \quad (8)$$

where ϕ_n and ϕ_p are the quasi-Fermi levels for electrons and holes and χ_c is the electron affinity of the device..

3.3.3 J_n and J_p are given by

$$J_n=-q\mu_n n\frac{d\phi_n}{dx} \quad (9)$$

$$J_p=-q\mu_p p\frac{d\phi_p}{dx} \quad (10)$$

where μ_n and μ_p are the electron and hole mobilities, respectively.

3.3.4 Boundary conditions

The spatial boundary conditions are given by the particle currents at the contacts. For the barriers and biases considered here thermionic emission dominates tunnelling, so that thermionic emission and its time reversed process combine to establish quasi-equilibrium carrier densities at the injecting contacts for electrons and holes,

$$n_e(E_L) = n_0 \exp(-\psi_L / kT) \tag{11}$$

$$p_e(E_R) = n_0 \exp(-\psi_R / kT) \tag{12}$$

$$\psi_{L,R} = \phi_{L,R} - e\sqrt{\frac{e|E_{L,R}|}{\varepsilon}} \tag{13}$$

where $E_{L,R}$ is the electric field at the left (right) contact, *k* is Boltzmann's constant, *T* is the temperature, ε is the dielectric constant, $E_{L,R}$ is the density of conjugated chain segments times the number of ways a chain segments can be occupied by a carrier, $\phi_{L,R}$ is the Schottky energy barrier at zero field at the left (right) contact, and $\psi_{L,R}$ is the field dependent energy barrier to injection at the left (right) contact which includes image force lowering of the barrier if the field has the correct sign for barrier lowering.

Table 3.1 Parameter value list

Parameter Definition	symbols	Units	PPV	HTL
Temperature	T	K	270	270
Workfunction	χ_c	eV	2.6	2.4
Highest occupied molecular orbitals	HOMO	eV	5.0	5.02
Lowest unoccupied molecular orbitals	LUMO	eV	2.6	3.42
Electron mobility	μ_n	$m^2/(V\ s)$	1×10^{-9}	1×10^{-9}
Hole mobility	μ_p	$m^2/(V\ s)$	1×10^{-8}	1×10^{-6}
Density state in conduction band	N_c	m^{-3}	2.5×10^{25}	2.5×10^{25}
Density state in valence band	N_v	m^{-3}	2.5×10^{25}	2.5×10^{25}
Electron recombination lifetime	τ_n	s	1×10^{-6}	1×10^{-6}
Hole recombination lifetime	τ_p	s	1×10^{-8}	1×10^{-8}
Donor concentration	N_D	m^{-3}	1×10^{21}	-
Acceptor concentration	N_A	m^{-3}	1×10^{15}	1×10^{15}

3.4 Simulation results

In this section, single PPV layer device and double layer HTL/PPV device structure have been simulated. The parameter values are given in Table3.1. The programme is done using Matlab software.

3.4.1 Simulation of single layer device ITO/PPV/Ca

In this simulation, PPV material considered with an energy gap of 2.4 eV, HOMO level at 5.0eV and LUMO level at 2.6eV. The electron and hole mobilities are given 10^{-9} and 10^{-8} m^2 /(Vs). For most typical OLED device, ITO has been used for anode; its workfunction is considered as 4.8eV. Low work function Ca has been used for cathode; its workfunction is considered as 2.9eV. For this simulation, ITO and Ca are also used for anode and cathode, except the anode and cathode variation cases. Figure 3.1 shows the schematic diagram of device structure which is going to be simulated. ITO is 100nm, cathode is 20nm. Device with different PPV thickness is also simulated and it is found out that 100nm PPV has the highest power efficiency, therefore in this simulation work, 100nm PPV is used.

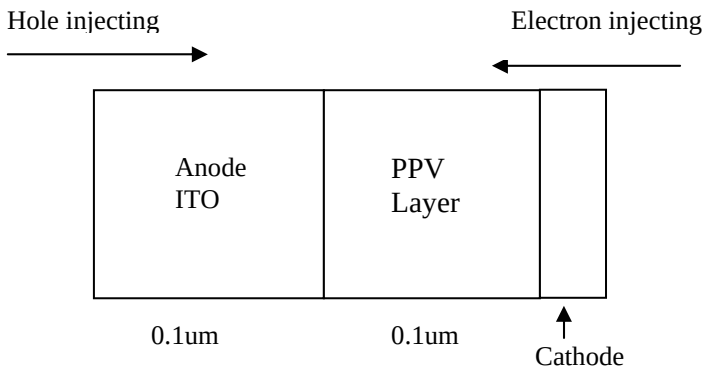

Figure 3.1: Schematic diagram of device structure simulated. ITO is used as anode and Ca is used as cathode. PPV thickness is 100nm.

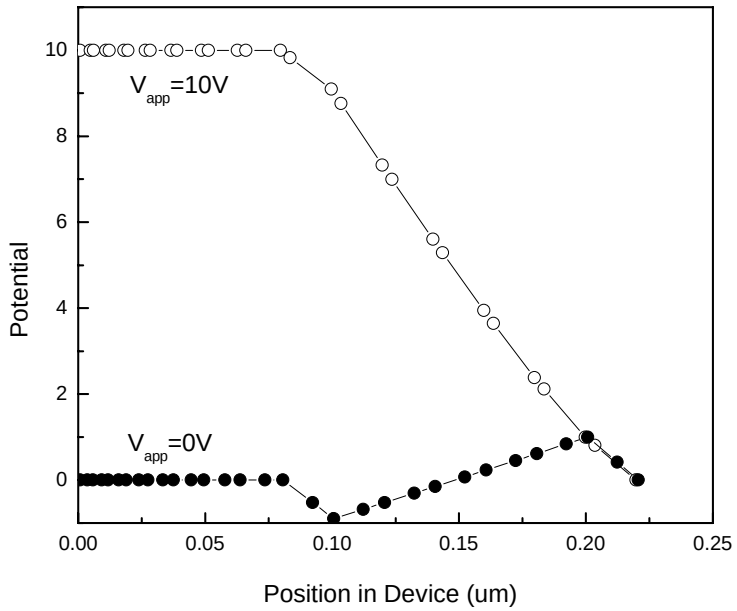

Figure 3.2: The potential curve for V_{app}=10V (open circle) and V_{app}=0V (solid circle)

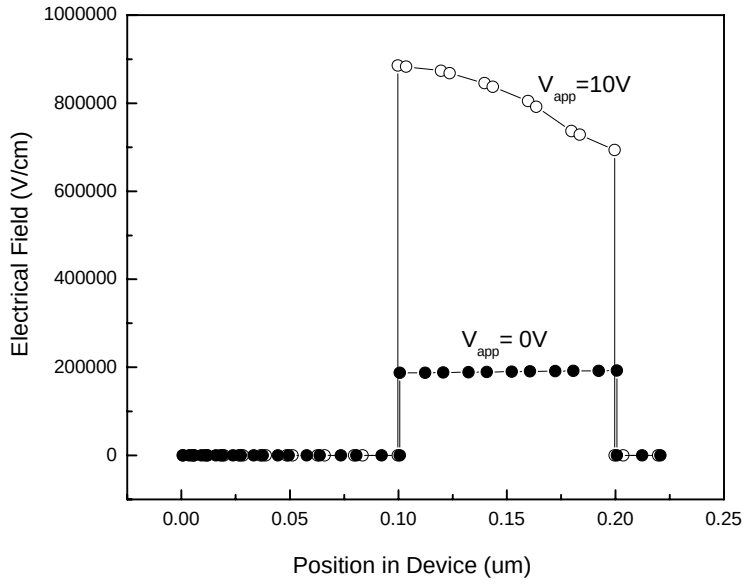

Figure 3.3: The electrical field curve for V_{app}=10V (open circle) and V_{app}=0V (solid circle)

Figure 3.2 shows the potential distribution and Figure 3.3 shows the electrical field distribution for device structure shown in Figure 3.1. Two cases are presented: without any bias 0V and device operating at 10V. Built-in potential and electrical field are existed, which is shown clearly in the figures.

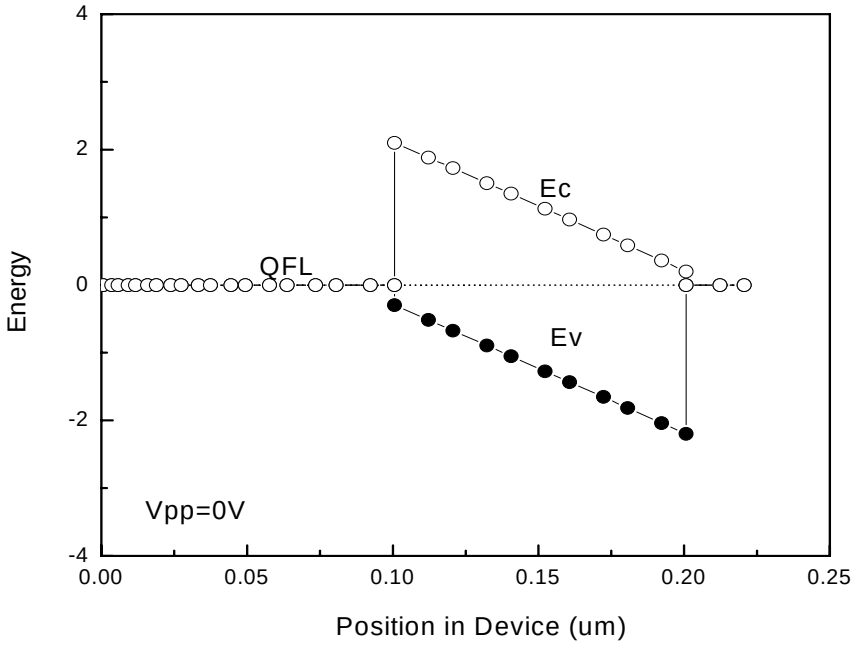

(a)

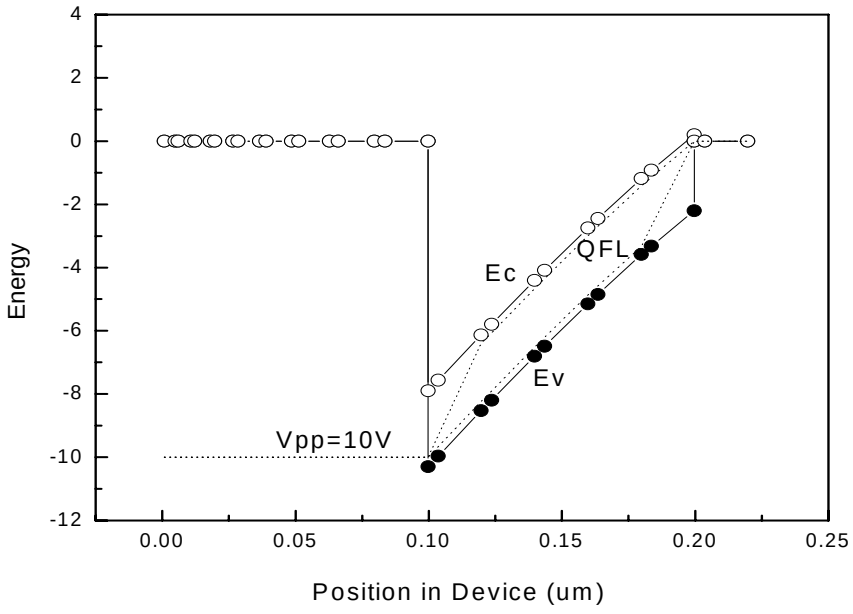

(b)

Figure 3.4: The conduction band (open circle), valence band (solid circle), electron quasi-Fermi energy (dot line) and hole quasi-Fermi energy (dot line) for V_{app} = 0 V (panel a) and for V_{app} = 10 V (panel b).

The conduction band, valence band and electron quasi-Fermi energy and hole quasi-Fermi energy for single layer device structure for V_{app} = 0 V and 10V are shown in Figure 3.4 panel a and panel b respectively.

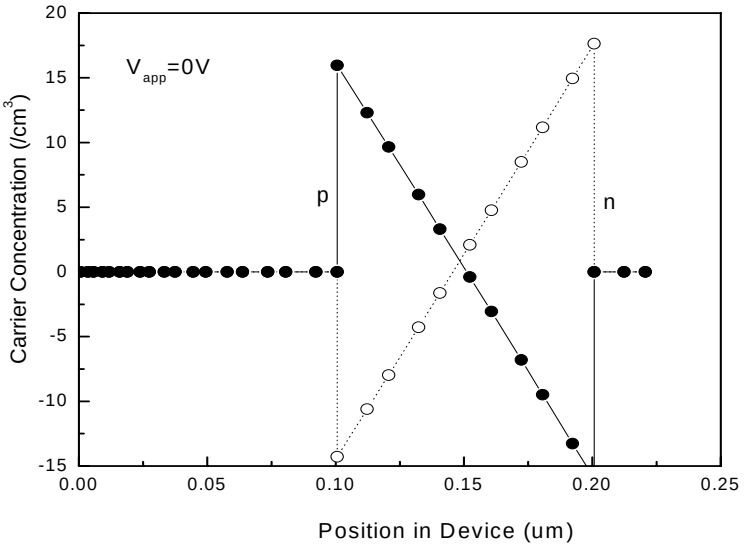

(a)

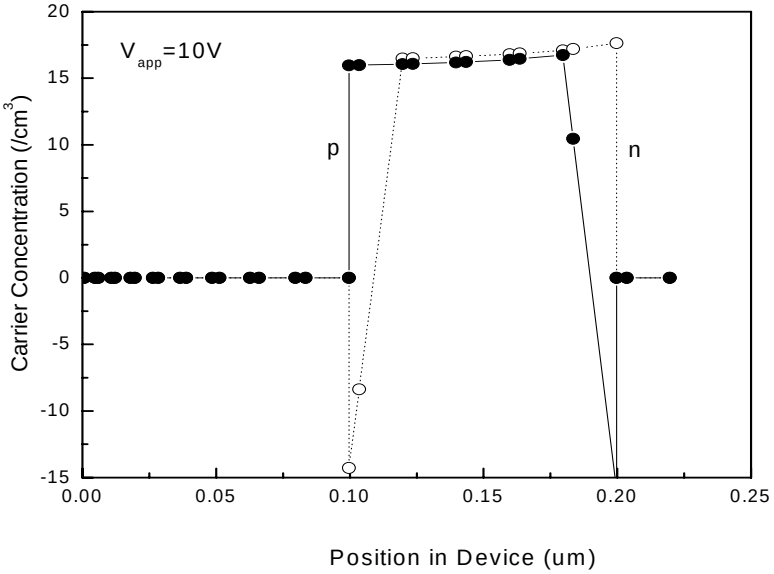

(b)

Figure 3.5: electron concentration (open circle), hole concentration (solid circle) for V_{app}=0V (panel a) and V_{app}=10V (panel b).

Figure 3.5 shows the electron concentration (open circle) and hole concentration (solid circle) for V_{app}=0V and 10V, respectively.

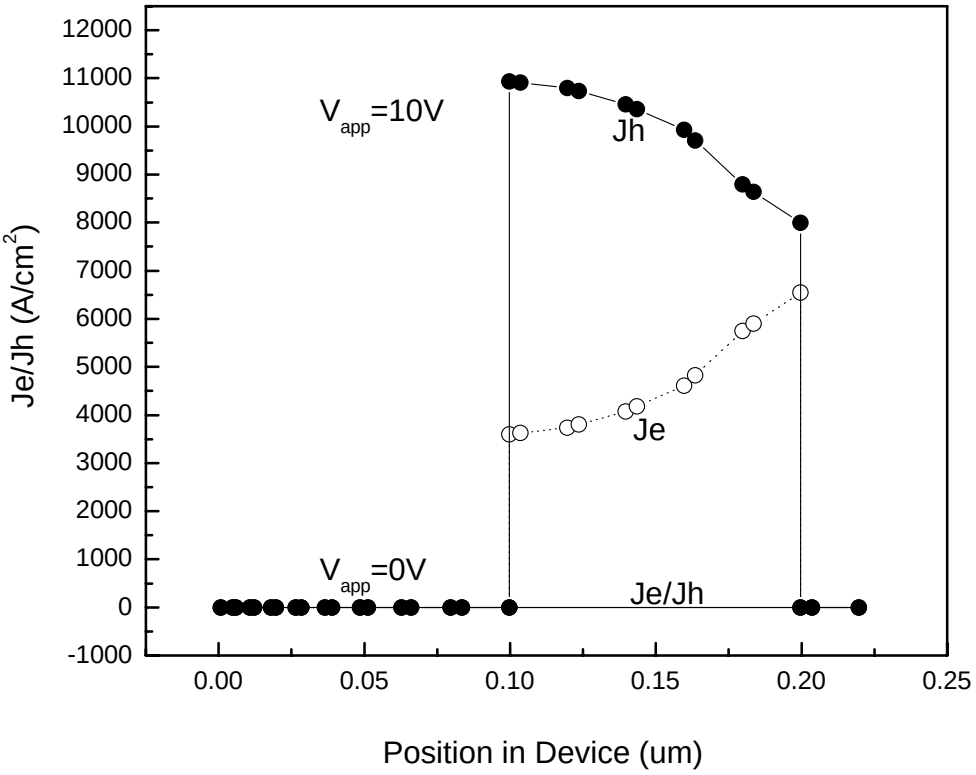

Figure 3.6: The hole current (solid circle), and electron current (open circle), for V_{app}=10V. Hole current and electron current for V_{app}=0V (straight line) are zero.

Figure 3.6 shows the hole current density (solid circle) and electron current density (open circle), for V_{app}=10V. Hole current density and electron current density for V_{app}=0V (straight line) are zero which are also shown together in the Figure 3.6. The anode side hole injection barrier is decided by the difference of workfunction of ITO and PPV HOMO which gives 0.2 eV difference and cathode side electron injection barrier is decided by the difference of workfunction of Ca and PPV LUMO which gives also 0.2eV difference. However, the PPV materials have the special property that the electron is easily trapped inside. And the hole mobility is 1-2 order larger than electron mobility, which gives much larger hole current than electron current.

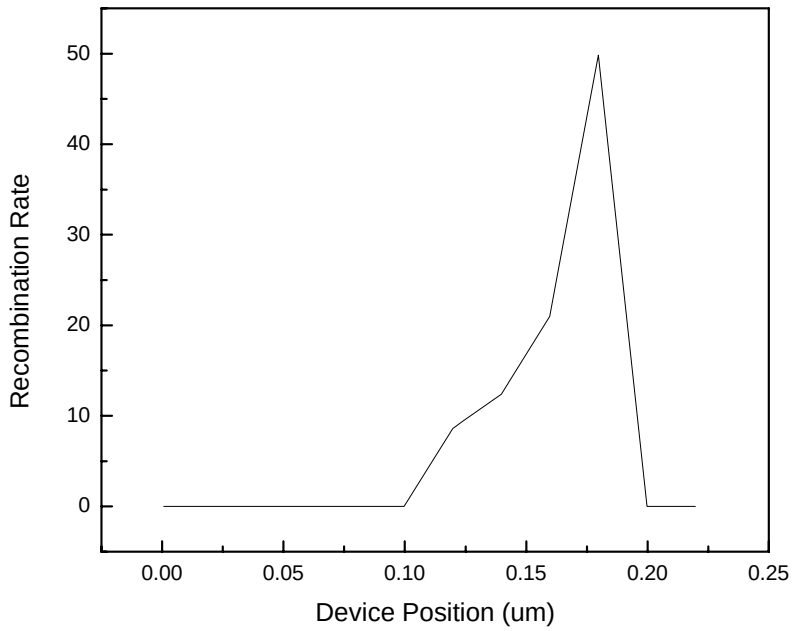

Figure 3.7: Recombination Rate versus device position for single layer device structure.

Figure 3.7 shows the total recombination rate profile for this single PPV device structure with ITO as anode and Ca as cathode. Due to the hole mobility is larger than electron mobility, the recombination centre deviate from the centre of PPV layer and located near the cathode interface.

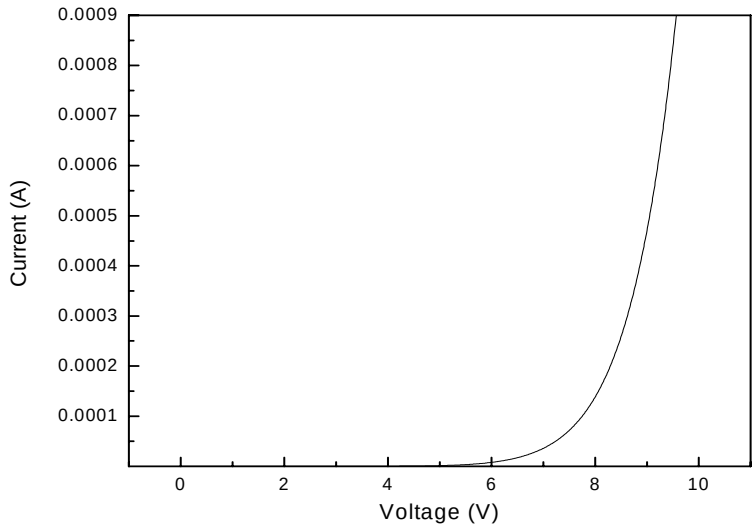

Figure 3.8: Current – voltage behavior of device structure shown in Figure 3.1.

Finally the Figure 3.8 gives the current –voltage behaviour of this device structure.

3.4.2 Simulation of device performance improvement

In order to understand more deeply about the typical OLED device electrical behavior, device with different hole injection barrier and electron injection barrier are simulated also.

3.4.2.1 Anode barrier variation

Figure 3.9 shows the hole current density (solid circle), and electron current density (open circle) for anode with 0 barrier height at V_{app}=10V. For barrier height 0.1eV, hole current density (solid upper triangle) and electron current density (open solid upper triangle) at V_{app}=10V are also shown. When the barrier at anode is lower, the hole current density and electron current density become more unbalanced, hole current density is much more than electron current density.

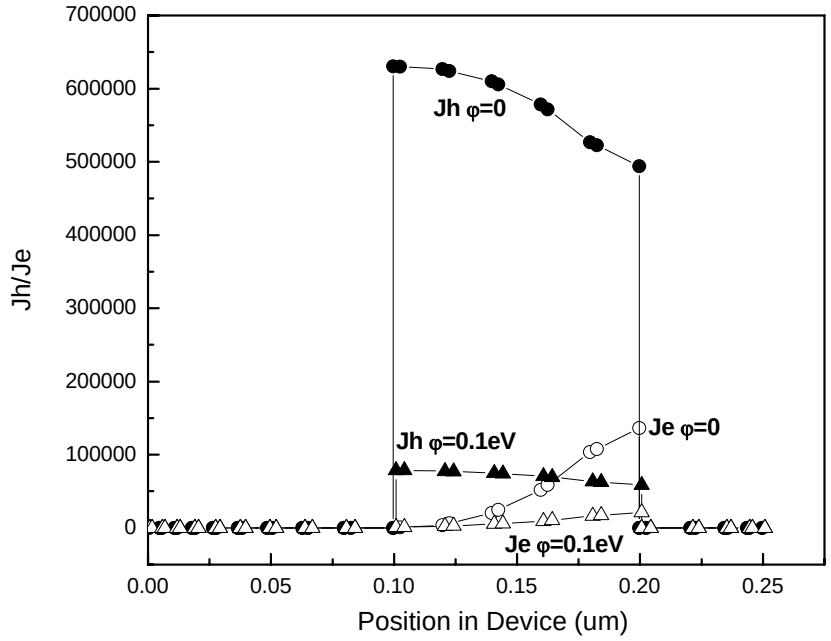

Figure 3.9: Hole current density (solid circle), and electron current density (open circle) for anode 0 barrier height. Hole current density (solid upper triangle) and electron current density (open solid upper triangle) for anode 0.1eV barrier height. V_{app}=10V.

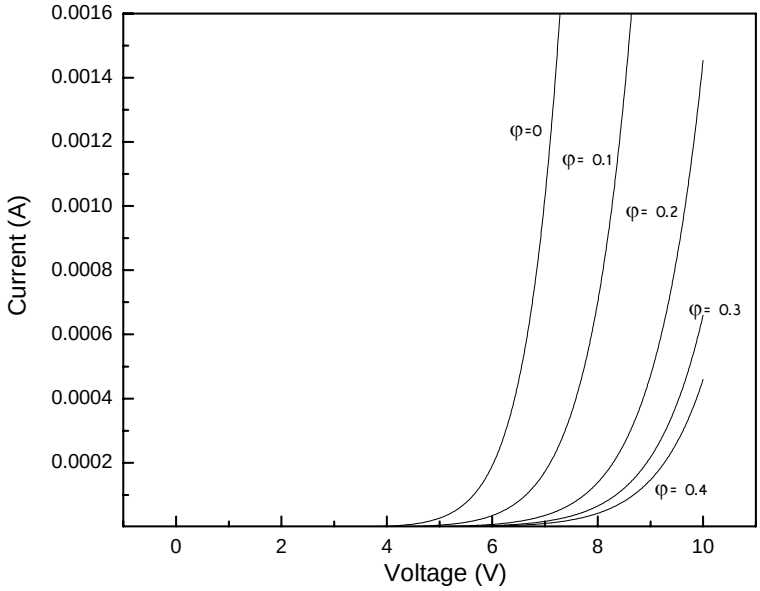

Figure 3.10: Current – voltage behaviour for anode hole injection barrier 0, 0.1, 0.2, 0.3 and 0.4eV.

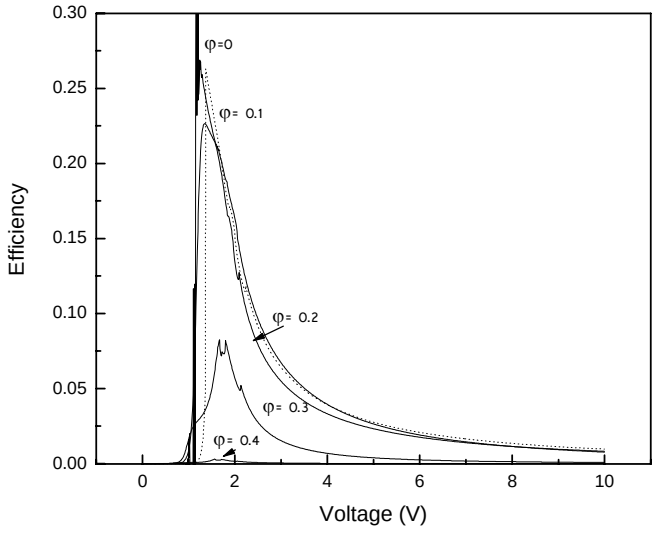

Figure 3.11: Power efficiency for anode hole injection barrier 0, 0.1, 0.2, 0.3 and 0.4eV.

Figure 3.10 and Figure 3.11 show current – voltage and power efficiency behaviour for anode hole injection barrier 0, 0.1, 0.2, 0.3 and 0.4eV. As the figures illustrated, the higher the hole injection barrier, the lower the device current and power efficiency.

3.4.2.2 Cathode barrier variation

Figure 3.12 shows the hole current density (solid circle), and electron current density (open circle) for cathode with 0 barrier height at V_{app}=10V. For barrier height 0.2eV, hole current density (solid upper triangle) and electron current density (open solid upper triangle) at V_{app}=10V are also shown. Contrary to the anode side, when the barrier at cathode is lower, the hole current density and electron current density become more balanced, electron current density is comparable to hole current density.

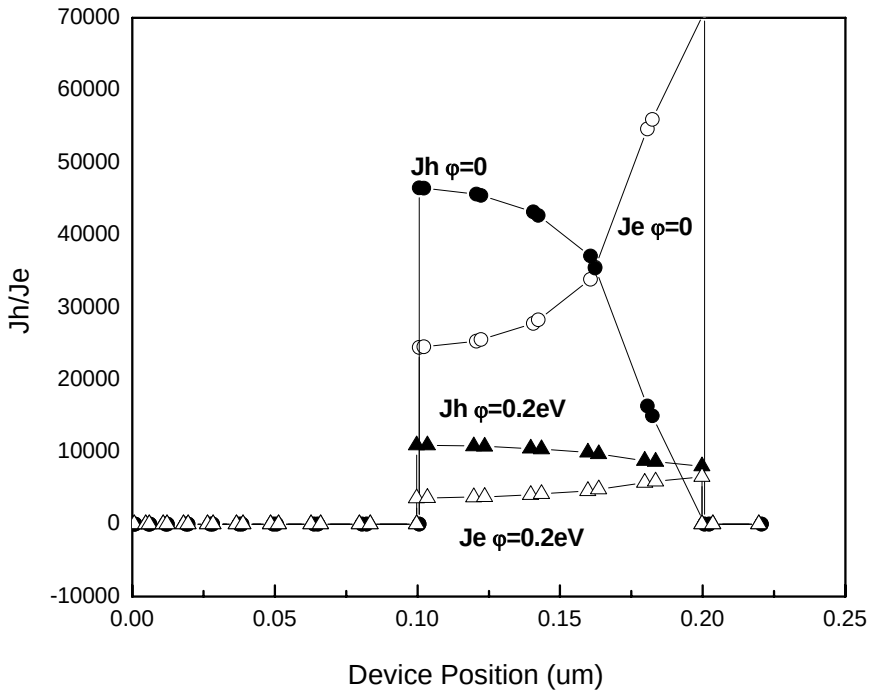

Figure 3.12: Hole current density (solid circle), and electron current density (open circle) for cathode 0 barrier height. Hole current density (solid upper triangle) and electron current density (open solid upper triangle) for anode 0.2eV barrier height. V_{app}=10V.

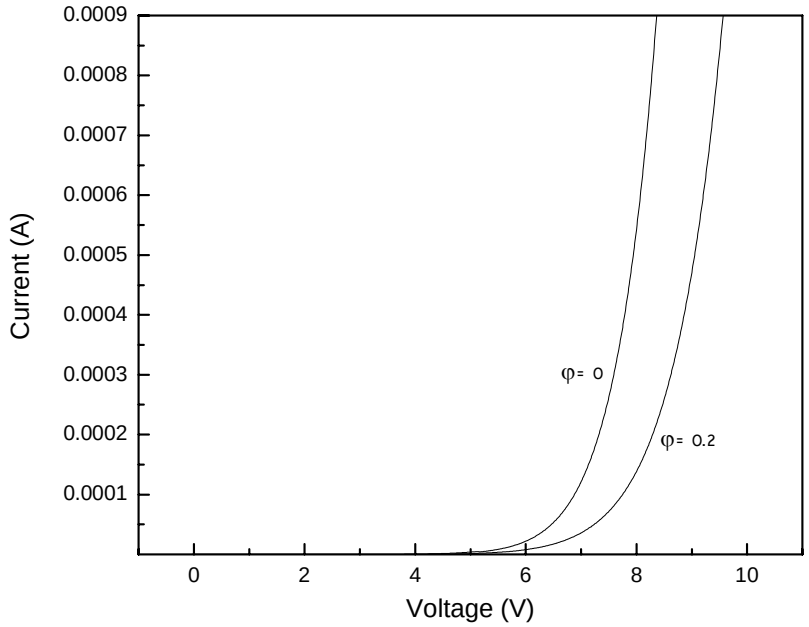

Figure 3.13: Current – voltage behaviour for cathode electron injection barrier 0 and 0.2eV.

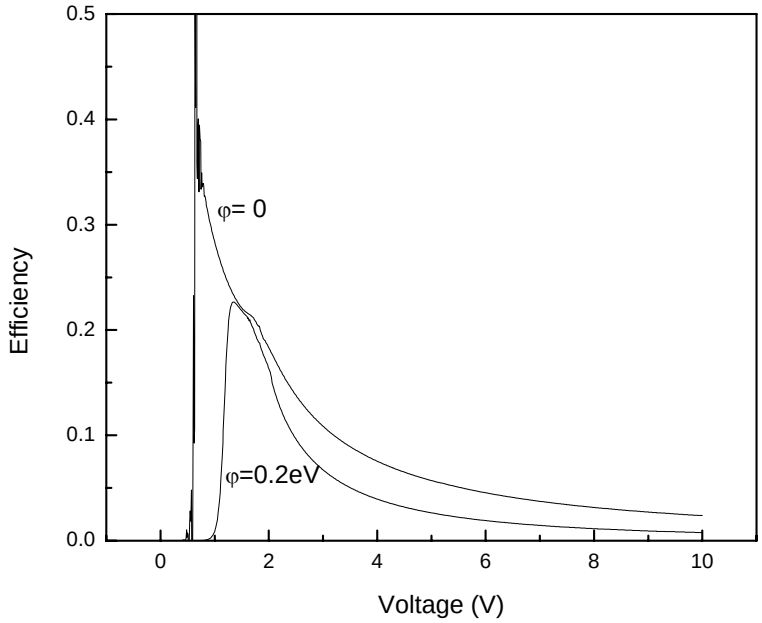

Figure 3.14: Power efficiency - voltage behaviour for cathode electron injection barrier 0 and 0.2eV.

Figure 3.13 and Figure 3.14 show device current – voltage and power efficiency behaviour for cathode electron injection barrier 0 and 0.2eV. It also shows that the higher the barrier, the lower of the device current and efficiency.

3.4.2.3 Inserting hole transport layer

Although ITO is widely used as transparent anode in OLED device so far, the problem associated with surface unevenness still hasn't been solved. Inserting a layer of hole transport layer (HTL) on top of ITO surface provide a way to smooth the interface and enhance the hole injection. Another advantage for inserting HTL is it can effectively move the recombination center from near cathode side to the center of the EL layer. The reason is hole mobility is much larger than electron mobility due to PPV property, the HTL layer will increase hole travel distance, so that the electrons can travel further into device center to meet with holes. The recombination center will move into the PPV layer. Figure 3.15 shows the recombination rate versus device position for double layer device structure. Compare Figure 3.7, the recombination rate for single layer device, the recombination center has moved inside into the device obviously.

.

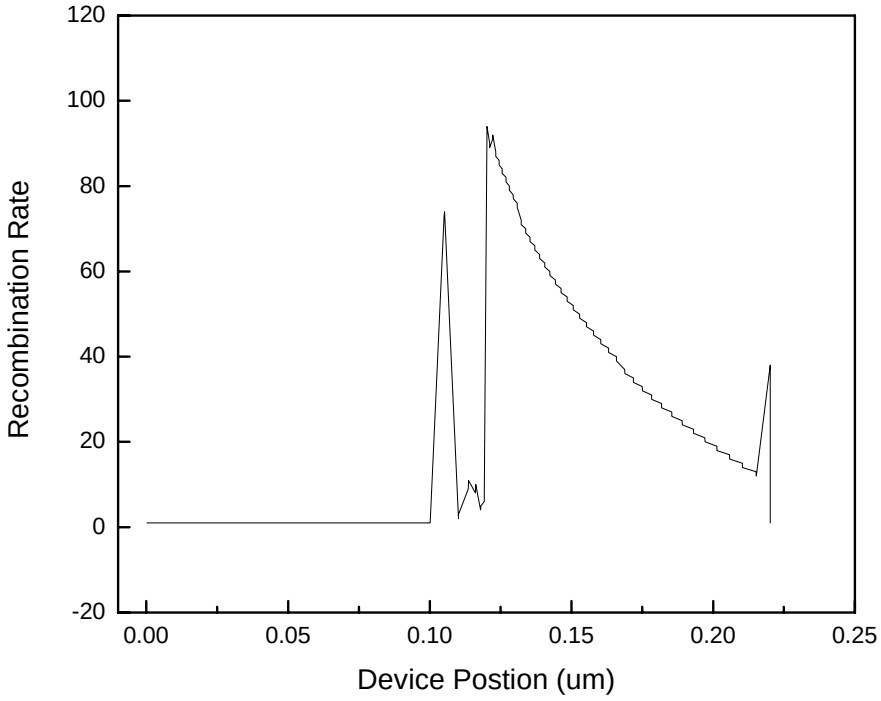

Figure 3.15: Recombination rate versus device position for double layer device structure.

.

3.4.3 Effect of interface roughness

Not only the ITO-polymer interface rough and full of the spikes, but the cathode side interface also rough due to thermal evaporation. Under electrical stress and metal migration, there are areas where Ca and In protrusions become close. A large electric field intensity and current density is created. The enhanced local luminescence and heating leads to instability and further growth of local current densities until the polymer breaks down; short circuit may be formed. The central dark spot is formed initially in this area. The detailed non-emissive area formation and growth will be illustrated in detail in the following chapters. Using the commercial semiconductor device simulator P-Spice, the device electrical field distribution with interface spikes is simulated. Figure 3.16 is the device structure simulated. Two big spikes from anode are simulated. Figure 3.17 is the

electrical field distribution in the device. It shows obvious un-uniformed electrical field distribution. The electrical field around spikes is one order higher than the surrounding area.

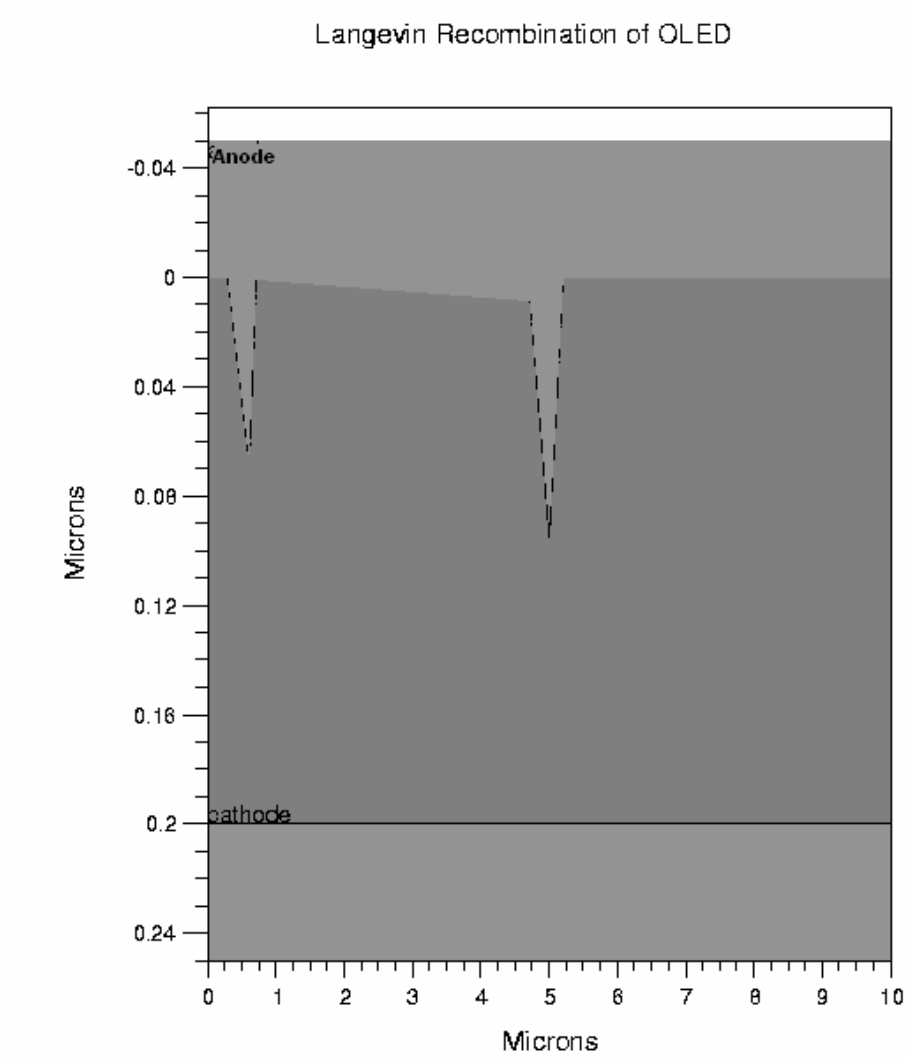

Figure 3.16 is the device structure simulated. Two big spikes from anode are simulated.

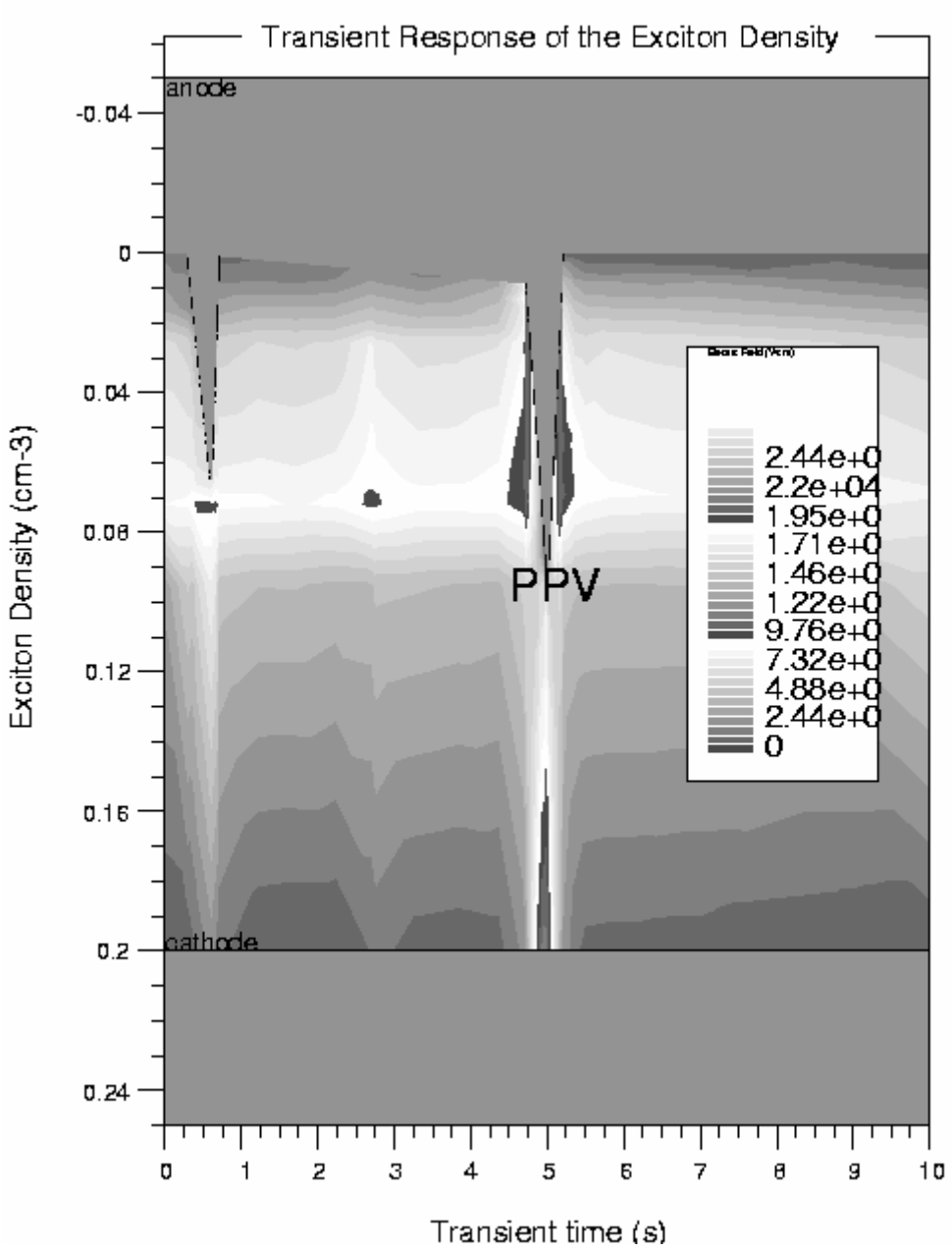

Figure 3.17 is the electrical field distribution due to ITO spikes. It shows obvious un-uniformed electrical field distribution.

3.5 Summary

The results of a device model for single layer and double layer organic LEDs are presented which includes charge injection, transport, recombination, and space charge effects in the organic material.

The best device performance regarding recombination rate is achieved where barriers to electron injection on the left and hole injection on the right are chosen such that injection is balanced, resulting in recombination rate profile which is significant throughout the emission layer rather than merely at the contacts. The two layer HTL/PPV device shows an improved recombination rate profile and substantially reduces the magnitude of the contact limited recombination seen in the single layer devices.

The interface also plays a very important role in device performance. The simulation results show that in the anode or cathode metal spikes, the local electrical field is increased by about at least order. The high electrical field and high local current will degrade the local polymer area, which is also the origin of display defect.

CHAPTER 4 POLYMER DEGRADATION DURING DEVICE OPERATION

4.1 Introduction

With the recent discovery and rapid development of polymers electroluminescent (EL) devices, there has been a concentrated effort to understand how these materials behave and how to improve device performance and device lifetime. There are many factors responsible for the reliability of the device, such as the EL material quality, the polymer metal electrode interface, environmental conditions during device operation, and so on. Among them the degradation of polymer is treated as intrinsic factor. In this chapter, I have studied the photo-stability of poly(*p*-phenylene vinylene) (PPV) when it is irradiated with UV light under different conditions. Detailed experiment conditions and results are reported. Furthermore, I examined the role of electrical stress on polymer degradation combine with the photo-oxidation effect with the organic device structure ITO/poly(*p*-phenylene vinylene)PPV/Ca/Ag which will explain polymer degradation mechanism during device electrical stress. This study will help to explain the organic light emitting device failure mechanism.

4.2 Experiments details

PPV was dissolved in toluene (approx.5 mg/ml) and was spin-coated at 1000 rpm for 60 sec. onto a quartz substrate. The films were then dried overnight in vacuum chamber to remove traces of the solvent. This gave films that were about 80-100 nm in thickness. The light source used for the degradation studies was provided by a 400W DYMAX 2000-EC Xenon lamp, Cut-off filters were used when necessary to restrict the wavelength of the incident light. The cut-off filters were placed directly in front of the lamp. The filters were chosen to pass wavelengths above 365, 300 or 254nm. The samples were placed approximately 10 cm away from the lamp

to avoid any heating effects.

UV–VIS spectra were measured with a Shimadzu 3101 UV/VIS/NIR spectrophotometer. The photoluminescence and photodegradation studies on light-emitting polymers were conducted with a conventional photoluminescence measurement system at room temperature. A He-Cd laser operating at a wavelength 325 nm and a power density of 2.0 W/cm2 at the sample surface was used for the excitation of photoluminescence as well as the photo-degradation of the sample. The luminescence signal was dispersed in a 0.75 m monochromator and detected by a GaAs photomultiplier using standard phase-sensitive lock-in amplification.

4.3 Photo-oxidation of poly(p-phenyl-enevinylene)(PPV)

Oxygen has been identified as the key contributor for the degradation of the active material. [61,62] Extensive and systematic investigations of the polymer stability have been carried out by a number of researchers. And photo-oxidation of poly(p-phenyl-enevinylene)(PPV) is considered an important effect upon the performance of EL devices. The mechanism of oxidative photodegradation of soluble derivatives of poly(p-phenylene vinylene)(PPV) has been studied by Scurlock et al.[63] and by Cumpston et al. [64,65] who have shown that oxygen binds to the vinyl bond, leading to chain scission and formation of carbonyl groups. Sutherland et al. [66] have also shown that photooxidation of poly[2-methoxy, 5-(2'-ethylhexyloxy)-1,4-phenylene vinylene](MEH-PPV) occurs in detectable amounts only if both oxygen and light are present. Similarly, the photodegradation of unsubstituted PPV subjected to laser illumination (458nm) in air was studied by Zyung and Kim, [67] who also identified a significant contribution of the environmental oxygen to the formation of carbonyls and thus to the PPV degradation. However the mechanism of the degradation process remains illusive. It is important to understand the mechanism of photo-degradation for further improving the performance of the device, especially prolonging the lifetime of the device.

4.3.1 Effects of Oxygen on poly(p-phenyl-enevinylene)(PPV) degradation

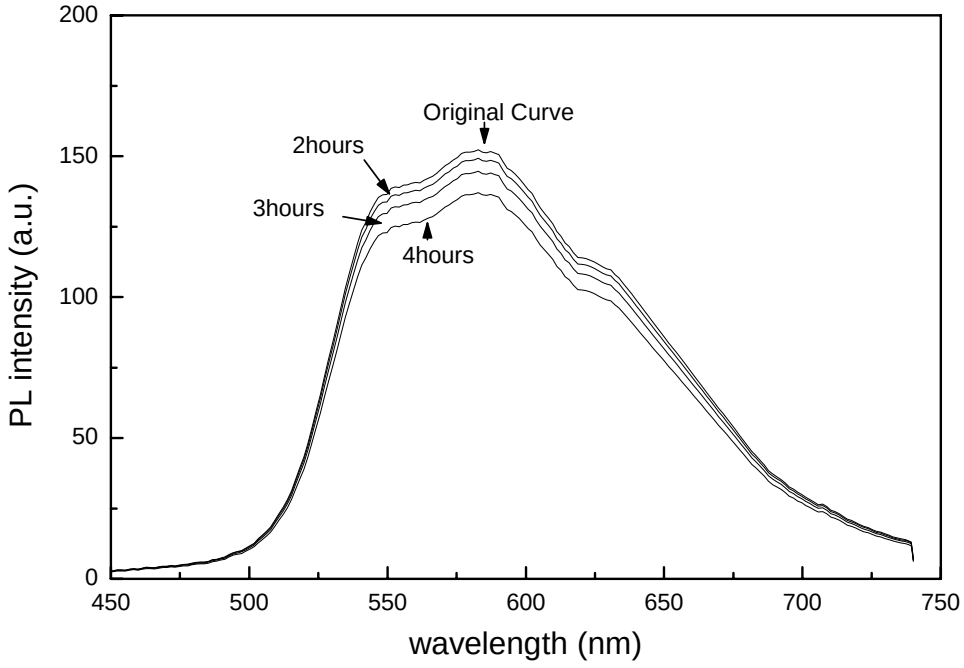

Figure 4.1: The PL spectra of film exposure to normal light with ambient condition.

PPV on quartz substrate samples were stored in glove box for days, weeks and months. Photoluminescence spectrum were taken on these samples, there is no significant intensity drop and wavelength shift, even for the samples stored for months. Samples were also tested under normal lab environment. Photoluminescence spectra show that no significant degradation was discernible. Figure 4.1 shows the photoluminescence spectra of device exposure to normal light with ambient condition. The peak shape and intensity did not change with the storage and exposure conditions.

4.3.2 Effect of UV exposure time under Nitrogen on poly(p-phenyl-enevinylene)(PPV)

degradation

Figure 4.2 shows 300nm 22mW/cm^2 strong UV light exposed to the sample surface in nitrogen environment. It is seen that the Photoluminescence intensity decrease very fast at the initial stage of the laser illumination, then the decrease becomes slower and finally it appears that there is no significant change above 2 minutes of exposure.

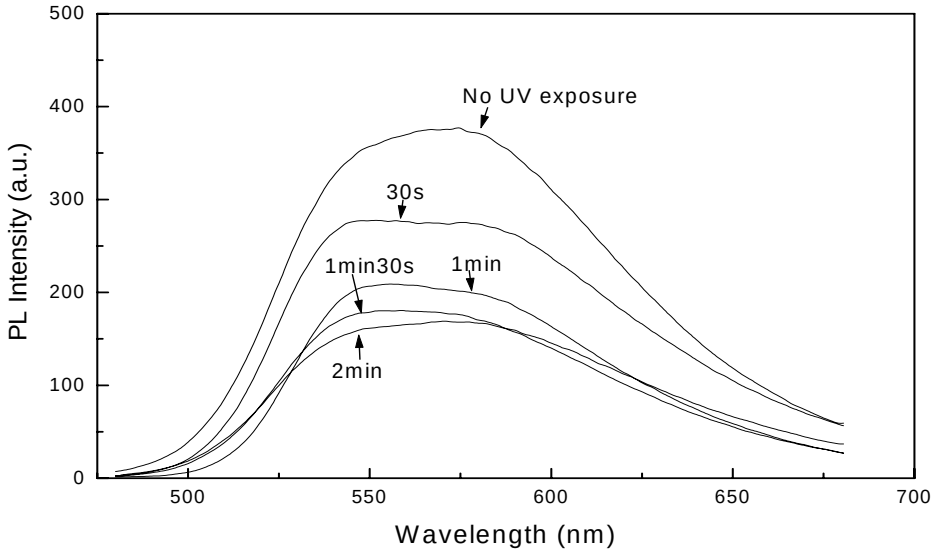

Figure 4.2: PL spectra of film exposure to 300nm 22mW UV light in nitrogen condition.

4.3.3 UV and oxygen on poly(p-phenyl-enevinylene)(PPV) degradation

In order to investigate the effect of photo-oxidation of poly[phenylene vinylene](PPV) when both oxygen and UV light are present, series of experiments with different UV power were carried out.

I. UV light of 300nm 22 mW/cm^2

Figure 4.3 shows the UV–VIS spectra of samples with different exposure time to the UV source at ambient atmosphere. The main absorption peak of the PPV film spin coated from a toluene solution occurs at about 460 nm. This absorption curve has been attributed to the electronic transition. The main absorption peak blue shifted with increasing exposure to the light source. In this case, the absorption peak shifts from 460 to about 410 nm after 2 min of exposure. Considerable loss in the intensity of the main absorption peak and the broadening of the absorption peak was also observed. These phenomena suggest the loss in effective conjugation length or scission of the polymer chain[63-65].

Figure 4.4 is the photoluminescence spectrum of the corresponding samples. The

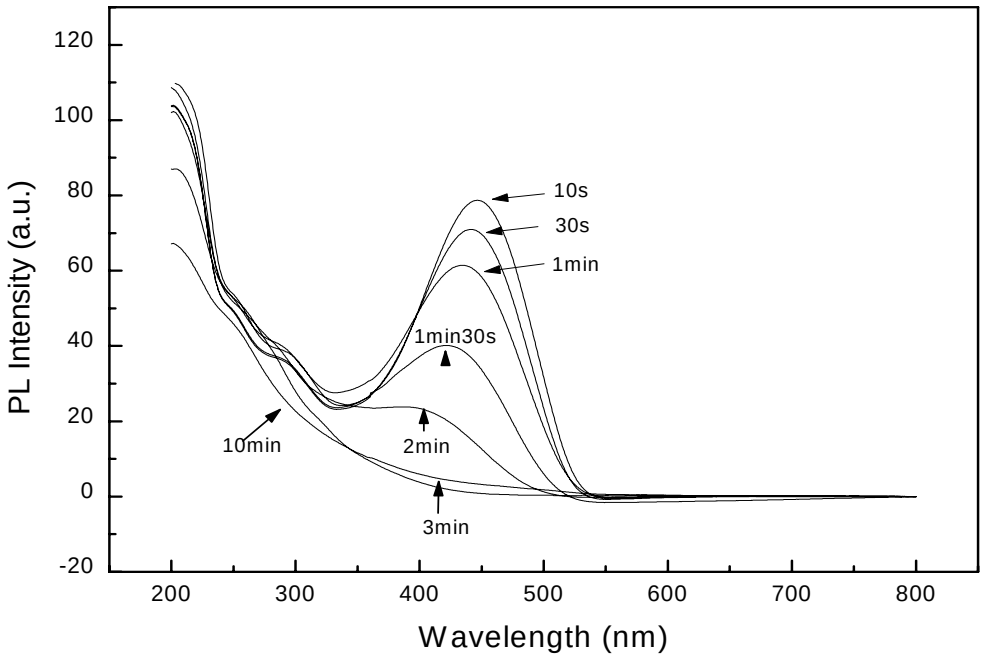

Figure 4.3: UV–VIS spectra of PPV film exposure to 300nm 22mW UV light in ambient condition.

photoluminescence decreased significantly. The photoluminescence spectra of the film disappeared almost completely after several minutes of illumination. At the end of the exposure, the color of the film has almost completely disappeared, indicating that UV illumination under atmospheric conditions had resulted in the disruption of the electron system and a significant

loss in the effective conjugation length of the polymer

This degradation process results in interruption of the conjugation of the polymer by breaking of the vinyl-bond and generated the carbonyl groups [63]. In order to explain this phenomenon, we assume that the carbonyl groups formed by photo-oxidation, act as quenching sites. With increase in exposure time indicates that the conjugation is reduced. As a result of the decreasing conjugation length, the polymer will bleach.

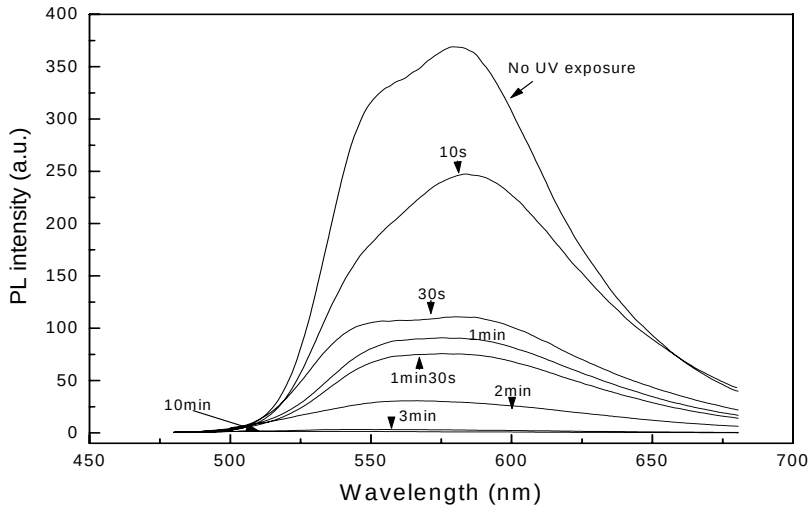

Figure 4.4: PL spectra of film exposure to 300nm 22mW UV light in ambient condition.

II.UV light of 300nm 9mW/cm^2

Figure 4.5 is the photoluminescence spectra of a series samples exposed to lower power of the UV source. When the photoluminescence reach saturated state, we switched off the UV source and put the sample in ultra high vacuum (UHV) chamber for overnight. Figure 4.6 is the photoluminescence spectra taken immediately after the sample was taken out from the UHV. Figure 4.6 indicates that part of photoluminescence intensity recovered. It has been well recognized that the optical

and electronic properties of a light-emitting polymer depend not only on its chemical structure but also on the physical states of polymer chain and intermolecular interaction.

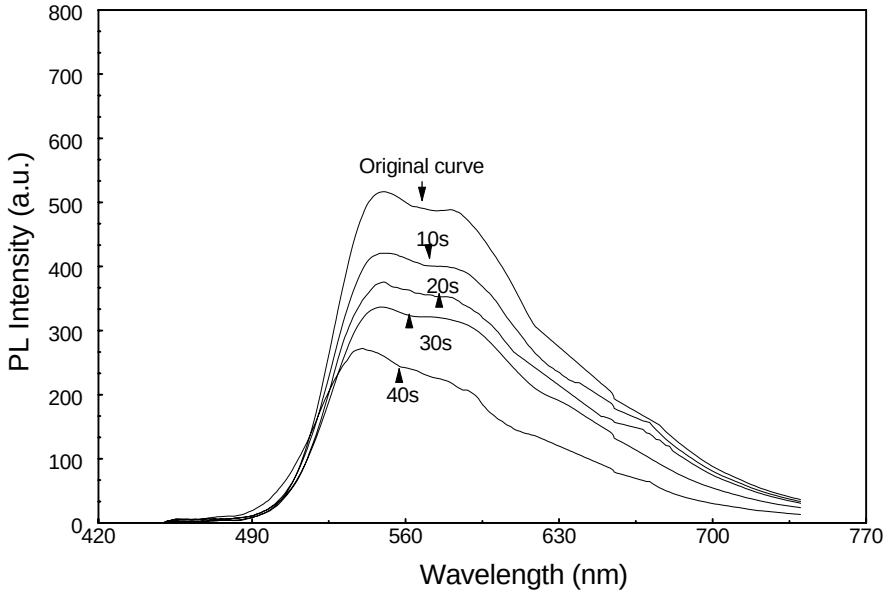

Figure 4.5: PL spectra of film exposure to 300nm 9mW UV light in ambient condition.

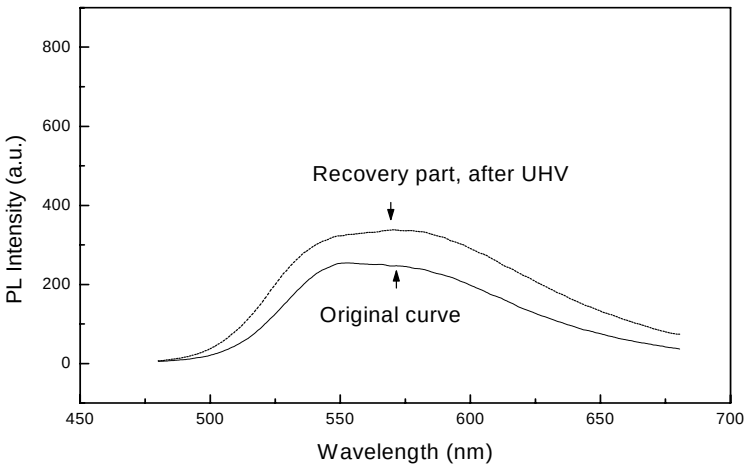

Figure 4.6: The recovery PL spectra of film taken out from UHV.

The reason for PL recovery is not fully understand but reported by other work also. [68]. I think it related to the special structure. There should not be chemical changes in the molecular structure or the PL intensity can not increase to nearly the initial value after PL degradation. We consider that the recovery of PL intensity associated with some conformational changes of the polymer chains, where the conjugation may be broken or the chain may be twisted by geometrical distortions upon UV illumination. Further study is needed to explain the PL recovery clearly.

III. UV light of 325nm 5mW/cm^2

We further lowered the UV power source with higher wavelength. Figure 4.7 shows a set of photoluminescence spectra measured at different exposure time. We found that the photoluminescence degradation induced by this irradiation condition can be self-healed. [69] Stopping the illumination on the sample, the photoluminescence recovers slowly on the order of hours. Figure 4.8 shows a set of photoluminescence spectra taken during the recovery. We postulate that this phenomenon is associated with conformation changes in polymer chain or electronic energy transfer in polymer upon exposing to laser beam. [69]

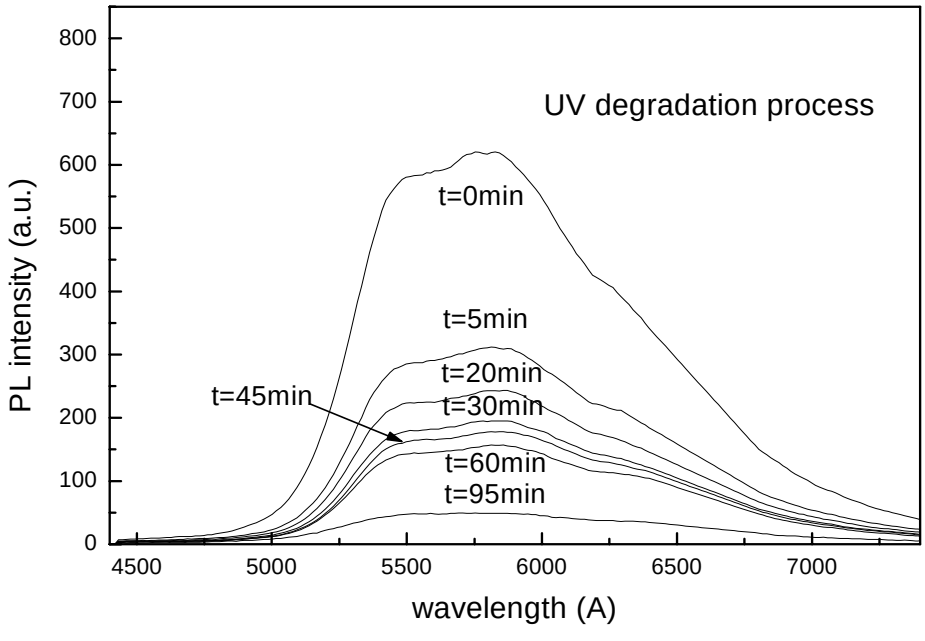

Figure 4.7: PL spectra of film exposure to 325nm 5mW UV light in ambient condition.

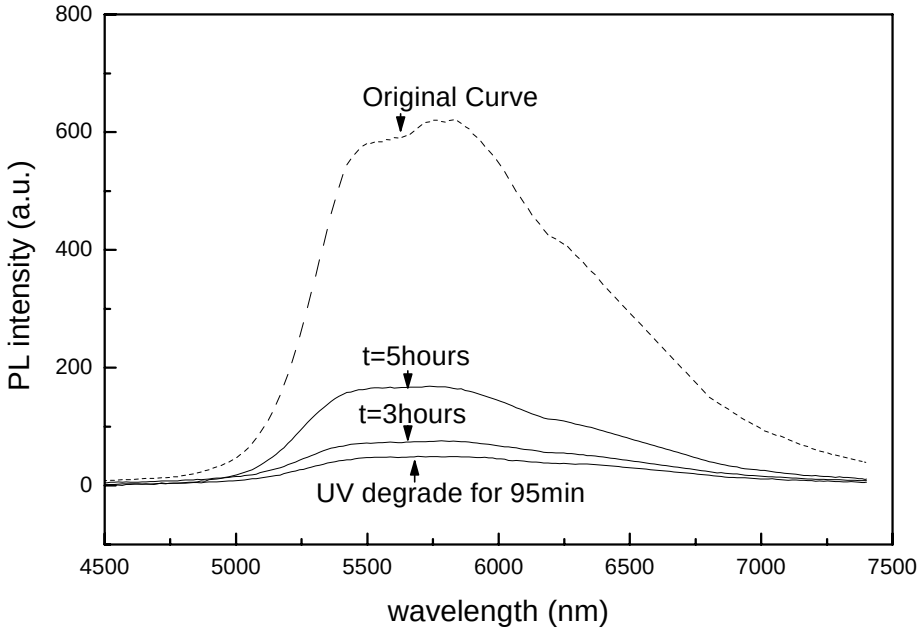

Figure 4.8: The recovery PL spectrum of film in ambient condition after UV exposure.

4.3.4 Conclusion of photo-oxidation effect on PPV

The experiment results presented above clearly indicate that the participation of oxygen in the photo-degradation process is important. When the PPV are irradiated with strong UV radiation, cross linking and/or chain scissions take place. The difference of photo-degradation from that of in inert conditions at room temperature indicates that UV light

alone does not significantly degrade the photoluminescence intensity. Only when both oxygen and light are present, significant photoluminescence intensity drop was detected.

Furthermore, we noticed that normal light and oxygen did degrade photoluminescence significantly, we postulate that only with strong UV energy chain scission occurred, followed by oxygen attack.

As presented above, the decrease in PL intensities is largely attributed to photo-oxidation of polymers. One of the most important species produced in the photo-oxidation process are carbonyl groups. They are normally one of the major constituents of the end products formed, for example, in the termination reactions. They can act as chromophores, and even play a primary role among the chromophores. If they are incorporated in the polymer backbone, they cause main-chain scission. The formation of carbonyl and other detrimental groups can also act as efficient quenching centers for excitons, because the electronegative carbonyl groups are strong electron acceptors, which can lead to the dissociation of excitons. These terminal groups destroy the extended conjugation of the polymer chains, and thereby eliminates the strong π-π* absorption. Thus we may consider that the photo-degradation mechanism of conjugated polymers is a chain scission reaction. Additional chromophores (e.g. carbonyl groups) are created during chain propagation. These chromophores can give rise to the initiation of new chain reactions upon continous irradiation and thus rapid deterioration of the polymer.

4.4 Electrical stress on poly(p-phenyl-enevinylene)(PPV) photo-oxidation degradation

When the device was driven at constant current and emitting at an initial luminance of around 100cd/m^2 in inert condition, the typical lifetime reached several thousand hours. In the initial stage of the lifetime test, there is a decrease in luminance followed by a slow rise to a broad plateau at around several thousand hours, after which it begins an ultimate decline in luminance. In order to investigate the influence of the electrical field on the polymer

degradation, three identical devices were electrically stressed for 50 hours, 100 hours and 200 hours under nitrogen environment. The electroluminescence intensities of the three devices yield little variation in the plateau region of the lifetime curve. One more device was left unstressed for comparison.

All experiments were carried out in glove box with pressure around 0.4mbar, H_2O and O_2 less than 1ppm and normal laboratory light unless otherwise noted. To examine the effect of the electric field on the crystalline structure of the polymer for both cases mentioned above, X-ray diffraction spectra from the samples were measured at room temperature.

4.4.1 Electrical stressed device in nitrogen environment

Figure 4.9 shows the photoluminescence spectrums of the devices which under electrical stress for 50 hours, 100 hours and 200 hours respectively. After the electrical stress, the devices were immediately encapsulated and the photoluminescence spectrums of the devices were recorded. The shapes of photoluminescence peaks remained the same, while the intensities of the peaks varied, with the sample stressed over a longer period of time giving a lower intensity. However the variation is not significant.

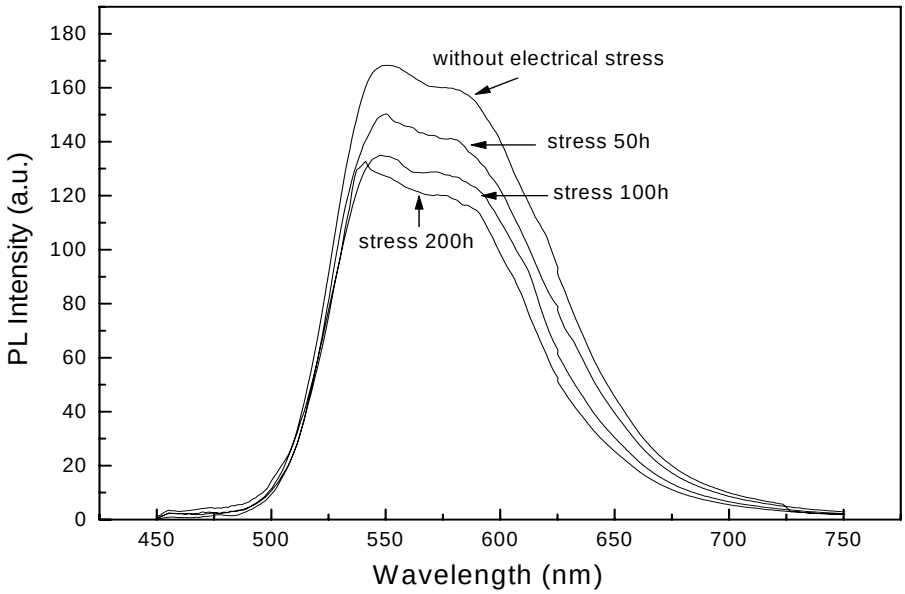

Figure 4.9: The photoluminescence spectrum of the devices in nitrogen environment without exposure to ambient. The stress time periods are 0, 50 hours, 100 hours and 200 hours respectively.

However, for the device without electrical stress, upon exposure to air and light even for several days, the photoluminescence spectrum exhibits the same shape and the intensities. X-ray diffraction spectra were scanned at room temperature for the devices after electrically stress but without exposure to air. There was no noticeable crystallization peaks formed for all these devices. For the device without electrical stress and exposed to ambient, the X-ray diffraction peak appeared much smaller compared with the devices which were previously electrically stressed.

4.4.2 Electrical stressed device with UV and Oxygen

Another series of three devices were also stressed in dry nitrogen ambient for 50 hours, 100 hours and 200 hours, and then exposed to oxygen and the normal laboratory light for the same time period of five hours. Four photoluminescence spectra were also recorded. To examine the effect of the electric field on the crystalline structure of the polymer for both cases mentioned above, X-ray diffraction spectra from the samples were measured at room temperature.

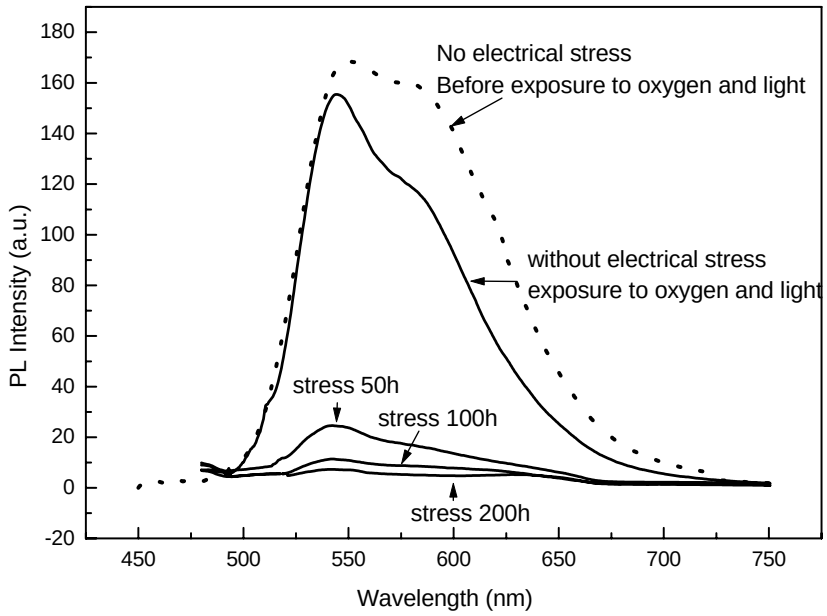

Figure 4.10: The photoluminescence spectrum of the stressed and exposed to ambient. The stress time periods are 0, 50 hours, 100 hours and 200 hours respectively.

Figure 4.10 shows the photoluminescence spectra of this series of three devices, which were stressed in dry nitrogen ambient and then exposed to oxygen and the normal laboratory light for the same time period of five hours immediately after electrical stress. It is noticeable that the photoluminescence intensities for the stressed devices decreased significantly upon exposure to air and light. The longer the devices were electrically stressed, the lower the photoluminescence intensities decreased.

The X-ray diffraction results from devices exposed to air after electrical stress showed the obvious crystallization peaks around 2θ of 8°. [64,65] The longer the stress time, the stronger the crystallization peak appeared. Figure 4.11 shows the X-ray diffraction spectra for the devices after electrical stress and exposure to air and light.

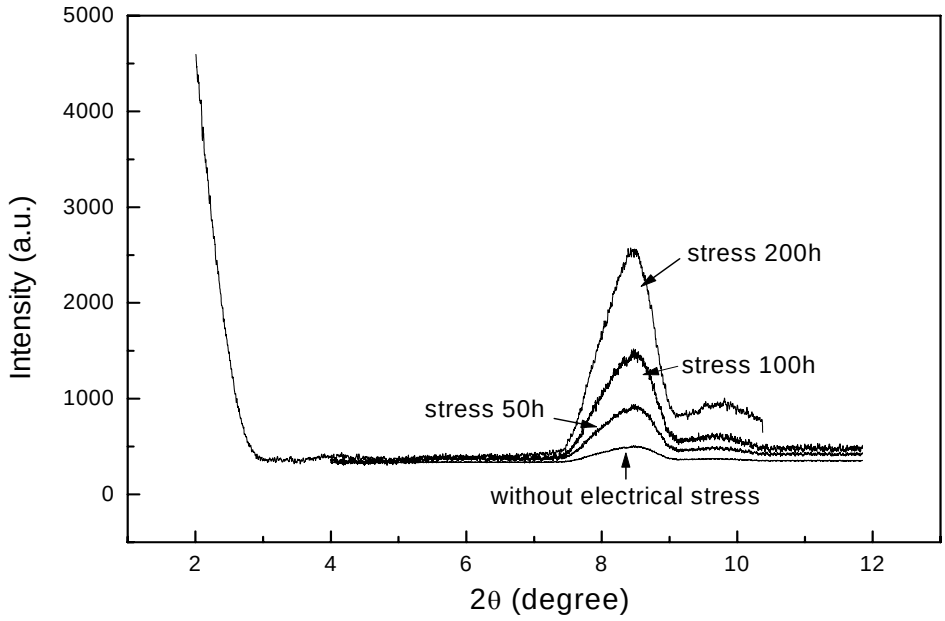

Figure 4.11: XRD spectrum of the devices stressed and exposed to ambient. The stress time periods are 0, 50 hours, 100 hours and 200 hours respectively.

4.4.3 Photo-oxidation of poly(p-phenyl-enevinylene)(PPV) under electrical stress

Figure 4.9 demonstrates that under electrical stress, but without exposure to air, the electrical stress has little effect on polymer photoluminescence spectra and the intensities were not significantly affected. From this it is inferred that the electrical field alone does not bring about the photoluminescence intensity degradation. The lifetime test results also demonstrated that with continuous operation in inert conditions up to several thousands hours, the voltage, current

and light output could be maintained very stable. These results indicate that photoluminescence spectra remain stable when the polymer is electrically stressed in inert conditions. Figure 4.10 shows that for a device exposed to light and air, but without being previously electrical stressed, the photoluminescence spectrum changes little and the decrease of the photoluminescence intensity is not significant. This result indicates that such a device did not suffer from much photo-oxidation. Extensive and systematic investigations of the polymer photo-oxidation degradation process have drawn the conclusion that oxygen binds to the vinyl bond, leading to the chain scission and the formation of carbonyl groups[63, 66-67]. The effect only acts when both oxygen and light are present. However, from Figure 4.10 it is clear that electrical stress followed by exposure to light and oxygen, photoluminescence spectra intensities of these devices decrease significantly, and the longer the stress time, the larger the decrease in the photoluminescence intensities. In order to clarify the effect of light, oxygen and electrical stress, a series of devices were electrically stressed and exposed to different conditions. The maximum photoluminescence values versus stress time are shown in Figure 4.12. The data presented in Figure 4.12 clearly show that either electrical stress or photo-oxidization alone slightly induced photoluminescence decrease. However, electrical stress followed by exposure to light and air, the decrease of the photoluminescence intensities became significant. The longer the stress duration, the more the intensity decreases.

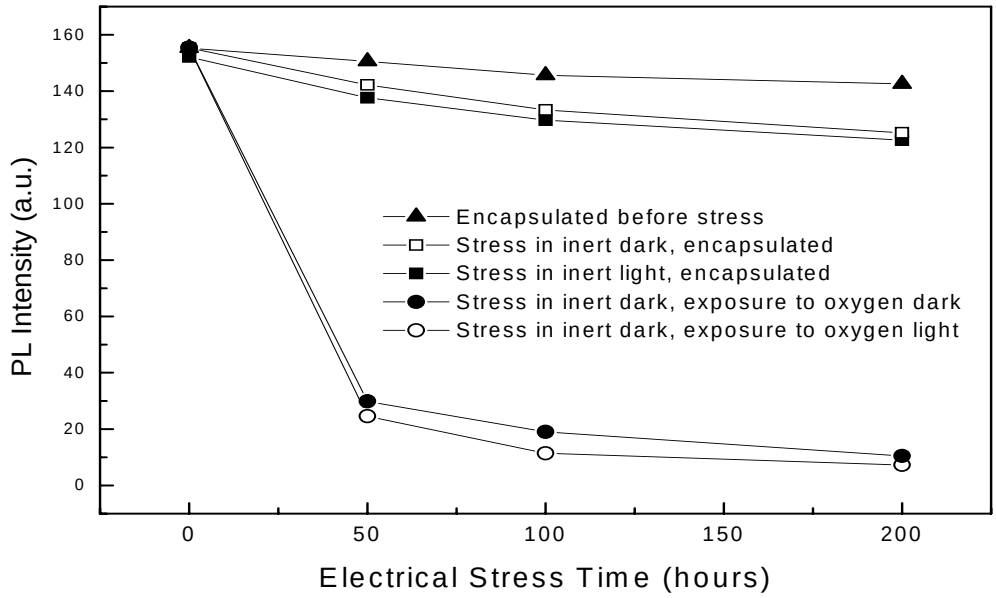

Figure 4.12: The maximum photoluminescence values versus electrical stress time. (▲Encapsulated before stress, □ Stress in inert dark, encapsulated, ■ Stress in inert light, encapsulated, ● Stress in inert dark, exposure to oxygen dark, ○ Stress in inert dark, exposure to oxygen light.)

It can be concluded from the above discussions that either electrical stress or photo-oxidization alone can't degrade the photoluminescence intensity significantly. However, when electrical stressed devices were exposed to ambient condition, the photoluminescence intensities decrease rapidly. The extent of the photoluminescence intensity decrease is related to the electrical stress duration.

The effects of the electrical stress and ambient conditions on polymer structure change can be monitored by the X-ray diffraction spectrum. After electrical stress, the devices were encapsulated and exposed to normal laboratory light. The X-ray diffraction spectra of the devices were recorded and the results show that all the devices do not show obvious

crystallisation. For the case of the stressed devices and with exposure to oxygen and light, the X-ray diffraction results show obvious crystallisation peaks. It is well known that for the conducting polymer using in the light emitting devices, the conductivity of the polymer decreases greatly and the device performance deteriorates rapidly with the increase in crystallisation. The X-ray diffraction results for the two cases, electrically stressed and encapsulated and electrically stressed followed by exposure to ambient, are consistent with the photoluminescence results. Either electrical stress or photo-oxidation alone did not cause the polymer crystallisation. When both electrical stress and exposure to oxygen and light take place, crystallisation is formed. This strongly suggests that the polymer structure change result in the rapid decrease in photoluminescence intensity and deterioration of device performance. The result from this work shows that the photoluminescence decrease is related to the increase in crystallization of the polymer materials. The longer the stress duration, the greater is the decrease in the photoluminescence intensities and the larger the crystallization peaks increase upon exposure to air and light.

4.5 Summary

The experimental results indicate that the decrease in photoluminescence is the effect of both the electrical stress and photo-oxidation. Either of the two factors can't cause the degradation significantly. The X-ray diffraction results indicate that the photoluminescence degradation is accompanied by the increase in the polymer crystallisation peaks. It implies that the photoluminescence intensity decrease is the result of the polymer structure change. In other words, the polymer structure changes bring about photoluminescence intensities decrease and device performance deterioration.

The devices were stressed in inert condition for the different time duration, while the electroluminescence intensities for all the devices remained no significant decrease.

Electrical stressed samples were under different environment exposure conditions and photoluminescence spectra were taken. Experiment results showed that either the electrical field or the photo-oxidation could not significantly cause the decrease of polymer photoluminescence spectra and the increase of X-ray crystallization peak. However, with the increase of the electrical stress duration, a much larger extent of the changes to the polymer intrinsic structure and the decrease of photoluminescence intensity upon the exposure to ambient conditions later. We interpret that the decrease of the photoluminescence intensities and the changes of polymer structure were due to the electrical stress as a precursor, followed by photo-oxidation degradation process.

CHAPTER 5 NON-EMISSIVE AREA FORMATION AND DEVICE FAILURE MECHANISM

5.1 Introduction

The non-emissive areas result in a decrease in device luminescence and reliability. There are many factors responsible for the reliability of the device as mentioned in chapter 1, such as the properties of the materials, process technology, and interfaces of the layers and environmental conditions etc. In this chapter, secondary ion mass spectroscopy, optical microscopy, scanning electron microscopy with electron diffraction x-ray and atomic force microscopy are used to examine the dark, non-emissive defects on the organic light-emitting device. [74,75] Both device fabrication and polymer blending are done in class 100 clean room environment in order to minimize the environment induced defects. The dark spot formations are systematically analysed and device degradation mechanisms are proposed.

5.2 Non-emissive area identification

Figures 5.1a&b show optical images under external illumination as viewed from the substrate side during the degradation process for two drive conditions (a: 6V, 2.32mA; b: 10V, 5.89mA). Device is driving at 6 V in the beginning. While when we suddenly increase the driving voltage to 10 V, clear two rings of shadow area can be seen as shown in Figure 5.1b. Under the higher drive conditions the low contrast rings seen in Figure 5.1a gives a discernable structure. A dark shadow forms around a non emissive site, in all cases the shadow is surrounded by hallow of intermediate brightness. The dark shadow area centre was burnt to irregular dark shape. Some dark shadow area's centre nucleation can not be clearly discerned in the beginning, after some period of time, dark centre part appears.

The driving voltage and device current with the ageing time elapse are also recorded and it shows fluctuation from stable operation to failed state. At all the constant voltage, current vibrations are observed, however, at higher voltage, the vibration is more obvious. In the beginning, dark shadow area shows two rings when we suddenly increase the voltage. And at certain constant V, the whole device luminance became dim with the driving time elapses accompanied by current drop. When the device luminescence became dim, we again increase the driving voltage; clear ring of light is detected. The first ring join together, the second ring is continuously growth, and the initiated centre of the dark shadow area became carbonated. The appearance of the fluctuations was coincidental with the start of the bubbles and carbonated area formation, growth and merge. This is also corresponding to the lifetime final stage, the variance in the voltage at constant current, which exactly correlates with light fluctuations, is obvious before the device fails.

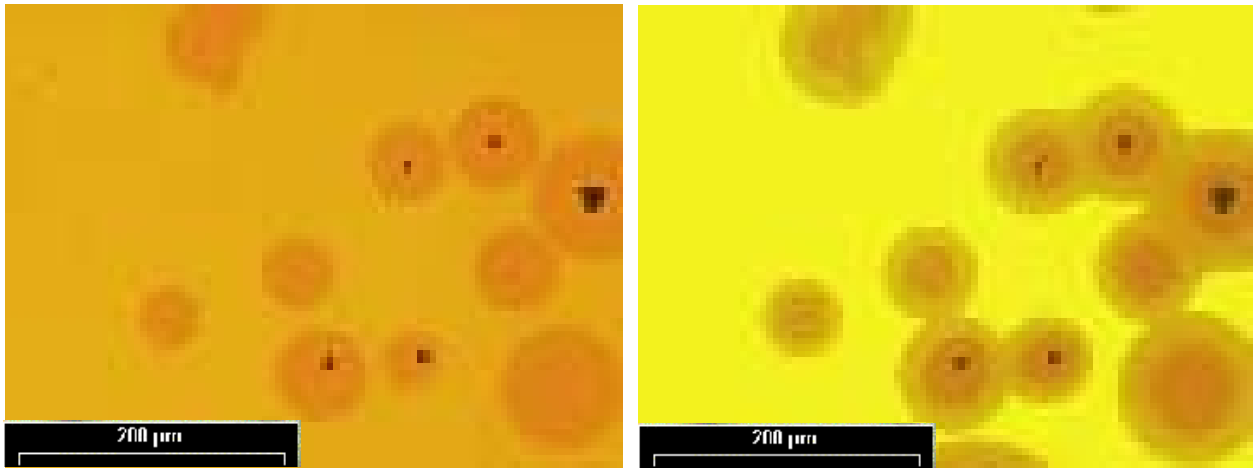

a b

Figure 5.1: Dark spot observed under the microscope (a): driving voltage: 6V, current: 2.32mA, duration of electrical stress is 20min; (b): driving voltage: 10V, current: 5.89mA, duration of electrical stress is 20m15s. Device structure:ITO/PEDOT/PPV/Ca/Ag.

5.3 Dark non-emissive area formation

In order to investigate the non-emissive area formation mechanism, Secondary Ion Mass Spectrometer (SIMS) depth profiling was used taken for Ag, Ca, C, In and O in the bright area and dark spot area in electrical stressed device(s). The Ag and Ca infer the cathode behaviour, while the C signal is from the electroluminescence layer and the In and O from ITO anode layer. The device(s) was prepared as follows. Device was taken out from the evaporator after cathode deposition and electrically stressed with constant voltage of 7 volt. The position of the dark spots formed in the active area was monitored and marked using an optical microscope (Olympus BX-30) with attached CCD camera. The sample was then loaded into SIMS vacuum chamber for analysis. The total time for device exposure to atmosphere was about half an hour. SIMS analysis was also performed on a device prepared together on the same ITO glass substrate, but without subjecting to the electrical stress test. Three cases, non-stressed device, bright and dark region in stressed device, were studied.

5.3.1 SIMS results for non-stressed device

Figure 5.2 demonstrates various elements C, In, Ag, Ca, O profiles for non-stressed device. The device structure is: ITO/PEDOT/PPV/Ca/Ag and the PPV is about 90nm. First in the case of non-stressed device, a severe Calcium tail has already been observed entering into the EL

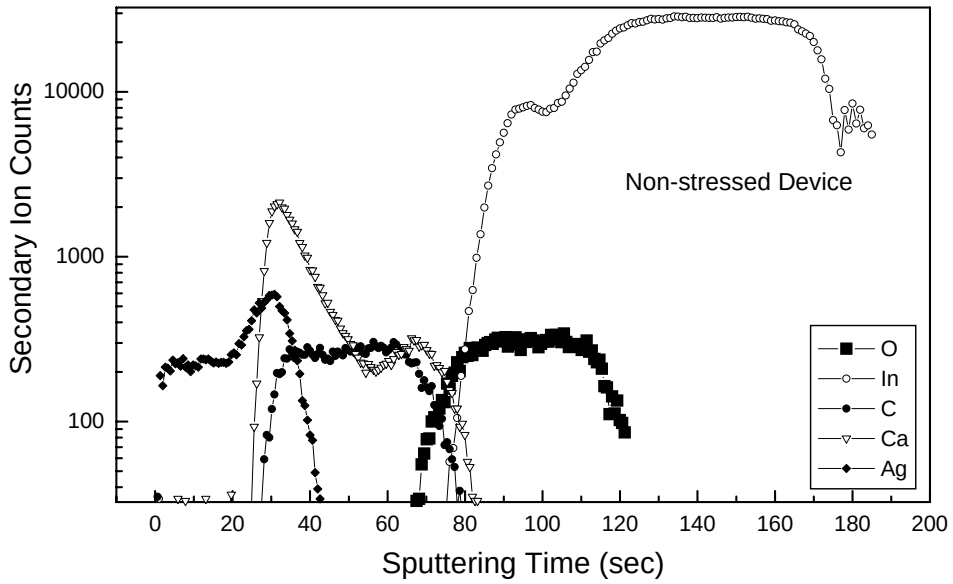

Figure 5.2: SIMS profiles for non-stressed organic light emitting device.

layer. This should attributes to the polymer inhomogeneity, such as pinholes, sharp edges, voids and pits. The solvent preparation and spin coating conditions are also shown to influence the properties of PPV polymer. There is significant roughness of interface during the cathode evaporation. SIMS measurement is an average effect, though Ca and In signals have a small overlapping; it has no substantial effects on device degradation.

5.3.2 SIMS results for emissive area in stressed device

Figure 5.3 demonstrates various elements C, In, Ag, Ca, O profiles for stressed device in emissive area. Substantive indium peak width changed compared the two cases: unstressed device and bright area in stressed device, the decrease of the width is observed in the latter case.

We interpret this phenomena is due to ITO surface roughness in the first place. Although In atom has the tendency to move towards the power negative pole direction under electrical stress, but the ITO and glass interface is remain unmoved, so the whole effect is the ITO layer became thinner and more smooth compared with the initial status.

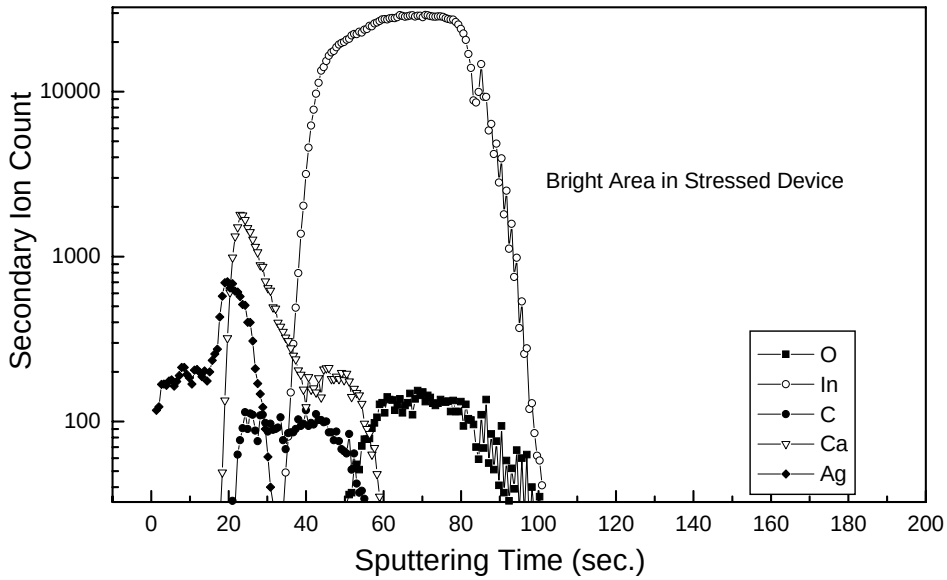

Figure 5.3: SIMS profiles for stressed organic light emitting device on emissive area.

5.3.3 SIMS results for non-emissive area in stressed device

Figure 5.4 demonstrates various elements C, In, Ag, Ca, O profiles for stressed device in non-emissive area. From Figure 5.4 we can see that the sputtering time of the whole device became shorter for dark shadow area than that of the normal bright area under the same conditions. This implies that the whole device shrunk in the failed dark shadow area and the stressed device caved in towards glass side. The In and Ca profiles have larger overlapping area in the dark shadow area. In certain localised area, Ca protrusion and In edge close faster. In the microscopic protrusion point, a very large electric field intensity and current density is created. The enhanced local luminescence and local heating around it lead to instability and further growth of local current densities until it reaches the catastrophe. Short circuit formed following by local heating and conduction path breaking. A surrounding circular region will be appearing as a growing dark spot on the cathode. It shows that Ag and Ca peaks have a

significant shift closing to the surface under electrical field. This is due to the cathode layers are fabricated using resistive heating induced thermal evaporation technique. The pinholes and other defects are almost impossible to be controlled by this evaporation technique. Under the electrical field, metal atoms move along the electrical field direction and tend to pack the pinholes and voids.

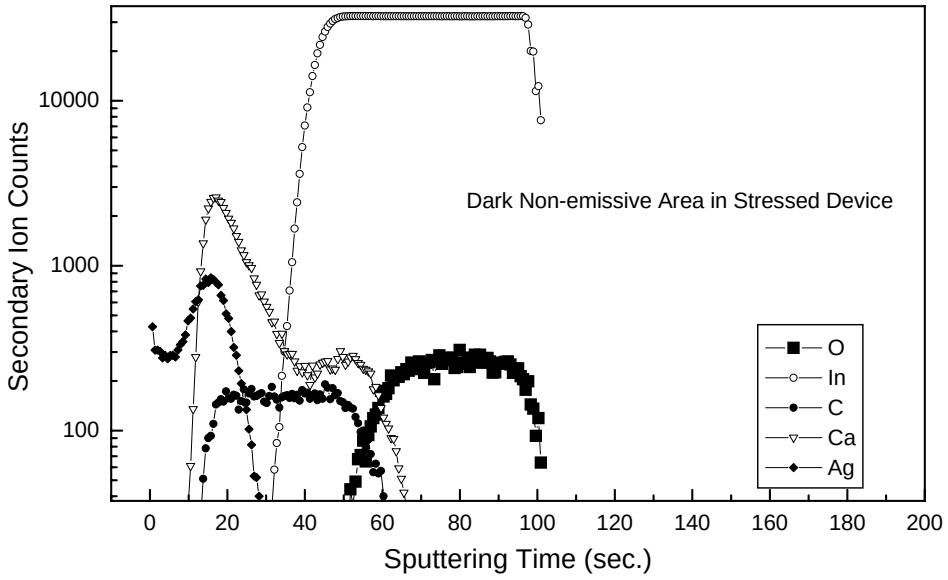

Figure 5.4: SIMS profiles for stressed organic light emitting device on non-emissive area.

Figure 5.4 demonstrates that Ca peak has a significant shift closing to the surface under electrical field. This is due to the cathode layers are fabricated using resistive heating induced thermal evaporation technique. The pinholes and other defects are almost impossible to be controlled by this evaporation technique. Under the electrical field, metal atoms move along the electrical field direction and tend to pack the pinholes and voids. At the same time, depleted the metal at the Ca and polymer interface. The cathode region near the surface became solid and sturdy during stress. The elastic property of PPV polymer became even movable under electrical heat, which result in interface fluctuation and roughness. There are

overlapping in all three cases; however it doesn't mean that all three cases have cathode and anode metal connection. First in the case of non-stressed device, a severe Calcium tail has already been observed entering into the EL layer. This should attributes to the polymer inhomogeneity, such as pinholes, sharp edges, voids and pits. The solvent preparation and spin coating conditions are also shown to influence the properties of PPV polymer. There is significant roughness of interface during the cathode evaporation reported by J. R. Rasmusson etc.[75] SIMS measurement is an average effect, though Ca and In signals have a small overlapping, it has no substantial effects on device degradation.

Figure 5.5 shows the photoluminescence spectrum on non-emissive area, weakly emissive area and non-stressed area. It clearly demonstrated that within the shadow area, the polymer materials show degradation. Therefore we could deduce from the above discussion that the dark shadow is the current density different area. And the growth of the dark shadow is due to polymer layer electrochemical or photochemical decomposition under electrical stress. The "thinner" polymer layer will come out lower current density, which shows the dark shadow area in the active area.

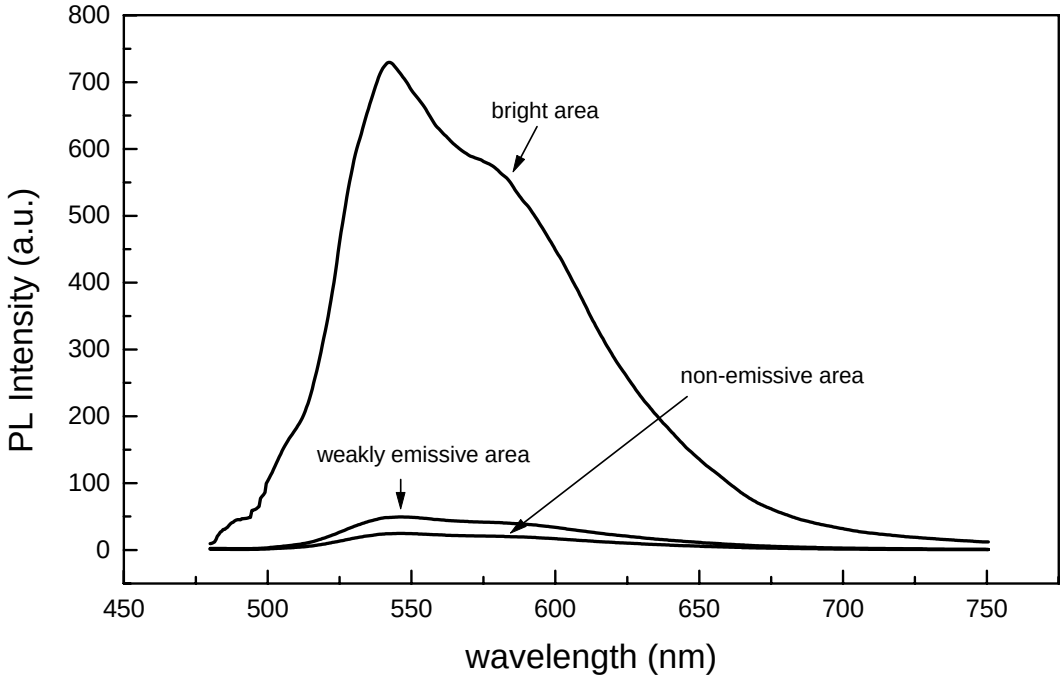

Figure 5.5: Photoluminescence spectrum on non-emissive area, weak emissive area and bright area on OLED device.

5.3.4 Conclusion from the SIMS experiment results

The SIMS observations made in this work reveals the distinct mechanism of the device failure in Organic Light emitting devices is due to cathode imperfection and interfaces roughness. We drew the Ca, Ag profiles for non-stressed device, emissive area and non-emissive area in stressed device, which shown in Figure 5.6 and Figure 5.7. The Ag and Ca peaks move towards surface direction when electrical stress is implemented. It implies that the metal movement will pack the pinholes and voids, which originated from the fabrication technique and also deplete the metal near the interface between cathode and EL polymer. The cathode imperfection causes the relative movements of the boundaries. The interface roughness due to the polymer inherent property resulted in the difference of the relative position variation in

different layers. This is clearly demonstrated when we drew In and Ca profiles together shown in Figure 5.8, in which Ca and In has a much bigger overlapping in dark non-emissive area. This will lead to local variations in the distance between the two electrodes. In certain localised area, Ca protrusion and In edge close faster. In the microscopic protrusion point, a very large electric field intensity and current density is created. The enhanced local luminescence and local heating around it lead to instability and further growth of local current densities until it reaches the catastrophe. Short circuit formed following by local heating and conduction path breaking. A surrounding circular region will be appearing as a growing dark spot on the cathode. Dark spot formed initially from here.

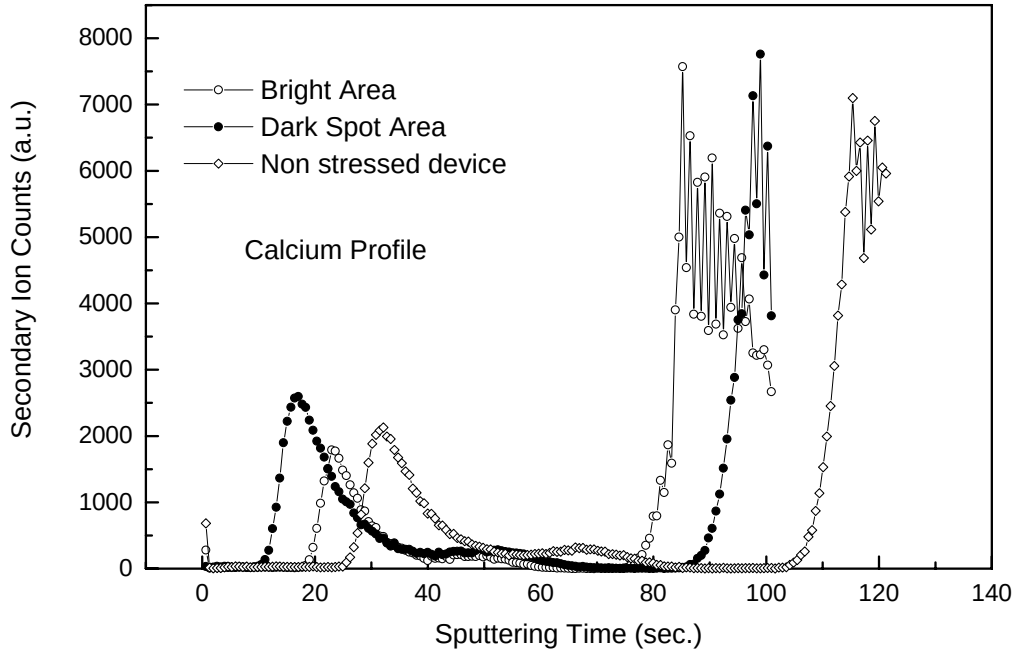

Figure 5.6: SIMS profiles for Calcium (Ca).

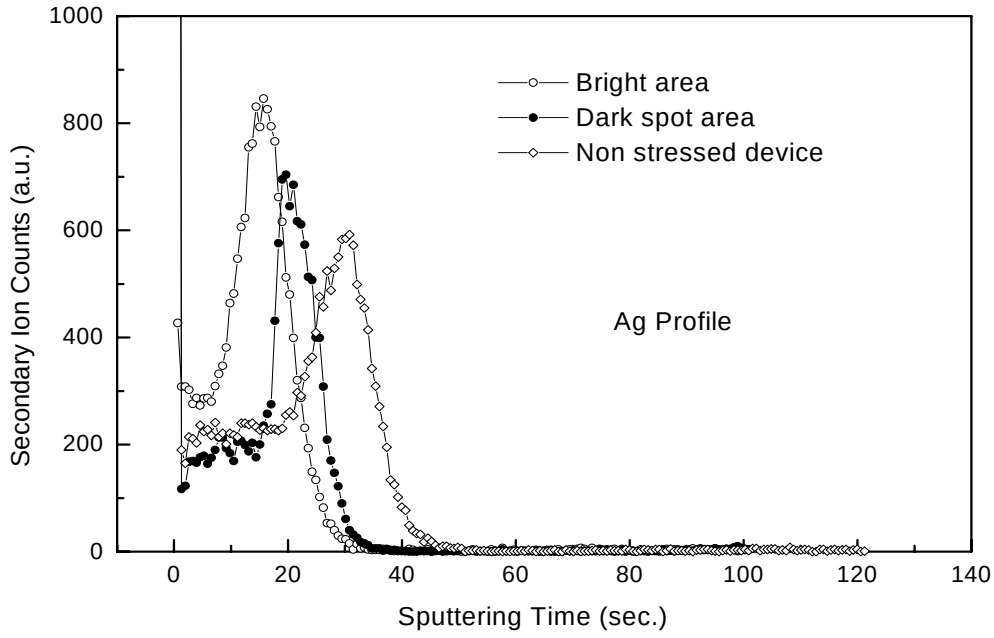

Figure 5.7: SIMS profiles for Ag (Silver)

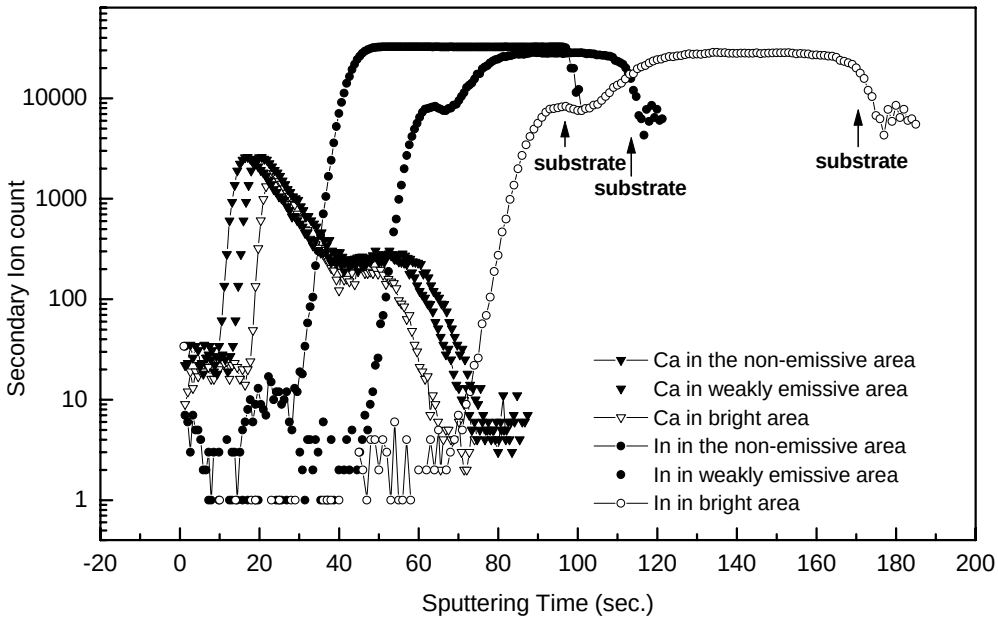

Figure 5.8: SIMS profiles for Calcium and Indium.

Figure 5.8 shows the results of Ca and In distributions. Obvious boundary movements for both bright area and defect area in stressed device were observed. However the distribution varied for both bright and dark area. The Ca profile expanded much larger in dark spot area, but narrow in bright area, strongly implies that when active area converted from emissive to non-emissive state, Ca and PPV polymer mixed up and interface became rougher. Ca and In overlapping became even serious. This will lead to local variations in the distance between the two electrodes, leading to differences in the electric field intensity and the local current densities.

Figure 5.9 shows the results of O and C distributions. Both O and C profile have relatively moved in dark area compared with bright area. Much bigger C expansion was detected in the dark spot area. Surprisingly cathode region and near surface region, the intensity variation of O signals was almost unnoticeable in all three cases. One of the most popular conjectures on dark spot formation in OLEDs is due to the moisture and oxygen penetrated into cathode and PPV interface, which oxidized the active metals. However from Figure 5.9, it explicitly shows that O signals near cathode area and interface between polymer and cathode have unnoticeable variations in all three cases. Figure 5.9 also unveil that C profile, corresponding to the polymer layer behavior, changes in dark spot area, are consistent with Ca profile variations in the dark region. Both demonstrate larger peak expansion in dark spot area than in emissive region. This also proved that the PPV and interfaces became rougher when device transited from emissive to non-emissive state.

SIMS results in Figure 5.10 clearly show that Ca and C moved synchronously in both dark and bright area in stressed device. And their front edge remained the same shape always,

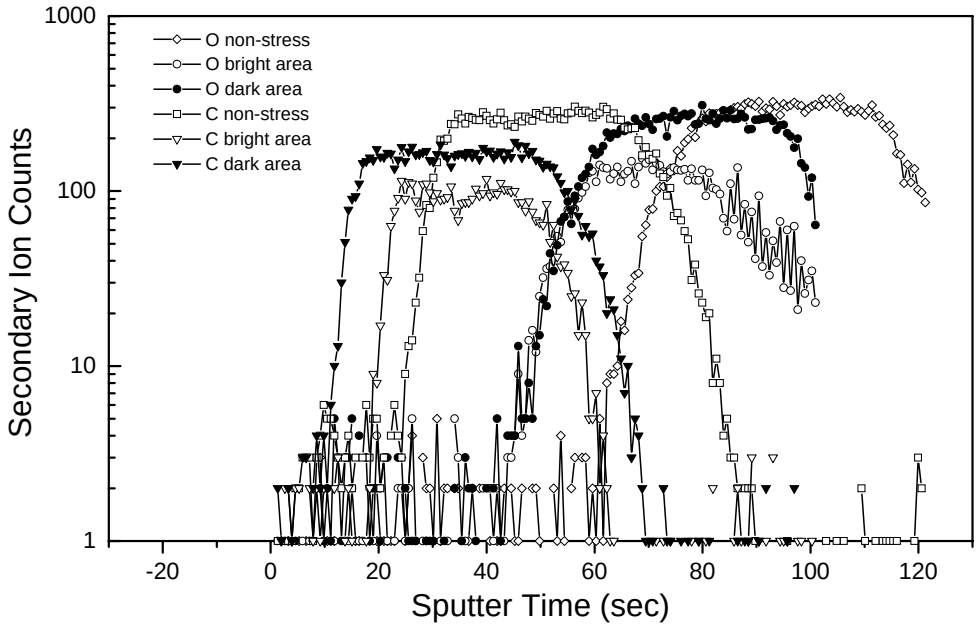

Figure 5.9: SIMS profiles for Carbon and Oxygen.

which strongly infers that no Ca and polymer separation during the device degradation process. Delamination of cathode and PPV polymer didn't show any trace in our SIMS results. We attribute this to the elastic properties of polymer. The electrical heating also enhances the flexibility and movability of the polymer, which ensures that polymer and cathode layers always stick together.

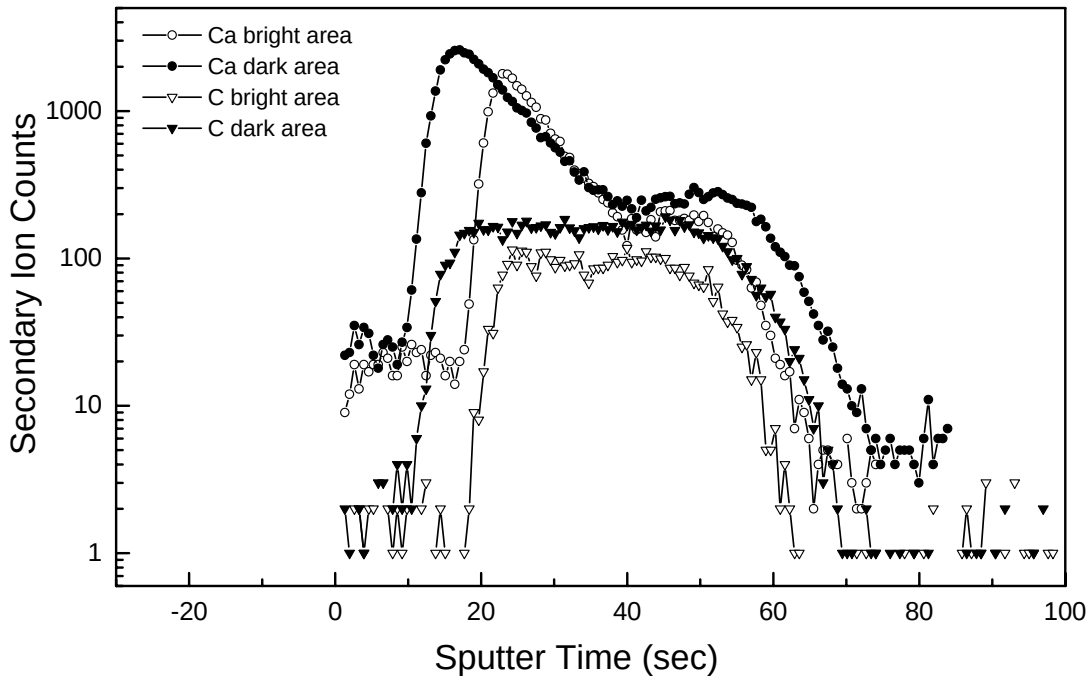

Figure 5.10: SIMS profiles for Carbon and Calcium.

5.4 Non-emissive area formation mechanism

From the discussion above we put forward that the device failure process is due to cathode pinholes and defects, all the boundaries relatively shift under electrical field. The material quality causes boundary movements are not in a good agreement. Interfaces became rough

and fluctuate. In some localised area Ca and In close faster, the mechanism by which this might occur is shown schematically in Figure 5.11.

The experimental observations of the high-localised current density initiating the dark spot point done by Vadim. N. etc.[77] also give our proposed failure mechanism a proof. Some other researchers using luminance scope observed that the precursor of the non-emissive, dark spot shadow is the sudden glare luminescence followed by abrupt annihilation, which is another evidence.

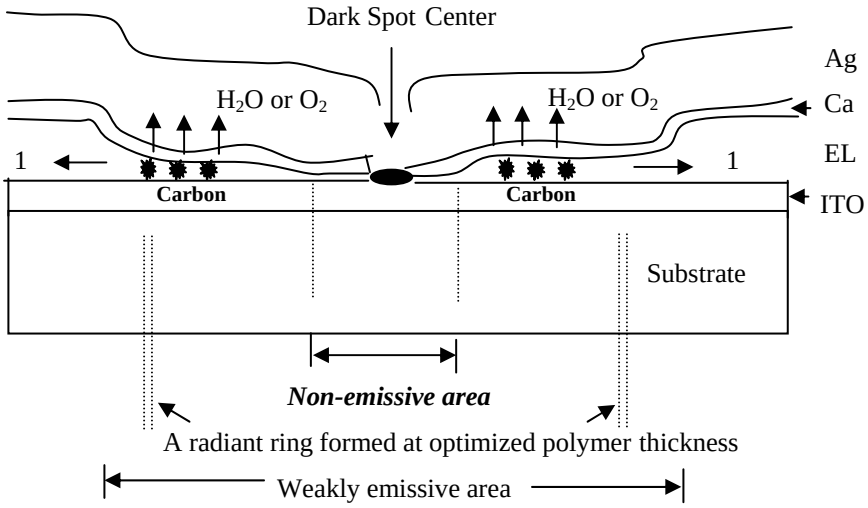

(a)

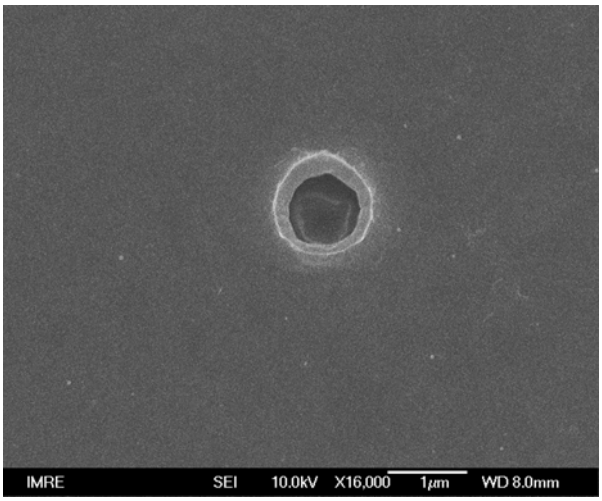

(b)

Figure 5.11: (a) Schematic diagram showing dark spot formation. (b) SEM picture of the dark spot.

Figure 5.11 is the schematic illustration of the device degradation mechanism. The interface roughness due to the polymer inherent property result in the difference of the relative position variation in different layers. In certain localised area, Ca protrusion and In edge close faster. A very large electric field intensity and current density is created. The enhanced local luminescence and local heating around it lead to instability and further growth of local current densities until it reaches the catastrophe. Short circuit formed following by local heating and conduction path breaking. Dark spot formed initially from here as shown in Figure 5.11. Following that due to polymer layer movability and local heating, the surrounding polymer will be pushed away as shown in Figure 5.11, arrow 1. At the same time the electrochemical, photochemical reaction and decomposition happened in the polymer layer under electrical stress. The disintegrated gas, like CO_2 and H_2O, could diffuse through Ca and Ag voids or evolve. If during the electrical stress, suddenly we higher up the driving current or voltage, part of the polymer materials didn't move faster enough to keep the pace, some lump will be left and accumulated to form the bubble structure. The residue gas remained in polymer during synthesis or trapped during polymer spinning, together with the gas raised from polymer decomposition, may also evolve into big gas bubbles during device stressing. With stress time elapse, the centre part of the polymer near the dark spot centre will become "thin" enough to become dark, truly non-emissive area. And the transit region with degraded polymer and normal polymer will become the second ring of the dark shadow area as shown in Figure 5.1. Some times the transit area with a certain optimised polymer layer thickness, there will showing a luminescent ring, which show brighter luminescence than other area in the dark shadow area, but definitely not as bright as outside normal luminance area.

5.5 Bubble phenomena identification

Figure 5.12 shows optical images of the nonemissive spots and bubble structures formed in OLEDs under external illumination as viewed from the side of ITO and glass substrate during the degradation process. Figure 5.12a shows a lighten-up device, 8V at 4.78 mA, within the

dark spot shadow and somewhere near the dark spot centre, there are three dark bubbles formed. However during the electrical stress, the bubbles grew to certain size and not continuously grew further. With time elapse, some foamy carbonised powder formed in the bubbles and the carbonised area accumulated. Figure 5.12b and 5.12c are images taken when the dark spot and bubbles grew to certain size and the device was powered off. For both of the cases, power off and power on the bubble remain there and the bubble continuously growth a lot with electrical stress resumed. Figure 5.13 shows images of the bubbles formed on the edge of the active area in OLEDs under external illumination. Figure 5.13a: ITO and Ca edge, formerly is the active area, during the stress, active area shrinks, and the outer side, the bubbles are averagely smaller and the inner side, where electrical stress sustained longer, the bubbles are larger. Lower part is the schematic diagram of the picture part. Figure 5.13b is the ITO and Ca edge where the device is no undergone electrical stress. Lower part is also the schematic structure of the image.

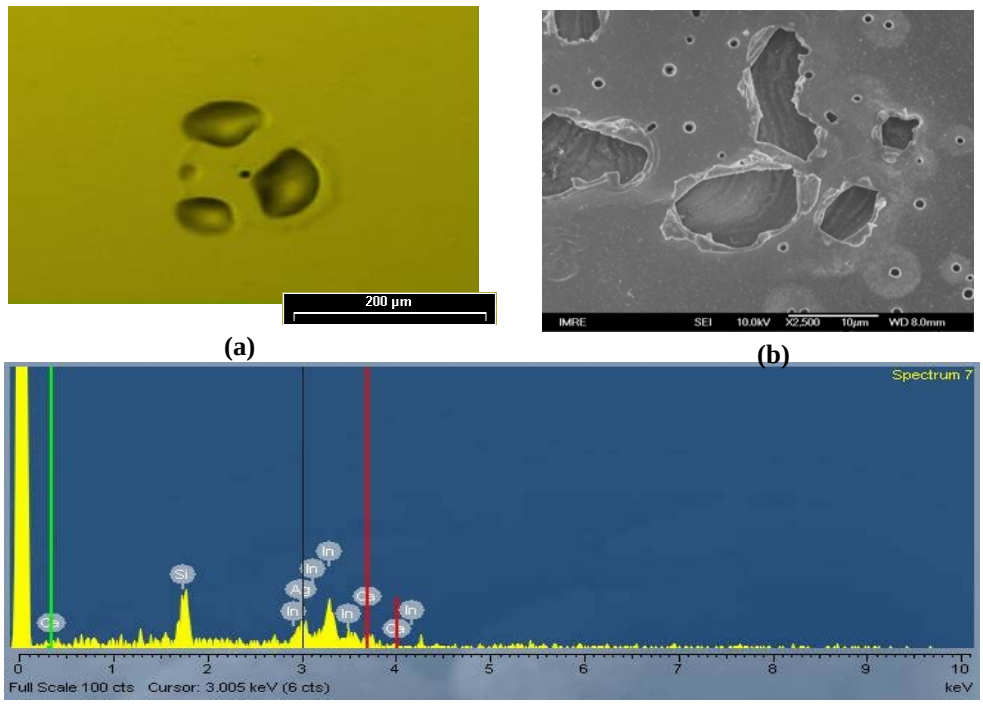

Figure 5.12: Typical bubble structures. (a) Optical image of bubble structures as viewed under external illumination from the glass substrate side. (b) SEM image of the sample surface at the sites of the dark spot and bubble structure. (c) EDX spectra at the sites where the bubble structures were formed.

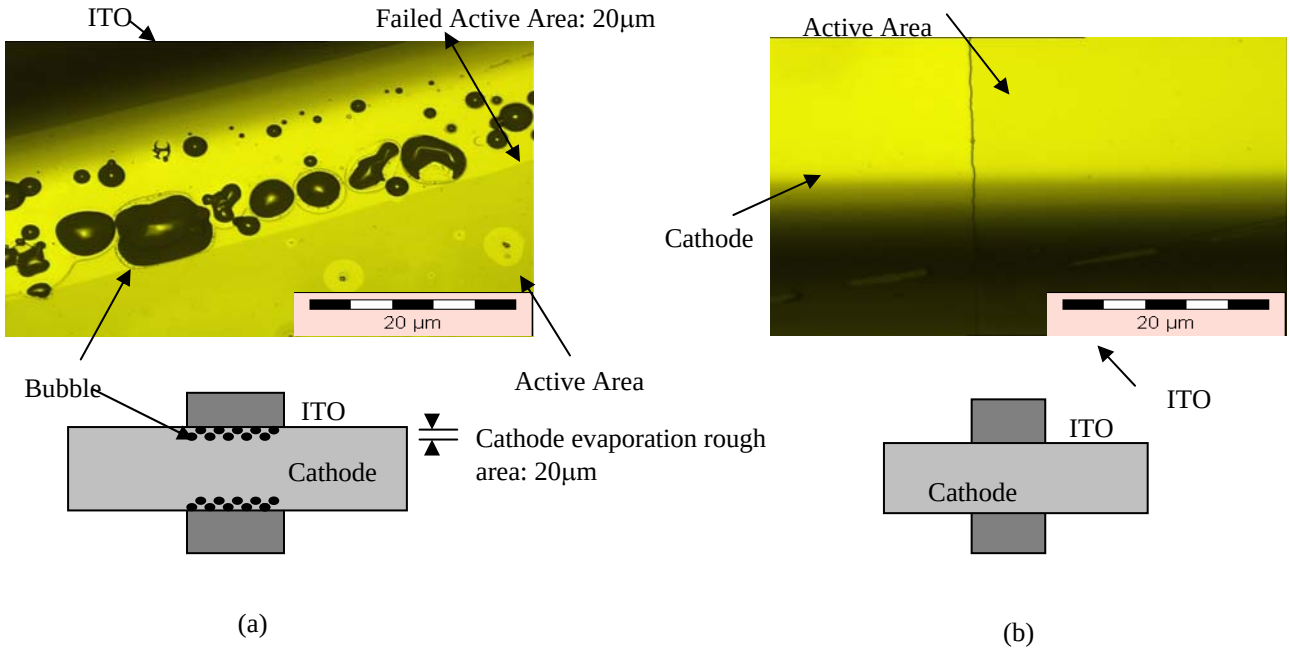

Figure 5.13: Bubbles formed at the edge of the active area. (a) The edge between the ITO and the calcium electrode. Larger bubbles are formed further away from the edge. The lower insert shows the schematic layout of the structure. (b) The edge between the ITO and the calcium before current stress. The lower insert shows the schematic layout of the structure.

5.6 Bubble formation within non-emissive region

The images shown in Figure 5.12 demonstrated that bubbles could be the melted polymer drops termed as liquid bubbles, or could be filled with gases mostly oxygen and moisture termed as gases bubbles. [20-22] The initiated points of the bubbles are not necessarily in the centre of the dark spot. The observed bubbles happened to start anywhere but within the area of the nonemissive spots. We observed the same bubble patterns in OLED devices under ambient atmosphere or under nitrogen atmosphere. This implies that the device inner factors

contributes to the bubble formation and growth, especially the liquid bubbles, although atmosphere moisture is reported to accelerate the bubble growth. The images showed in Figure 5.13 clarified that only electrical stress can initiate the bubble formation. The bubble formation and growth are also noticed to be dependent of the electrical bias period. The outer side of the active area, which has less lighten up time, the bubbles are averagely smaller. The inner side, which has longer lighten up time, the bubbles appear obviously larger. Deep inside the active area, the bubbles disappeared. The width of this bubble region near the edge is around 20 μm, which is almost equal to the Ca evaporation rough area. The electrode rough place, which has more chance to have short and high local current, there is high chance to have bubble formation.

Experiments also demonstrated that some bubbles appear much larger viewed from glass substrate side compared with that viewed from the cathode side, and some bubbles appear almost the same size viewed from the both sides. This shows that bubbles most likely situated in polymer layer or polymer: ITO interfaces.

Therefore, it can be deduced that the bubbles formations is due to the electrical stress and the position of the bubbles initiated most likely from the ITO and polymer interface or polymer layer.

To further investigate the formation mechanisms of the bubbles in the Ca:Ag cathodes device. OLEDs with only Ag cathode are studied. Like the case of Ca:Ag cathodes, clear big bubbles that grow during electrical bias are observed. The fact that these bubbles develop only during device bias and are enhanced in more humid atmospheres, regardless of the cathode metal, [3] strongly suggests that the bubbles are caused by gas evolution due to changes or decomposition in the underlying organic layers, not from cathode oxidation.

Secondary ion mass spectroscopy (SIMS) is used to examine the dark, non-emissive defects on the organic light-emitting device. SIMS results of Ca and C profiles are shown in Figure 5.10, which clearly show that Ca and C moved synchronously in both dark and bright area in stressed device. And their front edge remained the same shape always, which strongly infers that no Ca and polymer separation during the device degradation process. Delamination of cathode and PPV polymer is less likely happened. We attribute this to the elastic properties of polymer. The electrical heating also enhances the flexibility and movability of the polymer, which ensures that polymer and cathode layers always stick together. Furthermore, small atoms, Ca, could enter into polymer big molecular structure easily, which means that during the cathode evaporation, the cathode metals and polymer layer has already formed an entity.

5.7 Bubble formation mechanism

From the discussion above we put forward that the bubble formation and growth are due to interfaces rough and fluctuate, polymer material flexibility and elastic. In some localised area Ca and In is close, which result in local heating and shorts, dark spot centre is formed. Near the dark spot centre the local current is increase, the mechanism by which this might occur and bubble formation are shown schematically in Figure 5.14. Near the dark spot centre, very large electric field intensity and current density is created. Following that the surrounding polymer layer will be heated up, chain scission and decomposition happened, which result in local conducting path broken and luminance decrease. With stress time elapse, the polymer layer will appear “thinner” due to degradation and the edge of the dark shadow area expanded as shown in Figure 5.14, arrow 1. And at the same time the gas arise from decomposition of the polymer layer, like CO_2 and H_2O could diffuse through Ca and Ag void or evolved. If during the electrical stress, suddenly we higher up the driving current or voltage, part of the polymer materials didn’t move faster enough to keep the pace, some lump will be left and accumulated to form the bubble structure as shown in Figure 5.14 arrow 2. Residue gas remained in polymer during synthesis or trapped during the polymer spinning, together with

the polymer decomposed gas will also evolve into big gas bubble during device stressing as shown in Figure 5.14 arrow 3. With time elapse the centre part of the polymer near the dark spot centre will become “thin” (degraded) enough to became truly dark non-emissive area, and the transit region with “thinner” (less degraded) polymer layer will become the second ring of the dark shadow area as shown in Figure 5.1. Sometimes the transit area with a certain optimised polymer layer thickness, there will show a luminescent ring, which show brighter luminescence than other area in the whole dark shadow area, but definitely not as bright as outside normal luminance area. Once the bubbles are initiated, thermal runaway appears to accelerate their development. Both of these two kinds of bubbles will finally either be totally carbonised or broken under electrical field and form a completely hole, in which polymer layer is completely gone, only some metal particles fall inside. This is can be confirmed by observation under scanning electron microscope and also agree with Masamichi’s result. [76] The ultimate failure of the device occurs when the regions of damaged polymer start to carbonate, emerge and coalesce.

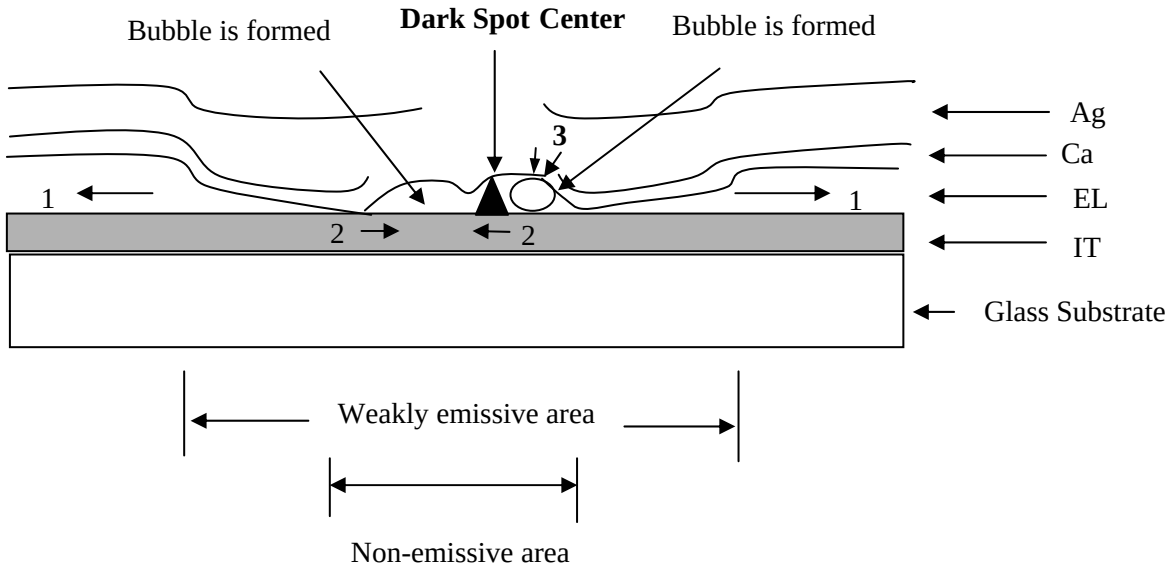

Figure 5.14: Schematic diagram illustrating bubble formation and the growth mechanism.

In conclusion, the elevated “bubbles” are either polymer material accumulation or the gas evolution due to polymer photoelectrochemical reaction. The formation of the bubbles is due to interface rough and polymer materials imperfection. Stabilising and smoothing the interface, which can also help polymer layer reduce deformation, will definitely minimise the chances for dark spot nucleation, furthermore, bubble structure formation.

5.8 Summary

In conclusion, the emissive or non-emissive areas in OLEDs have been identified as different current density areas. We show that due to the interface rough, the local current increase which causes the formation of the dark shadow centre. The degradation of polymer layer is the main reason to cause the dark shadow area growth. We demonstrated that stabilising the interface is the key point to maintain uniformed current density distribution and minimise the dark shadow formation in active area.

Boundary movements are originated from electrode imperfection. Due to flexibility and movability of polymer layer, distribution variations and a more severe Indium and Calcium overlapping are detected in dark spot defect area. Boundary movements are not in good agreement between different layers. Interfaces became undulate. The closeness and proximity between the In sharp spikes and cathode metal protrusion leads to the initial point of dark spot. We demonstrate that the presence of cathode imperfection and interface roughness of different layers correlated to the device dark spot formation. Fabrication of solid, pinhole and defect free cathode is the way to overcome this kind of device failure. Even in boundary movement situation, keeping the interface smooth, minimise the undulation by improvement of materials property or device structures is also a good alternative to prolong device lifetime.

CHAPTER 6 NON-EMISSIVE AREA GROWTH KINETICS

6.1 Introduction

The organic light emitting device lifetime strongly depends on the long-term stability of all components. In the previous chapters, I focused on the formation of the dark spots through studying the structural changes and analysing the EL material degradation. In this chapter, uniformly sized silica micro particles are used to intentionally create size-controllable pinholes on the organic light emitting devices. By this method, dark spot growth kinetics is studied easily. Some key factors that influent the dark spot growth behaviour, such as driving voltage, particle size and encapsulation, are examined. [79-81]

6.2 Obstacles in studying the dark spot

The important feature, which is observed in all of the previous studies, is that dark spots were randomly distributed within the sampling area of devices and that their sizes were scattered in a wide range. Experimentally, this presents an obstacle to *in-situ* monitoring of the dark spot growth, which in turn limits the study of the growth behaviour, and consequently, to the exploration of the degradation kinetics of entire devices. Therefore, the preparation of a device with predictable defects is the key to the study of the growth behaviour of dark spots and to an understanding of the controlling factors controlling formation and growth of dark spots.

6.3 Creation of pinhole defects on Ca and protective layers

6.3.1 Method description

In this work, micron-sized silica particles have been used to create defects. Due to the large size of the silica particles in comparison with the combined thicknesses of the cathode and protective layers, the silica particles gave rise to a shadow effect that prevented the Ca and Ag layers from covering the areas shadowed by the particles. Consequently, a “defect” was created in the organic light emitting device structure. The micron-sized silica particles used had a very narrow size distribution. Figure 6.1 is a schematic representation of the cross section of the structure formed under the silica particle. Figures 6.2 are SEM images providing evidence that defects were indeed formed under the silica particles. The defect size is 4 μm, which is similar to that of the particle size and the size distribution is believed to be very narrow due to usage of the uniformly sized silica particles. When such devices were exposed to an environment containing oxygen and/or moisture and light, the devices were degraded or corroded. Dark spots were initiated from the intentionally manufactured defects, thus enabling us to track the growth process of dark spots.

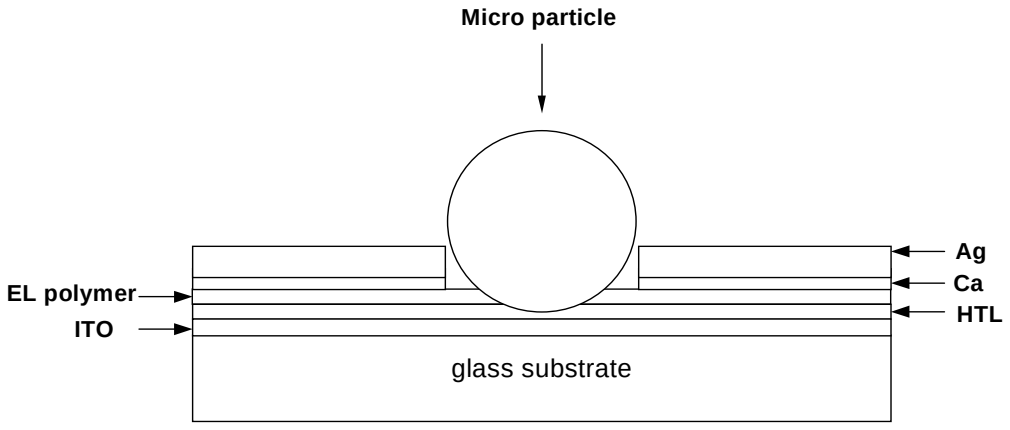

Figure 6.1: Schematic representation of the structure of silica particle in our devices.

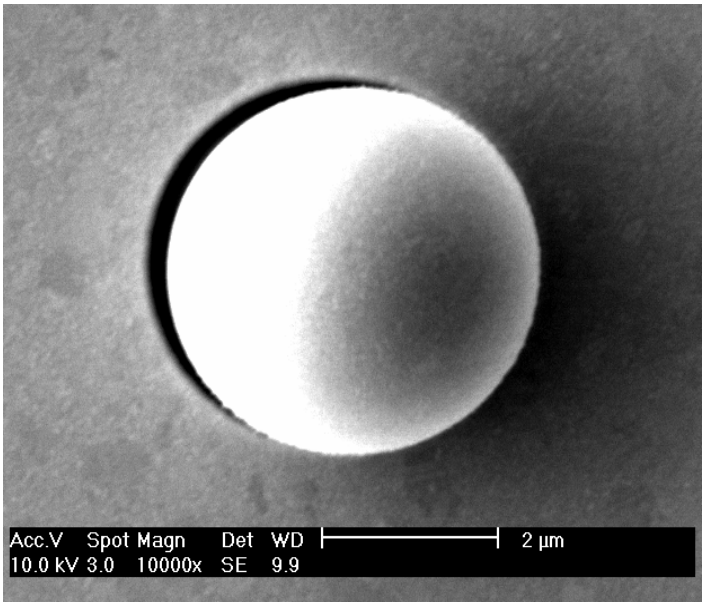

Figure 6.2: SEM images to evidence the pinhole defect formed under the silica particle.

6.3.2 Experiment details

In this experiment, the silica particles are mixed with a water solution of PEDOT to form a PEDOT/particle suspension solution with particle concentration in the range of 0.02-0.025wt% for 4.0μm silica particles. The PEDOT/particle suspension was spin-coated on the cleaned surface of the ITO-coated glass. After baking at 200^{o}C for 5 minutes to remove moisture, a toluene solution of the EL copolymer was spin-coated over the PEDOT. 5 nm of Low work function metal Ca was evaporated as cathode, finally 200nm of Ag was evaporated as a protective layer. This gave devices having the following multilayer structure: ITO/HTL/PPV derivative/Ca/Ag. Micron-sized silica particles with a narrow size distribution are used to create uniform pinhole defects on the organic light emitting devices. The dark spots initiated by these defects are monitored *in-situ* using optical microscopy in lit-up devices and their growth behaviour is further investigated. Some key factors that affect the growth behaviour of dark sports, such as driving voltage, particle size and encapsulation, are examined. Finally, the degradation process of entire devices is correlated with formation and growth of dark spots.

The results presented in this work enable us to discern the key factors that govern the formation and growth of dark sports.

6.4 General feature of dark spots growth

As shown in Figure 6.3, all the dark spots are circular in shape at the initial stage. Two kinds of dark spots can be seen: one with a black dot in the centre as marked by letters A and B, and the other without black dots as marked by letters C to G. The black dots are the silica particles. The dark spots A and B have almost the same size and their size always distributes in a very narrow range at a certain time. For dark spots without the centralised black dots, we observed that they are usually smaller sized and have a larger size distribution. Obviously, the centralised black dots allow us to easily identify the dark spots having the same initial defect feature and then track their growth. The narrow size distribution ensures the reproducibility of data measured from these dark spots. Therefore, such devices are valuable for routine investigation of the formation and growth of dark spots and further the degradation of entire devices.

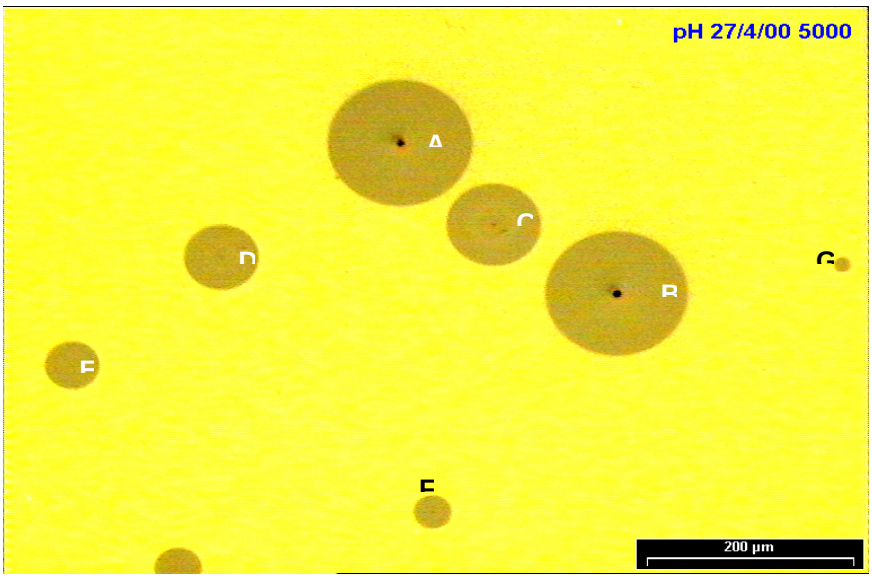

Figure 6.3: An optical image showing the general feature of the dark spots. Letters A and B mark dark spots with a centralised black dot (silica particle), while letters C to G mark another type without a centralised black dot.

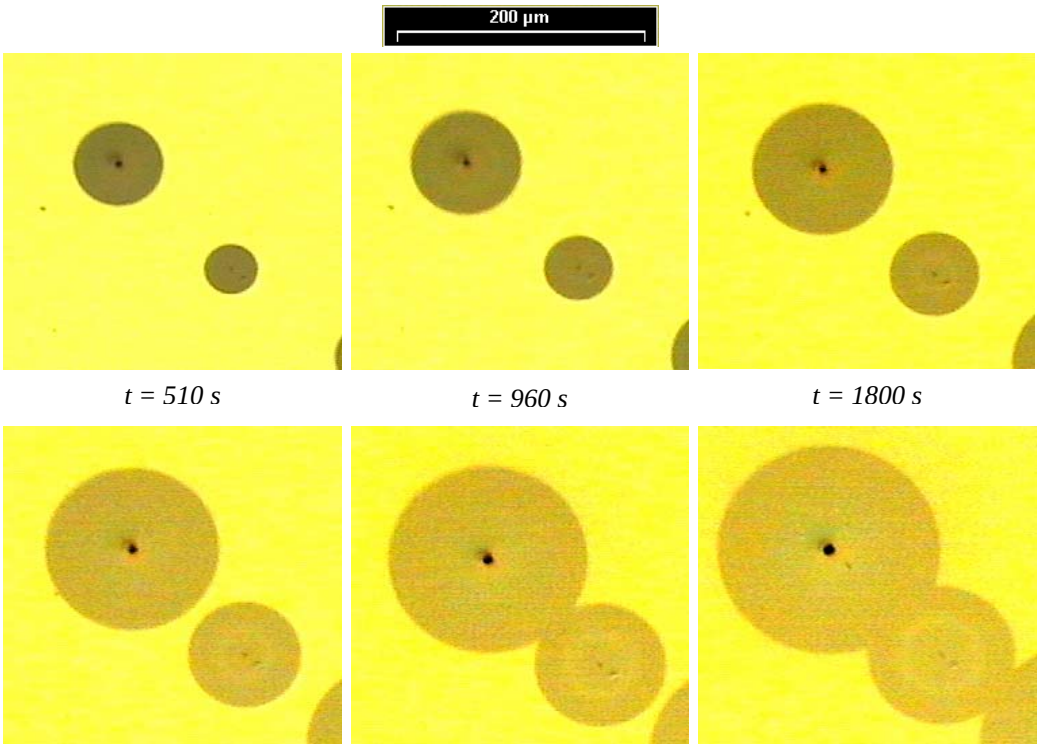

Figure 6.4: A series of optical images of the dark spots A and C taken from the device at different times.

In our *in-situ* observation, we noted that both kinds of dark spots do not grow in number, only in size. Figure 6.4 shows a series of optical images of the dark spots A and C taken from the device at different times. Their change in size illustrates the growth of the dark spots. As the dark spots grow in size, they coalesce with neighbouring ones, as shown in the image taken at t = 5400 s, to form non-emissive areas having irregular shapes. Figure 6.5 illustrates the growth of the dark spots with respect to time measured from the seven dark spots previously shown in Figure 6.3. The dark spot areas, A_{ds}, linearly increase in the time regime covered. The slope reflects the growth rate, G, of the dark spots. The inset graph shows the dark spot areas, A_{ds} with respect to growth rate, G. Linear fitting shows zero intercepts, indicating that corrosion occurred prior to commencement of the recording time. In addition, we can see that the larger

the initial size, the dark spots grew more rapidly if we correlate the growth rate derived from Figure 6.4 with the size shown in Figure 6.3.

Repetitive experiment reveals that the dark spot size and growth rate measured from those dark spots with centralised black dots are very reproducible. For example, the growth rate measured from different dark spots in the same device or different devices made under the same condition varies within a small range (see lines A and B in Figure 6.3). This implies that the data obtained from different devices are comparable and thus allows us to further explore the influence of some other factors on the growth of dark spots.

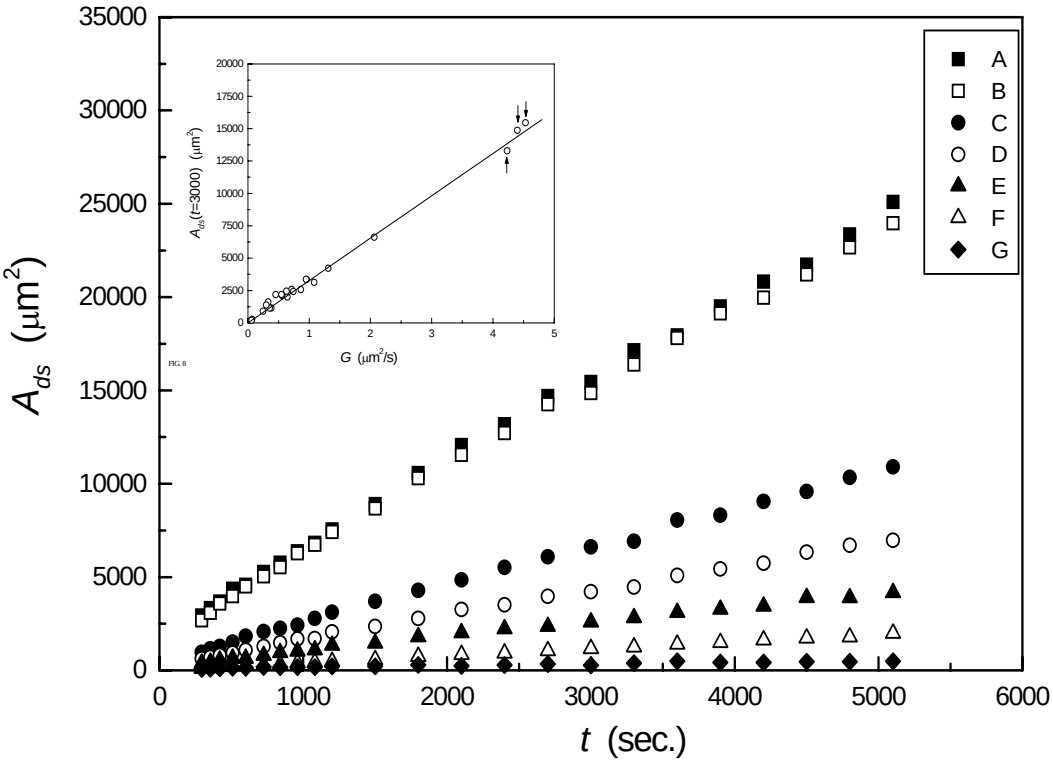

Figure 6.5: A plot showing the linear growth of A_{ds} for the dark spots shown in Figure 6.3. The letters A to G corresponds to the letters in Figure 6.3.

6.5 Dark spot growth rate

6.5.1 Particle size dependence

Figure 6.6 shows the growth of the dark spots with centralised silica particles. The diameters of the silica particles are 1.0, 2.0, 4.0 and 6.0 μm, respectively. G = 4.51 μm^2/s is for the dark spot with 4.0 μm silica particle, while G = 2.05 μm^2/s is for the dark spot with 1.0 μm silica particle. The inset graph shows the dark spot growth rate, G, linearly increase with the silica particle size, d_p and with a non-zero intercept. This is easily interpreted, as the pinhole defects created by 4.0 μm particle are larger than those created by 1.0 μm particle.

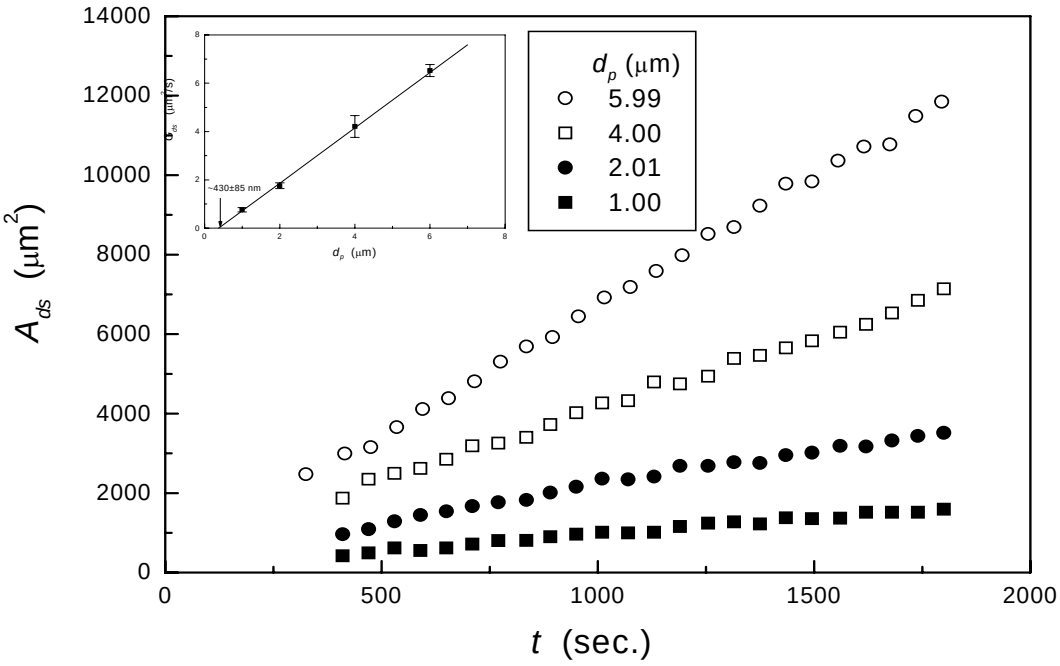

Figure 6.6: Particle size dependence of the dark spot growth. The particle size is 1, 2, 4, 6 μm respectively.

6.5.2 Driving voltage dependence

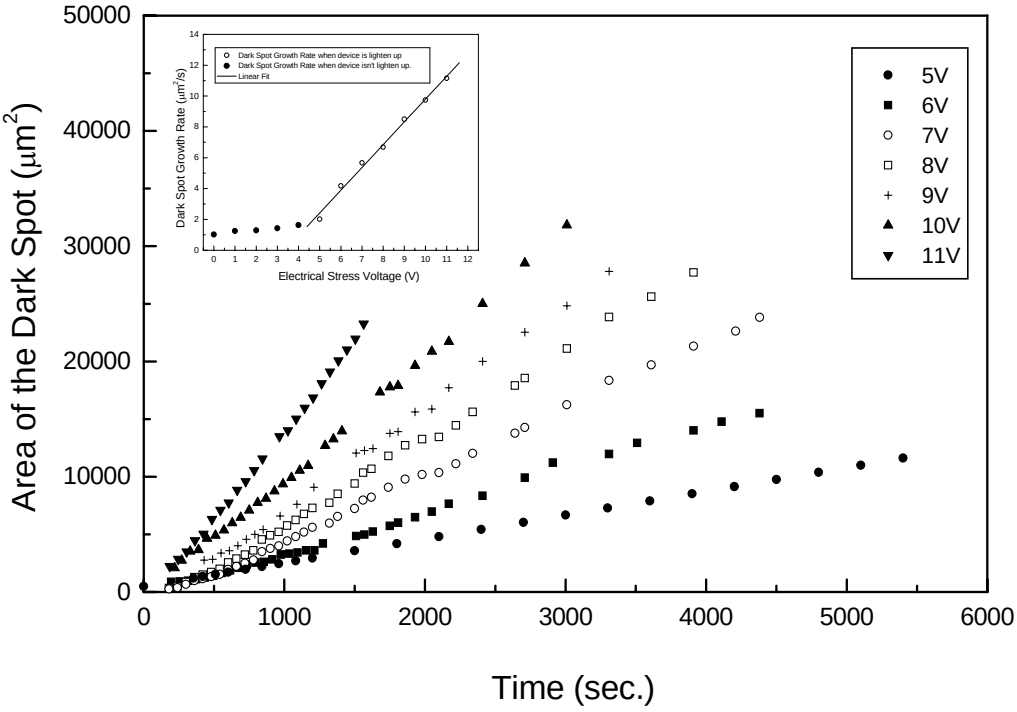

Figure 6.7: Driving voltage dependence of the dark spot growth. The particle size is 4 μm.

Figure 6.7 shows the effect of electrical stressing on the growth of the dark spots with the centralised 4 μm particles. The driving voltages were from 8 to 12 volts, respectively. Linear fitting shows that G = 4.53 μm^2/s at 8 V, while G = 11.2 μm^2/s at 12 V. Clearly, increasing the driving voltage expedites the growth rate of the dark spot. The inset graph shows the dark spot growth rate, G, versus electrical stress voltage, V. The black solid sample points smaller than 4V indicate the growth rate of the dark spot when the device was not lighted up. The observation is under optical microscope dark field. The void circle sample points larger than 4V indicate the growth rate of the dark spot when the driving voltages are higher than the turn on voltage. A linear growth rate with respect to the voltage was observed with fitting parameter better than 99.7% when the device is driven above turn-on voltage. The figure clearly shows that increasing the driving voltage expedites the growth rate of the dark spot. In other words, increasing the driving voltage speeds up physical and chemical change of the cathode layer. The interception of the fitting line with the voltage axis indicates the device turn-on voltage.

6.5.3 Encapsulated devices

When the diodes were covered with a glass cap and then were sealed with epoxy resins, we observed that the growth rate of dark spots was considerably slowed down. Figure 6.8 shows the growth of dark spot using a 4 μm silica particle for three devices encapsulated with different methods. G_{non} = 4.53 μm^2/s for a non-encapsulated device, G_{hc} = 2.26 μm^2/s for a device encapsulated with the heat curing epoxy resin at 60 °C for 10 min, and G_{uv} = 1.31 μm^2/s for a device encapsulated with the UV curing epoxy resin at room temperature for 1 min. Obviously, the reduction of dark spot growth rate after encapsulation is because the moisture and/or oxygen must at first penetrate some weak areas of encapsulated and sealed devices before they can attack Ca or other materials. In other words, the encapsulation and sealing cause a reduction of the concentration of moisture and/or oxygen inside devices. This is an indirect indication of the effect of the moisture and oxygen concentration on the growth behaviour of dark spots.

What is of more interest is the further comparison of the growth behaviour of the dark spots in

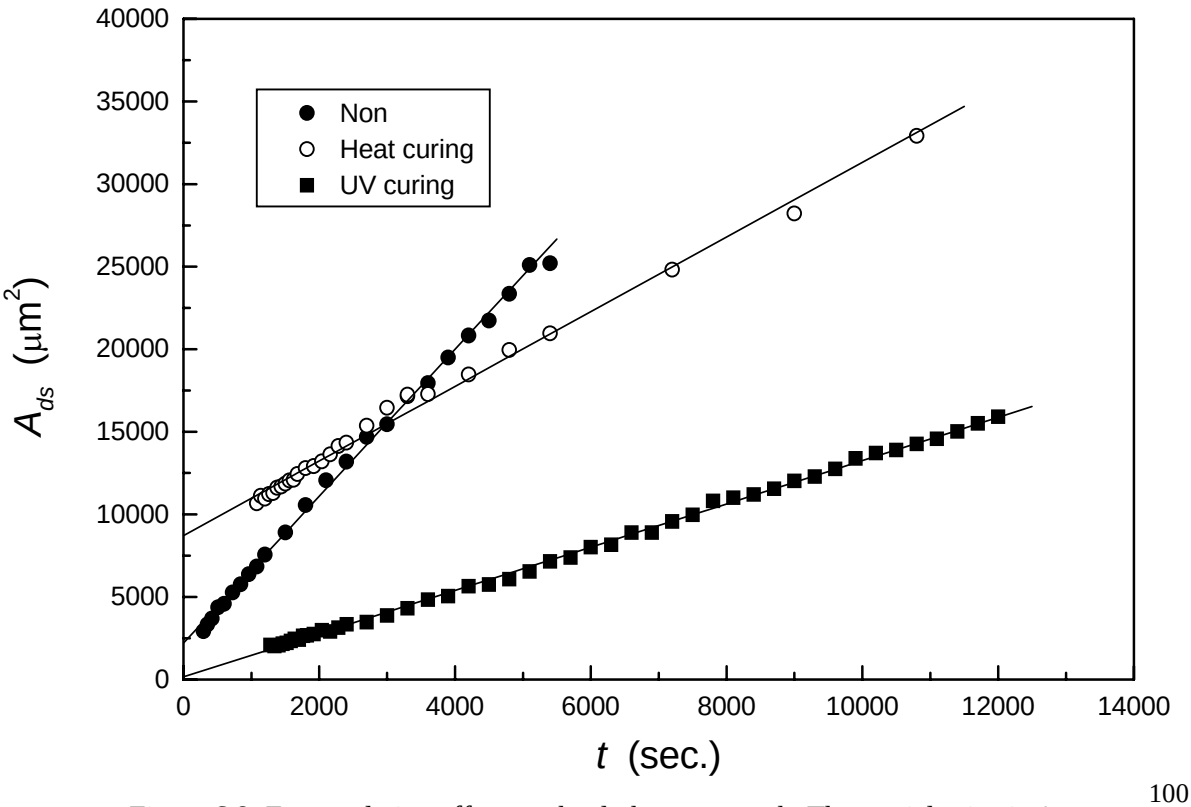

Figure 6.8: Encapsulation effect on the dark spot growth. The particle size is 4 μm.

the two differently encapsulated devices. First, the sealing quality of the UV curing epoxy resin is better than that of the heat curing epoxy resin because G_{uv} = 1.31 μm^2/s is smaller than G_{hc} = 2.26 μm^2/s. Secondly, there are different intercepts for two straight lines for the dark spots. The intercept for the device sealed by the heat curing epoxy resin is much larger than that for the device sealed by the UV curing epoxy resin. The larger intercept means a larger dark spot size at the initial stage. For the sealing process using the heat curing epoxy resin, we believe that curing at 60 °C for 10 min causes a rapid growth of the dark spot or conversely, a rapid degradation of polymer layer and deteriorate of the whole device with the limited amount of moisture and/or oxygen trapped within the devices. It is worth emphasising here that by comparing the growth rate and the intercept of dark spots in the devices sealed by different methods and different sealant, we can quantitatively check the sealing quality and also evaluate the sealing process.

6.6 Significant of this method

The study of the growth of individual dark spots can be correlated to the failure process of entire diodes. Figure 6.9 shows a linear growth of the fraction of the dark spots, ϕ_{ds}, obtained from the sampling area shown in Figure 6.3 and other data measured images taken at different times. The slope obtained by linear fitting is about 3.3×10^{-5} s^{-1}, implying that the sampling area will be fully covered by the non-emissive area at 30,300 s, implying that the device has a lifetime of about 8.4 hours. This is a proposed new method to estimate the lifetime of OLED devices due to the formation and growth of dark spots. In Figure 6.4 we have mentioned that some dark spots started to coalesce with neighbouring ones at t = 5400 s to form non-emissive areas having irregular shapes. It should be pointed out that ϕ_{ds} maintains its linearity even at t > 5400 s. This indicates a linear growth rate of the non-emissive areas having irregular shapes and that furthermore, their growth rate is controlled by the number and size of pinhole defects. Therefore, we can predict the degradation rate of entire devices simply by studying the sum of

the growth rate of individual dark spots. The linear growth rate of the dark spot fraction can be correlated with those of the individual dark spots. In accordance with the definition of fraction, we have

$$\phi_{ds} = \sum_{i=1}^{n} S_i^{ds}(t) \Big/ S \tag{6.1}$$

where $S_i^{ds}(t)$ is the area of *i* dark spot at time *t*, and *S* is the total area of the sampling area. We have found $S_i^{ds}(t) = a_i + b_i \cdot t$ in Figure 6, therefore, we have

$$\phi_{ds} = \sum_{i=1}^{n} a_i \Big/ S + \sum_{i=1}^{n} b_i \cdot t \Big/ S \tag{6.2}$$

If we take $A = \sum_{i=1}^{n} a_i \Big/ S$ and $B = \sum_{i=1}^{n} b_i \Big/ S$, we have

$$\phi_{ds} = A + B \cdot t\,. \tag{6.3}$$

This is a linear relation obtained in Figure 6.8. In Table 6.1, the slopes of the seven dark spots A to G in Figure 6.3 are listed. Clearly, their summary over the total area of the sampling area is very close to that of the fitted slope (3.3×10^{-5} s^{-1}) obtained in Figure 6.9. Furthermore, equations 6.1 to 6.3 demonstrate that we can predict the lifetime of entire device simply by studying the growth kinetics of individual dark spots having the same initial conditions, such as defect size and thickness of cathode and emitting layer.

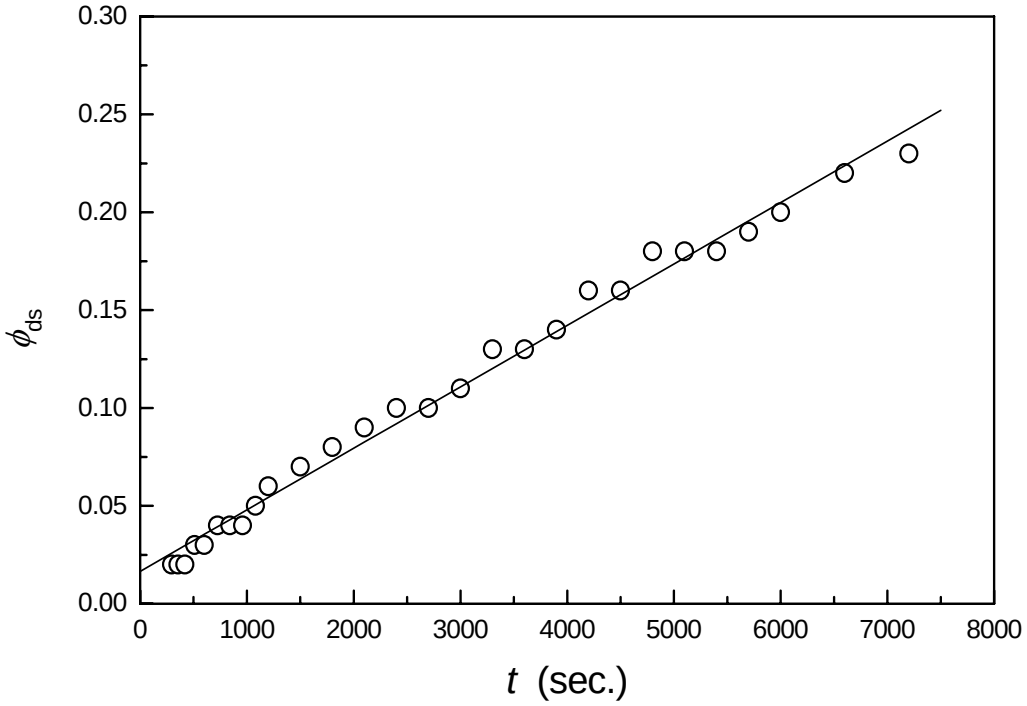

Figure 6.9 Linear growth of fraction of all dark sports in Figure 6.3.

6.7. **Failure of entire diodes**

Hence, we propose a new method to estimate the lifetime of OLED devices based on the formation and growth of dark spots. In Figure 4.5 we have mentioned that some dark spots started to coalesce with neighbouring ones *at* 5400 s to form non-emissive areas having irregular shapes. It should be pointed out that growth rate maintains its linearity even at $t >$ 5400 s. This indicates that non-emissive areas having irregular shapes also follow a linear rate of growth and that their growth rate is controlled only by the number and size of all pinholes. Therefore, we can predict the failure rate of entire devices simply by studying the sum of the growth rate of individual dark spots.

Dark Spot	Growth rate b_i $(\mu m^2/s)$	b_i / S $(1/s)$
A	4.53	10.88×10^{-6}
B	4.40	10.56×10^{-6}
C	2.06	4.94×10^{-6}
D	1.31	3.08×10^{-6}
E	0.72	1.71×10^{-6}
F	0.38	0.91×10^{-6}
G	0.067	0.15×10^{-6}
Total	$\sum_{i=1}^{n} b_i / S = 13.47$	$B = 3.22\times10^{-5}$

Table 6.1. Growth rate of all dark spots in Figure 6.3 and the calculated parameter, b_i / S .

6.8 Dark spot growth behavior analysis by diffusion reaction theory

Although dark spot formation and growth involves very complicated mechanism, its growth rate tracing experiment results performed on organic light-emitting device can be generally well-fitted by Fick's diffusion equation. In this work, diffusion coefficient in the ideal structure, which has no chemical reaction involved, using Fick's diffusion reaction theory is calculated. And then compare the ideal situation with the real device situation to explore the device degradation mechanism quantitatively.

6.8.1 Theoretical model of diffusion

Dark spot growth area can be mathematically analyzed by the diffusion equation model shown schematically in Figure 6.10. The interface (dark spot edge) is located at $r = r_0$, the diameter of the centre cylinder is the pinhole or particle size, while the centre of the top of the cylinder is at z=0. Some assumptions are made in order to simplify the problems:

1. There is no resistance to mass transfer at the environment-device interface. The interface is the equilibrium concentration.

2. Temperature remains constant during the test.

3. The diffusion coefficient (signify the dark spot growth behaviour), D, does not change significantly with concentration over the range of concentrations encountered in the test.

4. Due to the large size of the silica particles in comparison with the combined thickness of the cathode and protective layers, the thickness of the Ca has no significant influence on this case.

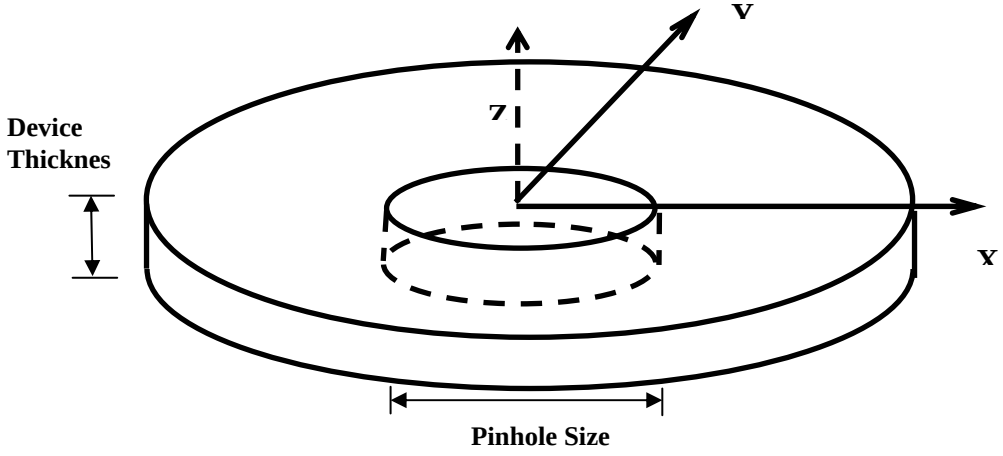

Figure 6.10: Theoretical model for calculation of diffusion coefficient in organic light emitting devices

Therefore, the general unsteady-state equation of three-dimensional diffusion with constant diffusivity is:

$$\frac{\partial C}{\partial t} = D(\frac{\partial^2 C}{\partial x^2} + \frac{\partial^2 C}{\partial y^2} + \frac{\partial^2 C}{\partial z^2}) \tag{6.4}$$

The boundary conditions applicable to the system are:

$$\begin{aligned} C(r = L, t) &= 0 \\ C(r_0, t) &= C_0 \end{aligned} \tag{6.5}$$

The initial condition is:

$$C(r, 0) = 0 \tag{6.6}$$

where C_0 is the concentration in ambient. The profile of the dark spot growth profile can be obtained:

$$C(r,t) = \frac{C_0(\frac{r}{L} - 1)}{\frac{r_0}{L} - 1} - \sum_{n=1}^{\infty} \frac{2C_0}{n\pi} \sin[\frac{n\pi(\frac{r_0}{L} - \frac{r}{L})}{\frac{r_0}{L} - 1}] \exp(-\frac{n^2\pi^2}{(1 - \frac{r_0}{L})^2} \frac{Dt}{L^2}), \tag{6.7}$$

where L is the radius of device material, which is assumed to be infinite long, and r_0 is the initial radius of the dark spot, which created by intentionally induced silica particles. D is the diffusivity.

Assume $\frac{r_0}{L} = S_0, \qquad \frac{r}{L} = S, \qquad T = \frac{Dt}{L^2}$

$$\frac{C(r,t)}{C_0} = \frac{S-1}{S_0-1} - \sum_{n=1}^{\infty} \frac{2}{n\pi} \sin[\frac{n\pi(S_0 - S)}{S_0 - 1}] \exp(-\frac{n^2\pi^2}{(1-S_0)^2} T), \tag{6.8}$$

6.8.2 Results and Discussions

Using the diffusion theory elaborated above, diffusion efficiency can be calculated based on experimental results. Two experiment results have been analysed in the following demonstration. First, for particle size variation experiment, which is elaborated in 6.5.1, Table 6.2 lists all the parameters including the dark spots starting size and dark spot growth rate. Initiated dark spot centres are 0.5μm, 1μm, 2μm and 3μm. L should be much larger than the dark spot initial size, in the following calculation L= 150 μm is assumed. Second case, two different device structures are also compared, which are Substrate/ITO/HTL/EL/Ca/Ag and Substrate/ITO/HTL/EL/Ag, the parameters for these two structures are shown in Table 6.3

Dark Spot	Initial radius (μm)	PPV Polymer (nm)	Ca (nm)	Ag (nm)	Experiment $G\ (\mu m^2/s)$
1μm*	0.5	90	5	300	0.83447
2μm*	1	90	5	300	1.78451
4μm*	2	90	5	300	4.44444
6μm*	3	90	5	300	6.52421

Table 6.2: Parameters for different size of induced dark spots in the device structure of substrate/ITO/PPV/Ca/Ag

Dark Spot	Initial radius (μm)	PPV Polymer (nm)	Ca (nm)	Ag (nm)	Growth rate Exp. $G(\mu m^2/s)$
1*	2	90	5	300	4.44444
2*	2	90	0	300	15.5

Table 6.3: Parameters for intentionally induced dark spots in substrate/ITO/EL/Ca/Ag and substrate/ITO/PPV/Ca/Ag respectively.

According to the theoretical model, theoretical calculation of diffusion efficiency, D, starts with plotting the relationship between $C/C_{0,}$ the normalized concentration, and r/L, the normalized dark spot radium, at selected normalized time instant T. Figure 6.11 shows the results. Figure 6.12 shows the dark spot area increasing with normalized time T. The slope of the curve indicates the area growth rate.

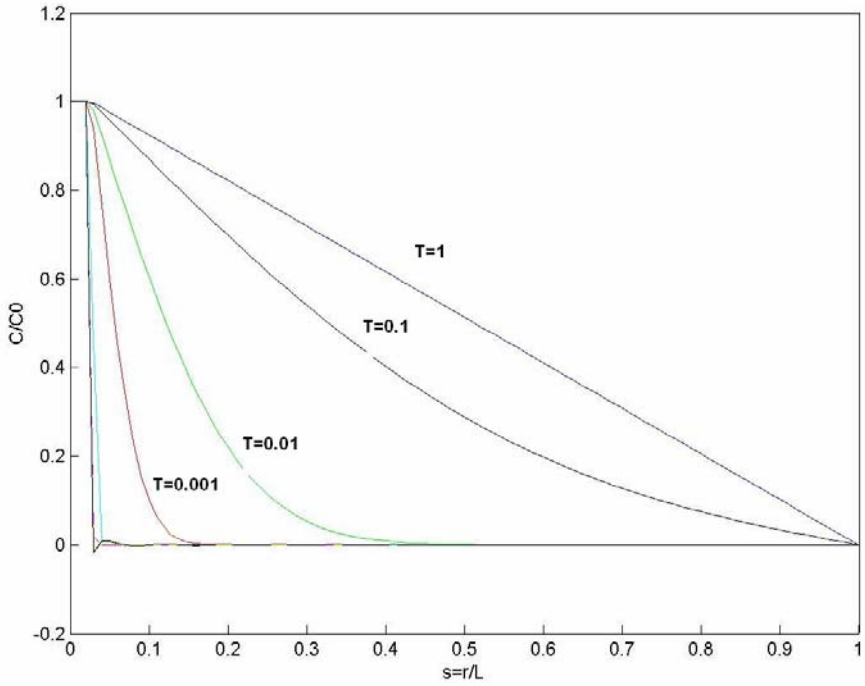

Figure 6.11: Normalized concentration C/C_0 vs. normalized dark spot radius r/L.

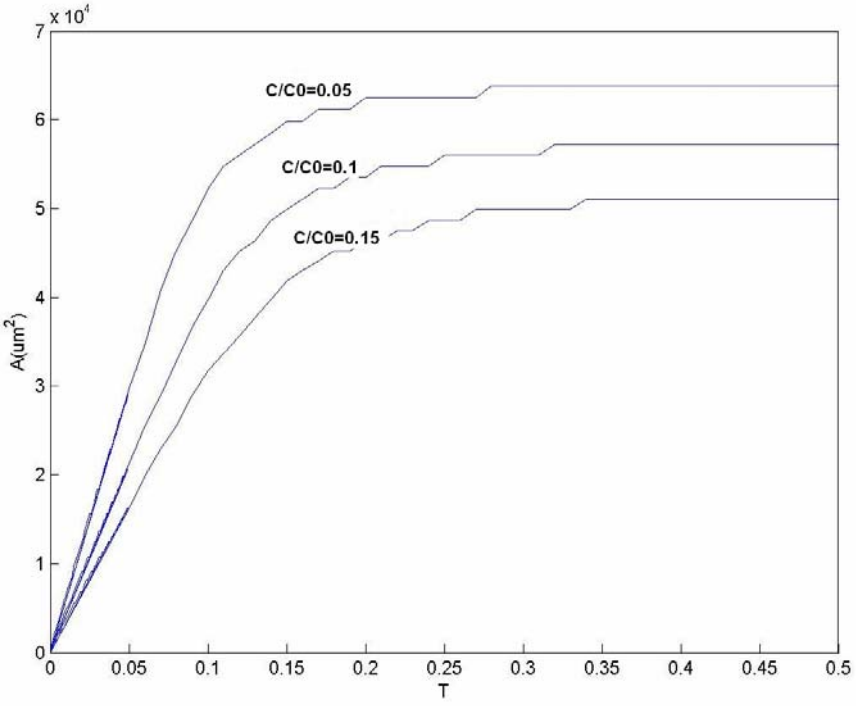

Figure 6.12: Dark spot area increasing with normalized time T. The slope of the curve indicates the area growth rate.

According to the formula $T = \frac{Dt}{L^2} \Rightarrow D = \frac{dA}{dt} \times \frac{1}{dA/dT} \times L^2$ (6.9)

The diffusion coefficient, D, can be extracted by combining the experimental result dA/dt and dA/dT read from the graphs plotted above.

Table 6.4 shows theoretical calculation of diffusion efficiency D, for L=150μm, with different induced initial sized dark spot. It can be seen that diffusion coefficient increases with dark spot starting radium and concentration. Repeat the calculation by using different L shows that the value of L almost has no effect on the diffusion efficiency results. Table 6.5 shows theoretical calculation of diffusion efficiency, D, for L=150μm, with device structure of substrate/ITO/EL/Ca/Ag and substrate/ITO/EL/Ca/Ag respectively. It shows a decrease of diffusion coefficient in the device with the structure of substrate/ITO/HTL/EL polymer/Ca/Ag compared with device structure of substrate/ITO/HTL/EL polymer/Ag. This shows that the device with structure of substrate/ITO/HTL/EL polymer/A has a faster dark spot growth rate and faster degradation process.

The experiment and the theoretical analysis provided an insight into the nature of the process of the device degradation. By strictly tracing the dark spot growth rate and calculating the diffusion coefficient, we could determine the moisture solubility and diffusivity in a polymer and furthermore determine the cathode materials and interface quality. Reversibly, this is also a way to determine the unknown diffusivity of gases in a polymer by putting in polymer layer in between two perfect contacts and performing the dark spot tracing experiments on this structure. This method could also be used to trace the dark spot initial size. For example, by fitting the dark spot growth rate curve shown in Figure 6.5, the dark spot initial size for C, D, E, F and G are 2.1μm, 1.6μm, 1.2μm, 0.8μm and 0.2μm respectively. This is a way to quantitive judge the device initial defect level.

Dark Spot	Initial radius (μm)	Experiment $G\,(\mu m^2/s)$	Diffusion Coefficient ($10^{-10}m^2/s$)	
1μm*	0.5	0.83447	C/C_0=0.05	0.0346
			C/C_0=0.1	0.0492
			C/C_0=0.15	0.0665
2μm*	1	1.78451	C/C_0=0.05	0.074
			C/C_0=0.1	0.1052
			C/C_0=0.15	0.1315
4μm*	2	4.44444	C/C_0=0.05	0.1741
			C/C_0=0.1	0.2420
			C/C_0=0.15	0.3275
6μm*	3	6.52421	C/C_0=0.05	0.2622
			C/C_0=0.1	0.3596
			C/C_0=0.15	0.4807

Table 6.4: Theoretical calculation of diffusion efficiency D, for L=300um, with different induced initial sized dark spot.

Cathode	Initial radius (μm)	Growth rate Exp. $G(\mu m^2/s)$	Diffusion Coefficient ($10^{-10}m^2/s$)	
Ca/Ag	2	4.44444	C/C_0=0.05	0.1741
			C/C_0=0.1	0.2420
			C/C_0=0.15	0.3275
Ag	2	15.5	C/C_0=0.05	0.6230
			C/C_0=0.1	0.8810
			C/C_0=0.15	1.0964

Table 6.5: Theoretical calculation of diffusion efficiency D, for L=300um, with device structure of substrate/ITO/EL/Ca/Ag, substrate/ITO/EL/Ca/Ag respectively.

In conclusion, the experiment and the theoretical analysis provided an insight into the nature of the process of the device degradation. The diffusion coefficient calculated from the diffusion equation combined with experimental results proposes a possible new way to explore device degradation mechanism quantitatively.

6.9 Summary

In summary, it is demonstrated that using silica particles is a convenient and efficient way of controlling the location and number of dark spots because uniform sized defects can be created on organic light emitting devices. Such controllable features allowed us to monitor *in-situ* the growth of the dark spots as well as their growth behaviour. After examined some key factors that affect the growth behaviour, such as driving voltage, particle size and encapsulation, we found that low driving voltage, small initial dark spot size and good encapsulation will reduce the dark spot growth rate. Clearly, summarize from the previous chapters, electrode defects and polymer degradation are the main causes of the formation of dark spots. It is via these draw backs that the driving voltage and concentration of moisture and/or oxygen will keep on degrade the device and speed up the growth of dark spots. At the same time, we found that the formation and evolution of bubble structures inside dark spots were greatly related to the applied electrical stress too. The diffusion coefficient calculation from the simplest and Fick's diffusion law fitted device structure to complicated device structure which including physics change and chemical reaction propose a possible new way to explore device degradation mechanism quantitatively. This may permit us in future to quantitatively judge the encapsulation and sealing quality of different encapsulation methods and also to estimate the lifetime of devices.

CHAPTER 7 NON-EMISSIVE AREA INHIBITION

7.1 Introduction

In the previous chapters, I have elaborated that interface problem; device high current, local heating, cathode pinholes and materials flaw etc. play an important role in the formation and growth of dark spots. However, device failure is a complicated process, which has been studying extensively and deeply by lots of researchers. The dark spot formation on OLED device may also due to a number of other factors, such as the cathode deposition technique, film synthesis, surface morphology, surface contamination, oxygen and moisture evolution within the OLED materials, permeation and diffusion through the substrates and through the device sealing etc. In this chapter, I will propose a novel OLED structure design and a suitable process technology for the effective control of non-emissive area formation and its growth. [75]

7.2 Review of Present Device Architecture Designs

A traditional and most popular organic LED consists of two electrodes with one or more polymer layers sandwiched in between the electrodes. The anode indium tin oxide is biased positively with respect to the cathode. Electrons and holes are injected into the EL layer, where they recombine to emit light. Usually, the anode (ITO) is transparent and the work functions of the electrodes are chosen to closely match the energy levels of the polymer (HOMO for the anode and LUMO for the cathode). Hence, the materials most widely used for cathode are calcium, magnesium and aluminium & lithium alloys. Considerable improvements have been made in materials and device architecture, which resulted in devices with high luminance and external quantum efficiencies.

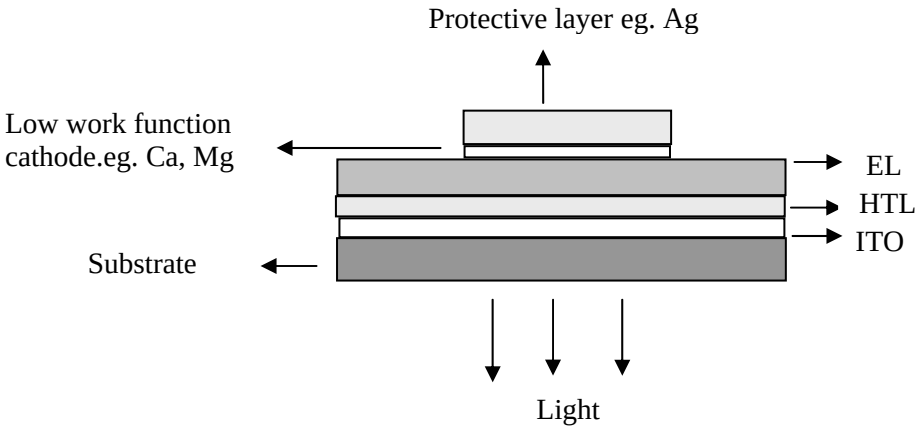

Figure 7.1. Typical two layer EL device structure

Figure 7.1 shows the typical device architecture consisting of the combination layers: Substrate/Indium Tin Oxide/Hole transport Layer/EL layer/calcium or magnesium/silver or aluminium. [76] It is generally agreed that besides the proper selection of organic materials, efficient carrier injection from both electrodes, and controlled electron-hole recombination within a well-defined zone are key factors in enhancing the performance of LEDs. Subsequent efforts that focused on increasing the charge injection by choosing a low work function metal cathode and on carrier confinement by using multilayer heterostructures have indeed led to remarkable improvements in device performance. These have lead to the improved popular device structure, which is shown in Figure 7.2. [77]

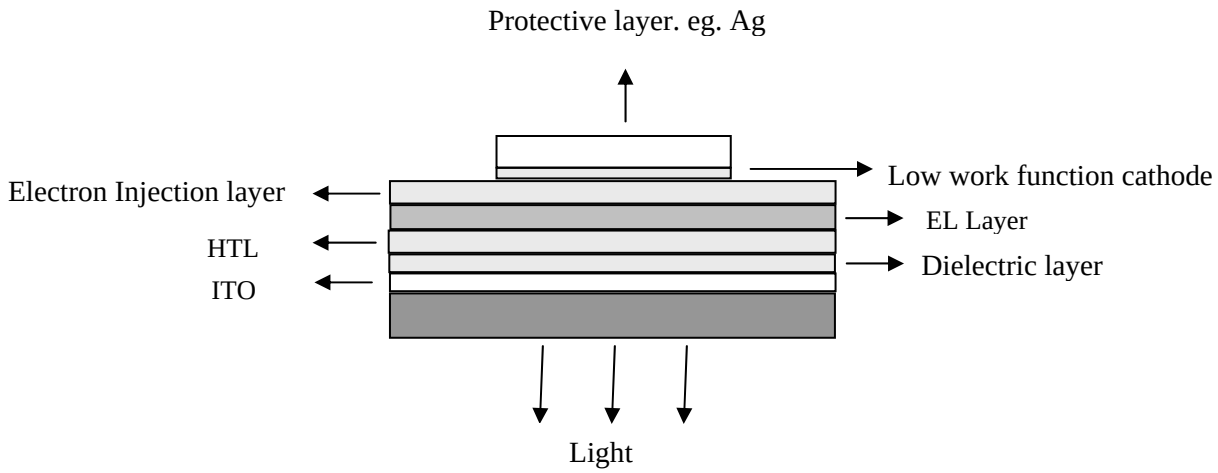

Figure 7.2: A typical multi-layer high efficiency device structure

Figure 7.2 shows the multi-layer high efficiency device structure. In the past, much research efforts have been put into achieving balanced injection of holes and electrons in order to improve the device efficiency. These include the formation of heterojunction or blending with electron transporting materials and synthesis of new emitting materials having high electron affinity. A multi-layer device structure has also been demonstrated to be efficient in controlling hole and electron injection. This is done by inserting a thin insulating layer between an emitting layer and a cathode as illustrated in Figure 7.2.

Extensive research has been carried out to improve the performance of the PLED by modifying its structure in order to achieve effective and balanced charge injections. The lowering of the effective barrier to carrier injection leads to more balanced injection of electrons and holes and the quantum efficiency will increase significantly. Recently Young-Eun et al. demonstrated that an extremely thin insulating PMMA buffer layer at the polymer/Al interface dramatically

improved the electron injection efficiency [78,79]. F. Li et al. describes the effects of a controlled Al_2O_3 buffer layer on the device structure of TPD/Alq/Al and showed that an optimised Al_2O_3/Al cathode yields high efficiency. [80] Others, such as, L. S. Hung et al. have demonstrated the PLED/OLED devices using LiF and CuPc as a electron injection layer in order to improve the device luminescence efficiency. [81,82] A good barrier layer is necessary for blocking the migration of oxygen from Indium Tin Oxide to the polymer and cathode materials. Figure 7.2 shows a device structure with thin dielectric layer inserted in between the ITO and the HTL layer.

Charge injection at the electrodes can be modified in a few ways. At the cathode side, Magnesium and Calcium are often used because of their low work function. However, Calcium and Magnesium are very sensitive to oxygen and water vapour. Due to the oxygen and moisture present within the OLED materials, and also through permeation & diffusion through the substrates and the encapsulation, reacts with the electrode and oxidise it. The oxidized cathode will decrease the efficiency and increase the bias threshold. It is well known that pinholes are formed due to resistive evaporation technique and control of pinholes and other defects is almost impossible by this technique. Although sputtering is one of the commonly used methods in the semiconductor industry for the deposition of thin films, it is not suitable for OLEDs because the devices are extremely sensitive to radiation, charging, heating and ion bombardment. Hence, the sputtering method is not normally used. Furthermore, without improvement in device lifetime, improvement made in device luminescence and efficiency will still limit the commercialization of the OLED. So far none of the device structures mentioned above can significantly overcome device degradation problems.

7.2 New device structure for non-emissive area inhibition

I have proposed a new OLED architecture design, which is proved to be a suitable solution for the reduction of dark spot formation and the control of its growth. This new device structure introduced one new barrier film which constitutes three more layers, and the new film has the following functional advantages:

1. The film reduces the permeation of oxygen and moisture through substrate, encapsulation and interlayers and hence reduces the reaction with the Ca and Mg electrodes.
2. The film retards metal migration of the electrodes during electrical stress and hence reduces the initiation of sharp points that lead to high electrical field, which cause electrical break down in the active polymer.
3. The film retards the migration of the active polymers through metal grain boundaries and pinholes in the films. This will reduce the chance leading to short circuit between the two electrodes at the sharp points.
4. The film is made thin enough that current can tunnel through the film. Such a film formed between the electrode and the active polymer can lead to a matching of the energy levels leading to more efficient current tunnelling.

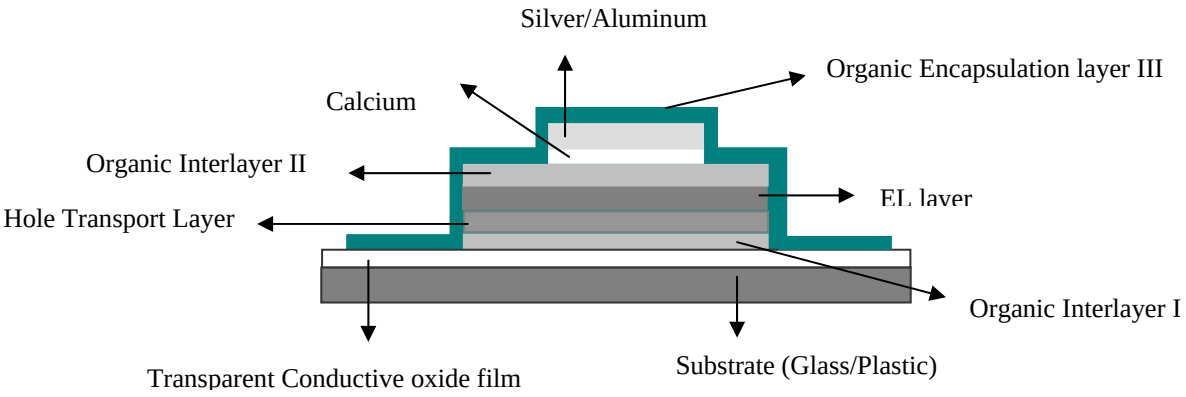

Figure 7.3: New device structure with organic interlayer I and II, organic encapsulation layer III

Figure 7.3 shows the newly designed multi-layer device structure. In this device structure, an organic interlayer I is introduced in between the transparent conducting electrode and the hole transport layer or in between the hole transport layer and the EL polymer layer. An organic interlayer II is introduced in between Electron Transport Layer and the Cathode or in-between the EL polymer and Cathode. Finally an organic interlayer III is introduced to cover the whole device to provide a double protection before final device encapsulation. The new film is pinhole free and this film may be Polyimide, Teflon, Parylene or other kinds of low moisture permeation polymer films. Spin coating or CVD or any other suitable deposition methods could be used to deposit these films. This organic inter layers should have good moisture barrier property in the range of 0.1cc/m2/day to 100cc/m2/day at 39°C @ 95% RH. It should also be transparent in the visible wavelength range and resistant to metal ion migration under electrical fields. The most preferred material would be Parylene series which can be deposited at room temperature. It has been proven that parylene does not alter the electronic parameters of devices. Furthermore, it has excellent step coverage and provides conformal coverage of OLED devices. It possesses very good oxygen and moisture barrier properties and the moisture absorbance is less than 0.1% by weight. Detailed experimental investigation has been done to prove that the new device structure is efficient in controlling dark non-emissive area formation and growth and the results are shown in section 7.3.

7.2.1 Organic Interlayer I

A new pinhole free parylene film introduced in between the transparent conducting electrode ITO and the hole transport layer is used for our experiments. The main roles of this film, Organic Interlayer I, are to serve the following functions:

- It should possess high water and oxygen permeation barrier properties and can effectively prevent oxygen diffusion from the ITO film to the HTL and EL polymer.
- It can also act as thermal barrier film and effectively prevent the heat transfer from the ITO to EL polymer during device operation.
- This film should be 100% pinhole-free, seal other defects and provide a smooth morphology for HTL deposition.
- This film should also be capable of reducing the strong electric field at ITO spikes.
- It should increase carrier injection efficiency by lowering the metal work function through the potential drop across the layer.

The performance improvement of the device with Organic interlayer I is confirmed with different experiments and the results will be discussed in section 7.3.

7.2.2 Organic Interlayer II

Another new pinhole free parylene film introduced in between EL material Layer and the Cathode is used for our experiments. The main roles of this film, Organic Interlayer II, are to serve the following functions:

- It should possess high moisture and oxygen permeation barrier properties and moisture can effectively prevent oxygen from diffusing to the EL polymer and reacting with the Cathode.
- This film should be 100% pinhole-free and provide a smooth morphology for cathode deposition.
- This film allows for sputter deposition of the cathode. Hence, pinholes formation on the cathode would be drastically reduced.

In the section 7.3, I will demonstrate the experiment results for performance improvement of device with Organic Interlayer II.

7.2.3 Organic Interlayer III

Finally a new pinhole free parylene film introduced to cover the whole device before final encapsulation. It is an excellent barrier to moisture permeation and protects devices after encapsulation. It is well known that with epoxy, moisture and oxygen permeation takes place which is a major factor for the oxidation of devices after encapsulation. With this design, it can be ensured that the devices could be sealed hermetically. In the section 7.3, I will demonstrate the experiment results for performance improvement of device with Organic Interlayer III.

7.3 Performance improvement using new device structure

The experiments were proceeded in three phases. In the first phase experiments, I introduced thin organic interlayer I (parylene) on top of the ITO and constructed the device comprising the structure of ITO/parylene/HTL/EL/Ca/Ag. The parylene layer's thickness is 3nm, 5nm and 10nm fabricated by U-system Com. on cleaned ITO substrate. After that HTL and EL polymer were spin coated on the top of parylene layer. Ca of 5 nm and Ag of 200 nm were deposited using ULVAC system. Then dark spot image of the sample was taken under microscope immediately after the sample has been take out from the evaporate chamber. After the dark spot's position was recorded and marked, the sample has been loaded to SIMS UHV chamber for SIMS element profile measurement. SEM, AFM experiments are also done on these samples.

In the second phase experiments, thin organic interlayer II (parylene) is introduced on top of the EL layer and constructed two types of the device comprising the structure of either ITO/parylene/HTL/EL/parylene/Ca/Ag or ITO/HTL/EL/parylene/Ca/Ag. The parylene organic layer II's thickness are 3nm and 5nm fabricated by U-system com. After we spin the HTL and EL

polymer, the devices were taken well care of avoiding light. On the top of EL layer, the parylene layer was deposited, and then Ca of 5 nm and Ag of 200 nm were deposited using ULVAC system. Dark spot observation, SIMS, SEM and AFM experiments are also done on these samples.

Finally in the third phase experiments, organic interlayer III (parylene) is introduced on top of the whole device and constructed type of the device comprising the structure of ITO/HTL/EL/Ca/Ag/parylene. The lifetime of this new structure is compared with traditional device structure.

7.3.1 Device with traditional structure

Novel structure device and traditional structure device were fabricated together for comparison. Figure 7.4 demonstrates various elements C, In and Ca profiles for non-stressed device, bright area and dark spot area in stressed device. Figure 7.5 is the I-V-L curve of the traditional structure device. Figure 7.6 is the efficiency curve of the traditional structure device. The turn on voltage for traditional device structure is 4.3V and the maximum efficiency is 5.762Cd/A.

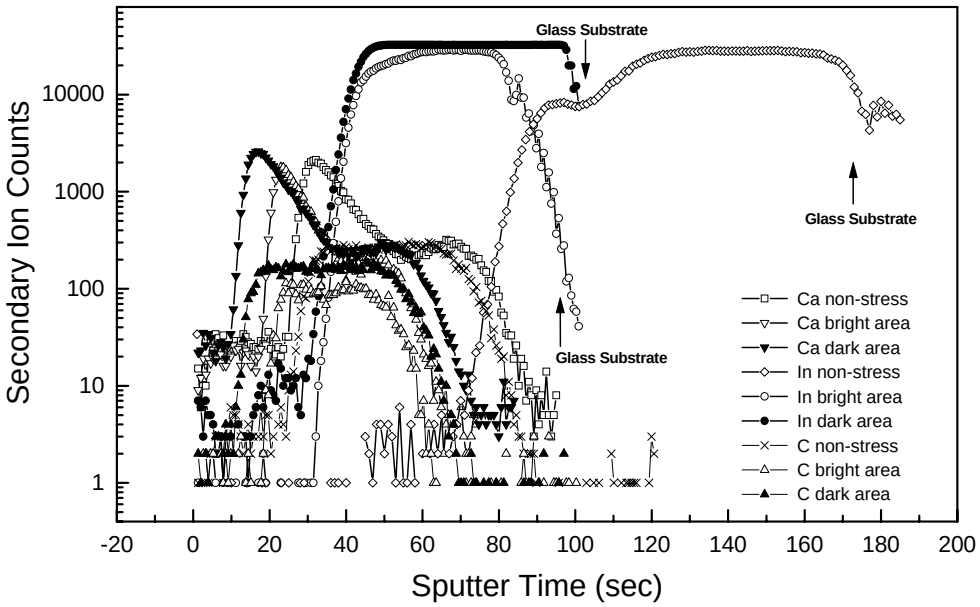

Figure 7.4: SIMS profile of In, Ca and C in traditional organic device structure.

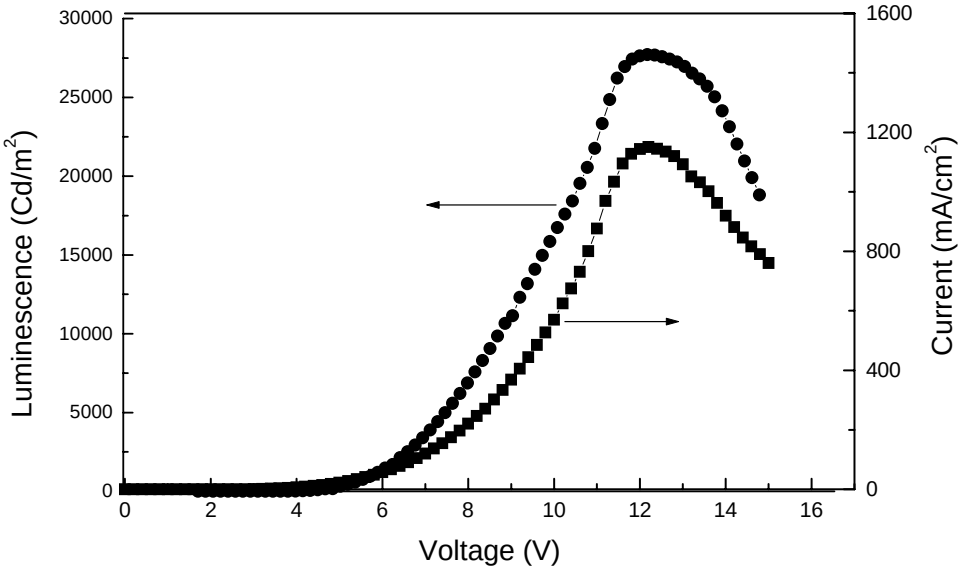

Figure 7.5: Traditional Structure: Turn on voltage: 4.3V

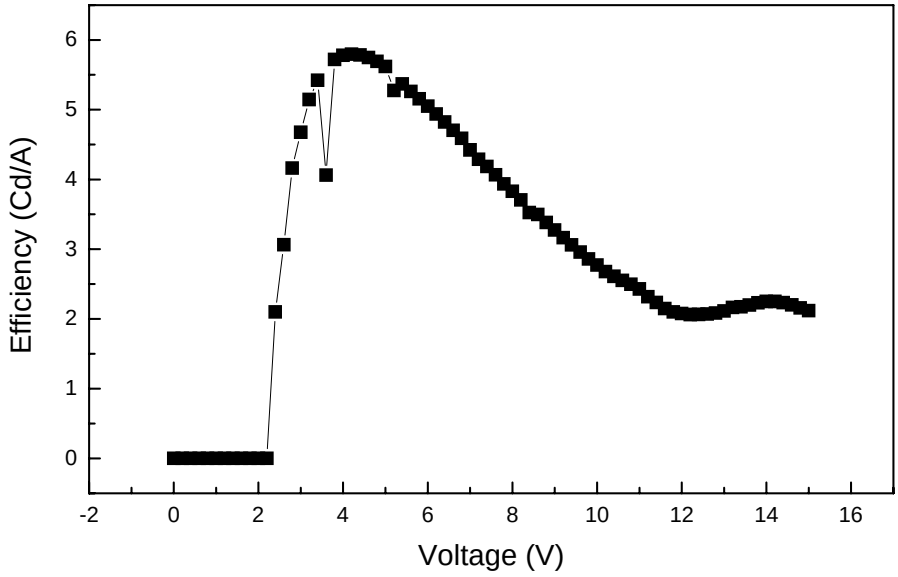

Figure 7.6: Efficiency curve for traditional Structure: maximum efficiency: 5.762Cd/A.

7.3.2 Device with organic interlayer I

Figure 7.7 is the I-V-L curve of the device structure of: ITO/3nm parylene/HTL/EL/Ca/Ag. The turn on voltage for modified device structure is reduced from 4.3V to 3.8V and the maximum efficiency is increased from 5.762Cd/A to around 7Cd/A.

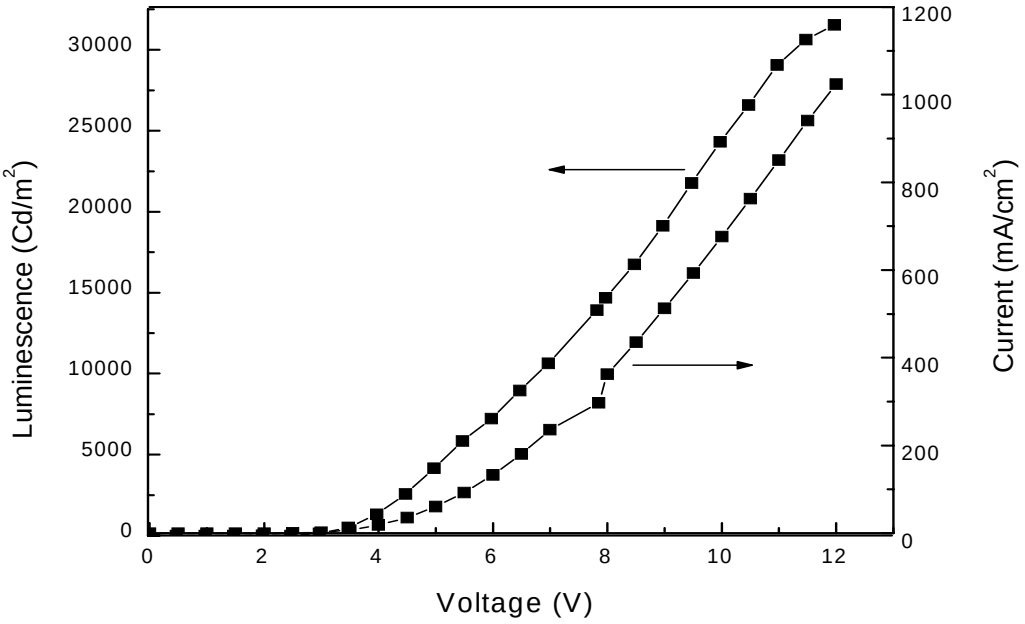

Figure 7.7: I-V-L curve for device structure of: ITO/3nm parylene/HTL/EL/Ca/Ag, Turn-on Voltage is 3.8V.

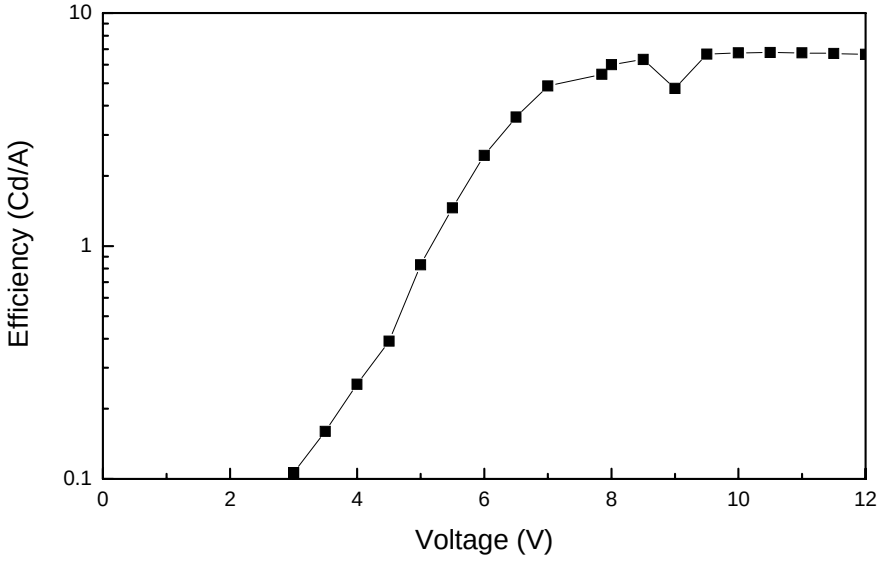

Figure 7.8: Efficiency curve for device structure of: ITO/3nm parylene/HTL/EL/Ca/Ag: maximum efficiency: 7 Cd/A.

Figures 7.9-7.12 show the Ag, Ca, C and In. SIMS profiles on the novel structure device of: ITO/3nm parylene/HTL/EL/Ca/Ag. SIMS experiment shows that In profile in bright area in the device with parylene structure is restrict to the original position compared with normal device, in which In profile moves into PPV layer as long as electrical stress has been exerted. However in dark spot area, In were found go deep into PPV layer. Because of this parylene layer smooth the ITO and PPV interface (only little area formed into dark spot, which means only little interface area is rough), we expect that other layers and interfaces will become better also. Just as we expected we found that the C profile expansion remains little variation compared with normal device, which has large changes on profile expansions. Following relatively smooth PPV surface, Ca profile and Ag profile were also observed position stable. Figure 7.13 (a) and (b) are AFM surface topography of ITO surface and parylene surface. Original ITO roughness is 2.8nm. For ITO with parylene surface, the roughness is 0.889nm. AFM experiments were performed on polymer surface on both normal device and device with parylene layer also. Figure 7.14 (a) and (b) are AFM surface topography on ITO/HTL//EL polymer and ITO/parylene/HTL/EL polymer. It shows that PPV became smoother in device with parylene layer and the roughness is improved from 1.15nm (ITO/HTL/polymer) to 0.78nm (ITO/parylene/HTL/polymer).

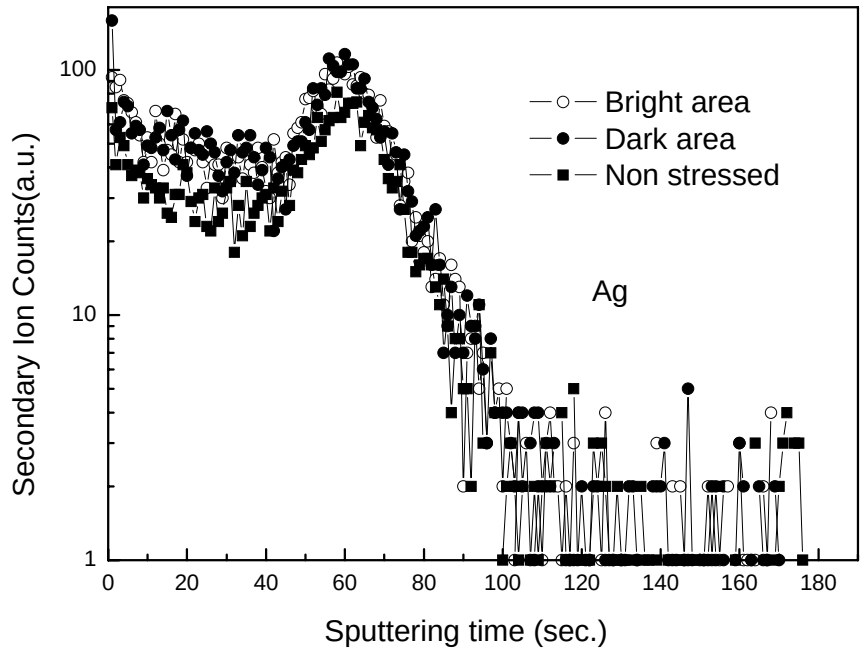

Figure 7.9: SIMS profile of Ag in device structure of: ITO/3nm parylene/HTL/EL/Ca/Ag

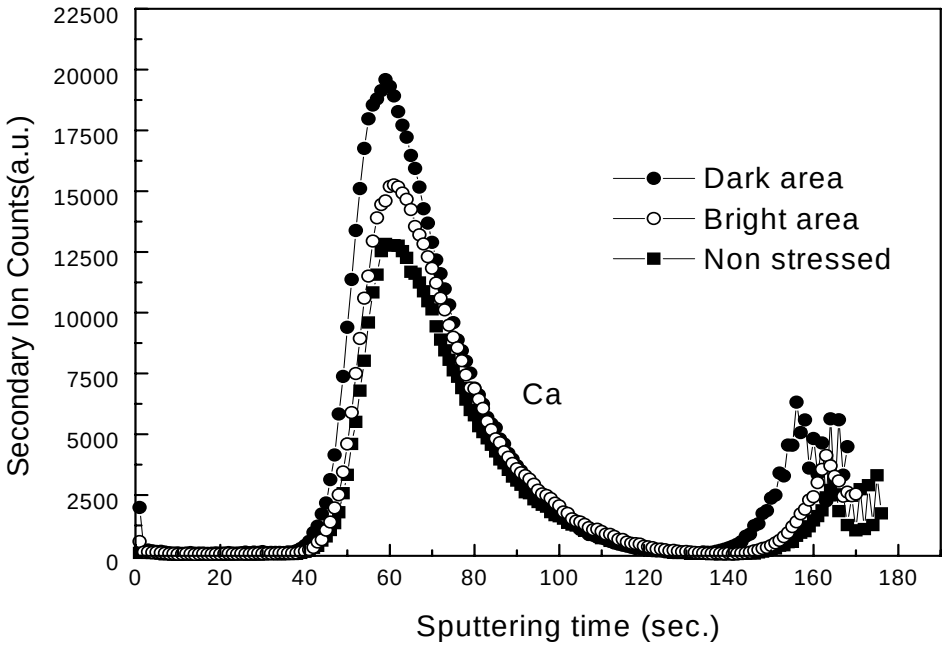

Figure 7.10: SIMS profile of In in device structure of: ITO/3nm parylene/HTL/EL/Ca/Ag

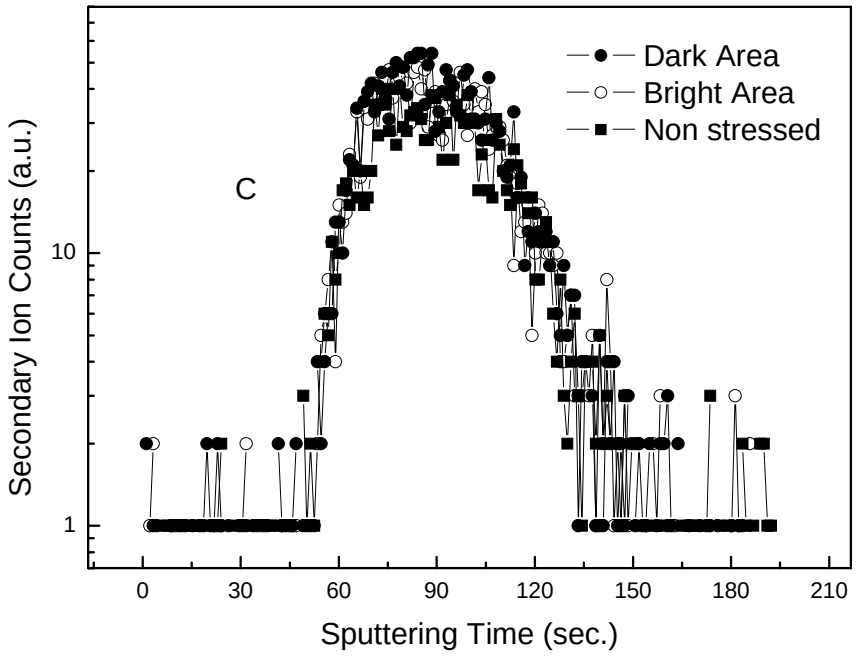

Figure 7.11: SIMS profile of C in device structure of: ITO/3nm parylene/HTL/EL/Ca/Ag.

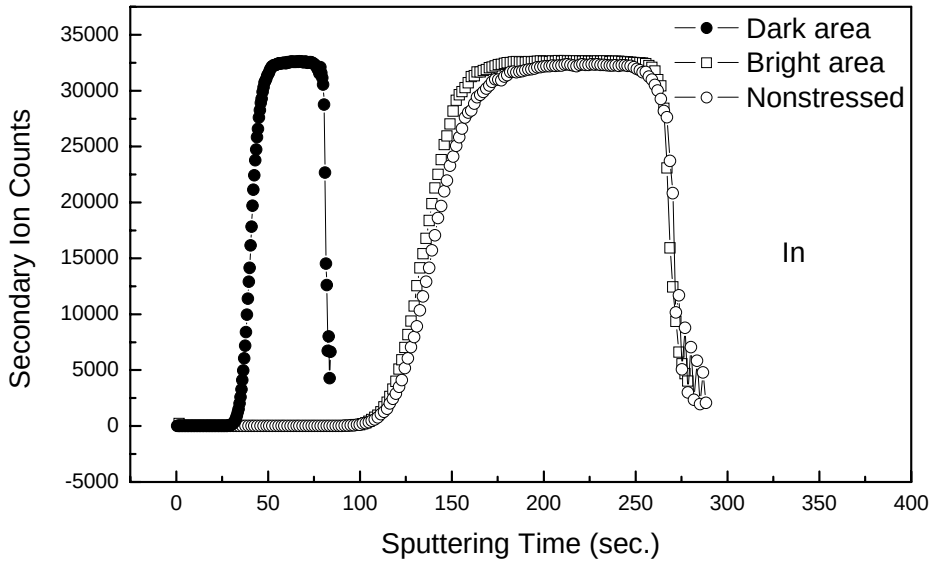

Figure 7.12: SIMS profile of In in device structure of: ITO/3nm parylene/HTL/EL/Ca/Ag.

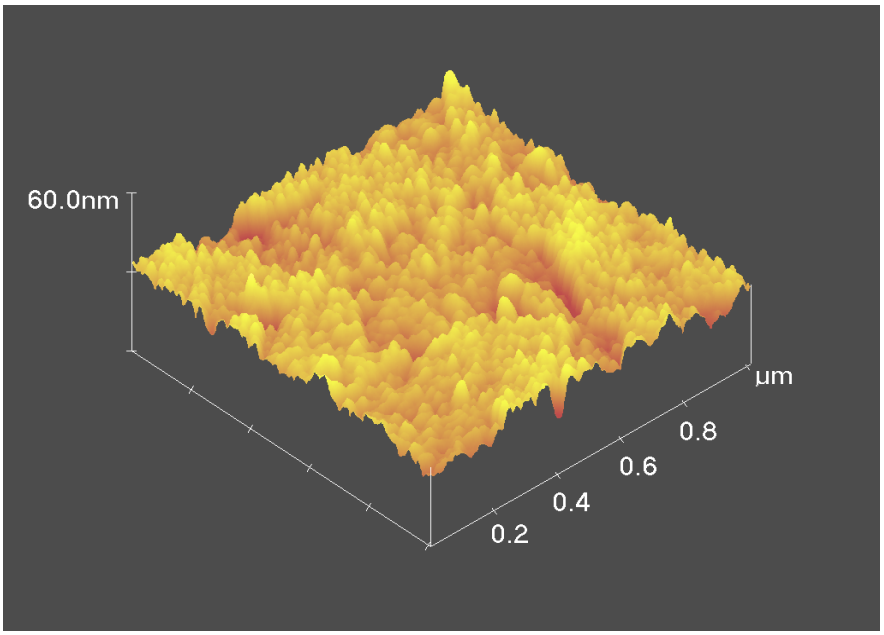

(a)

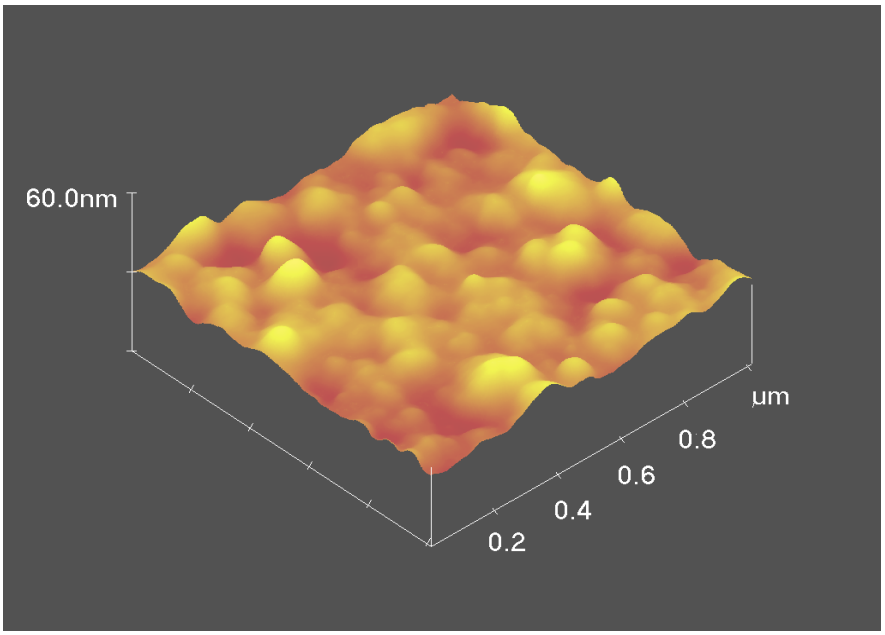

(b)

Figure 7.13: (a) Traditional Structure ITO surface Roughness: 2.879nm
(b) For ITO with parylene surface, the roughness is 0.889nm

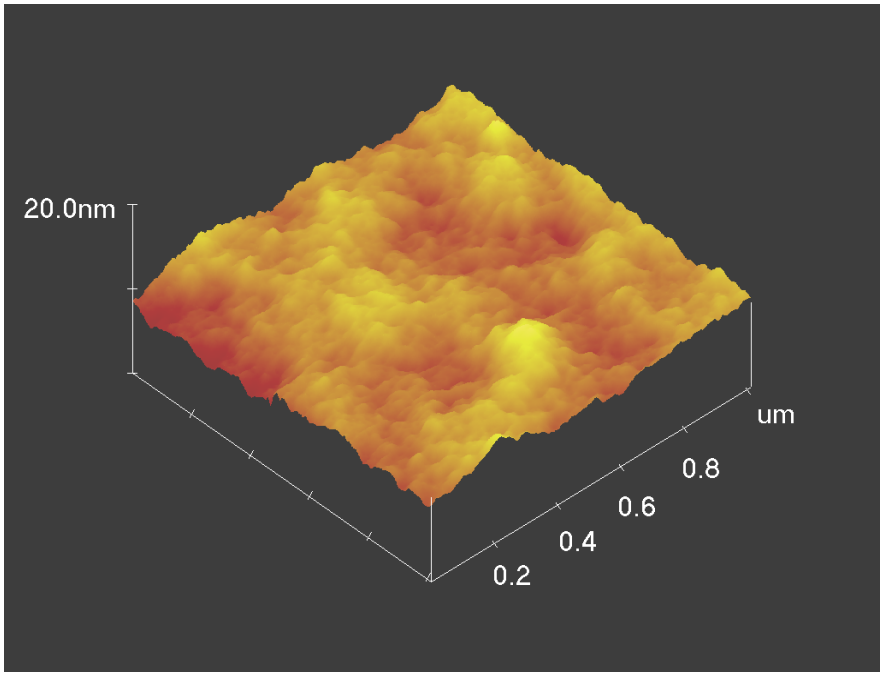

(a)

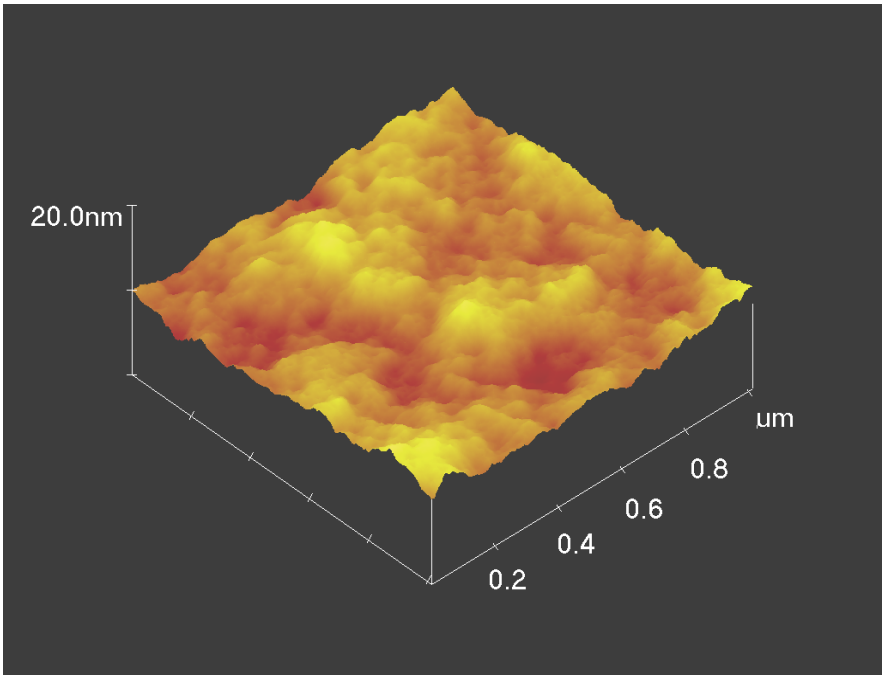

(b)

Figure 7.14: (a) AFM results on ITO/HTL//EL polymer surface, roughness is: 1.15nm. (b) Results on ITO/parylene/HTL/EL polymer surface, roughness is: 0.78nm.

The dark spot image taken under microscope shows that the number of dark spots in modified device structure reduced significantly and the growth rate is much slower. Figure 7.15 shows that dark spot growth rate in device structure with 3nm or 5nm parylene layer/HTL/EL/Ca/Ag. Dark spot growth rate reduce 27% and 36% respectively for novel structure devices with 3nm parylene layer and 5nm parylene layer.

The ITO and organic interface plays an important role in device failure. Parylene barrier has a better adhesion (organic-organic contact) compared with organic-inorganic contact, which also enhance the hole injection into the electroluminescent polymer. It also increases the efficiency and inhibits electrical shorts. The first phase experiments already significantly reduce the dark spot number and its growth rate.

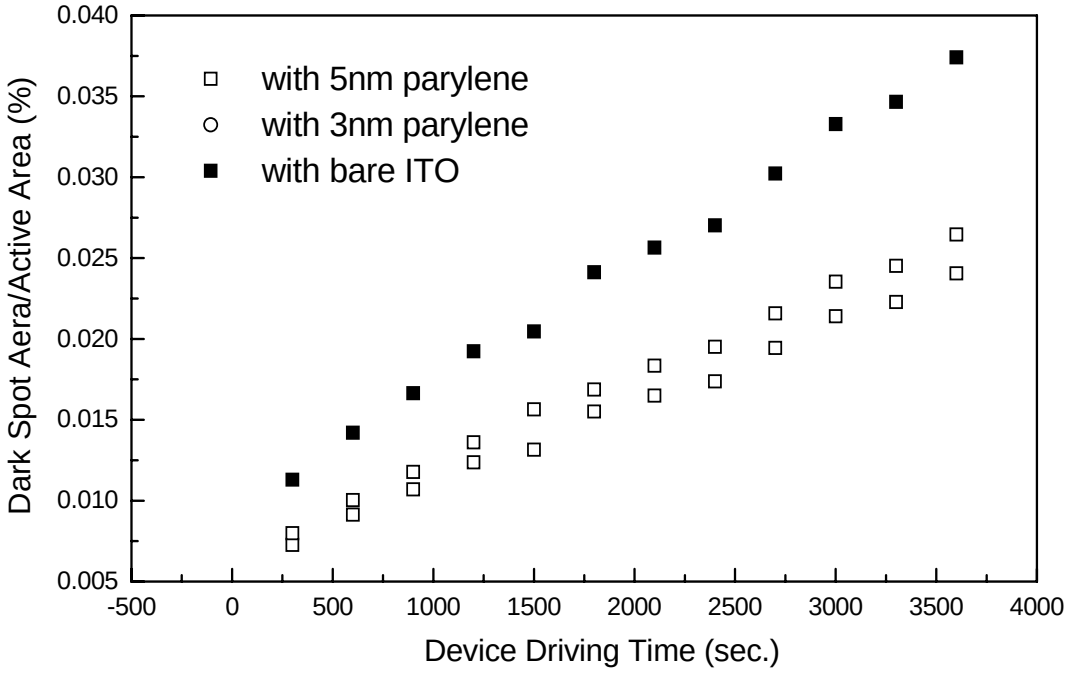

Figure 7.15: Dark spot growth rate in device structure of: ITO/3nm parylene/HTL/EL/Ca/Ag.

7.3.3 Device with organic interlayer II

Figure 7.16 is the I-V-L curve of the device structure of: ITO/3nm parylene/HTL/EL/3nm parylene/Ca/Ag. The turn on voltage for modified device structure is around 8.12V. Although the device show larger turn on voltage and reduced luminescence, the device shows much more stabilized structure and uniformed current and heat distribution.

Figures 7.17-7.19 show the Ca, C and In SIMS profiles on the novel structure device of: ITO/3nm parylene/HTL/EL/3nm parylene/Ca/Ag. Results show that In profile in bright area in the device with parylene structure is restrict to the original position compared with normal device, in which In profile moves into PPV layer as long as electrical stress has been exerted. In dark spot area, In profile was found still remain stable. Ca, profile and C profile are also remain stable no matter it is bright area or failed area. The reason for dark spot formation, as demonstrated in previous chapter, is EL polymer layer failed.

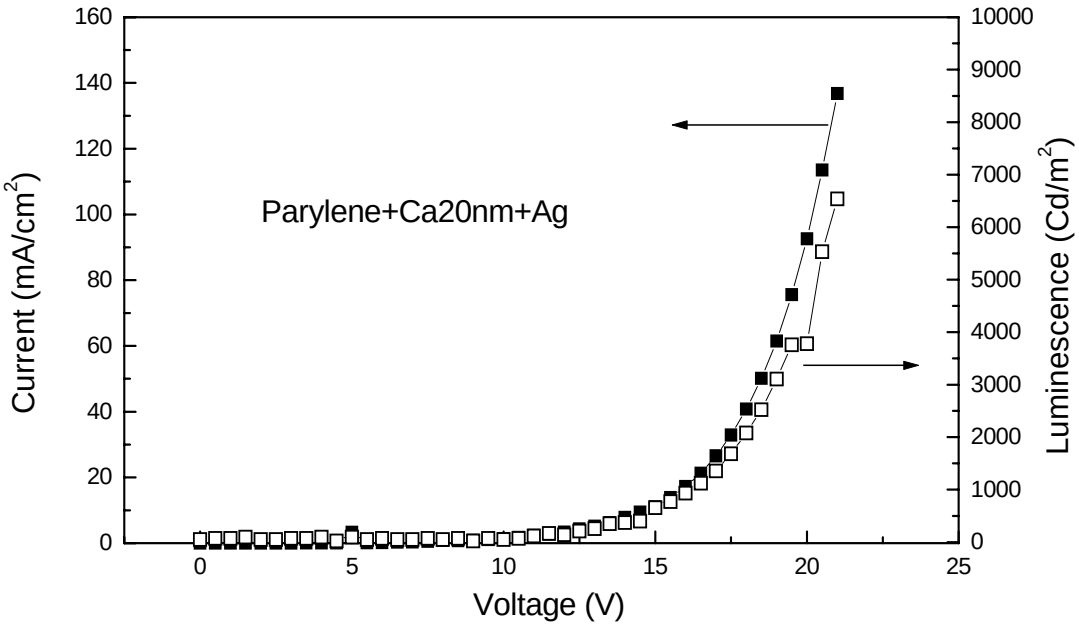

Figure 7.16: I-V-L curve in device structure of: ITO/3nm parylene/HTL/EL/3nm parylene/Ca/Ag.

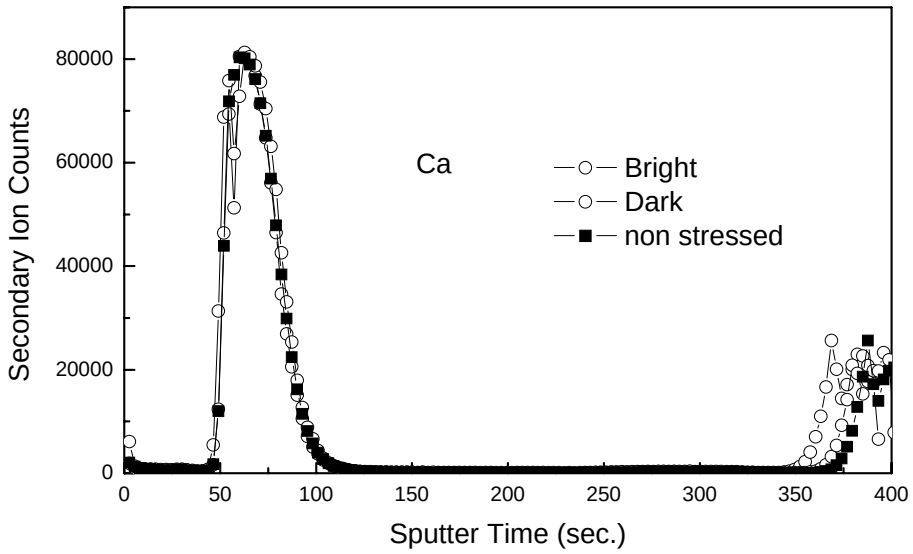

Figure 7.17: SIMS profile of Ca in device structure of: ITO/3nm parylene/HTL/EL/3nm parylene/Ca/Ag.

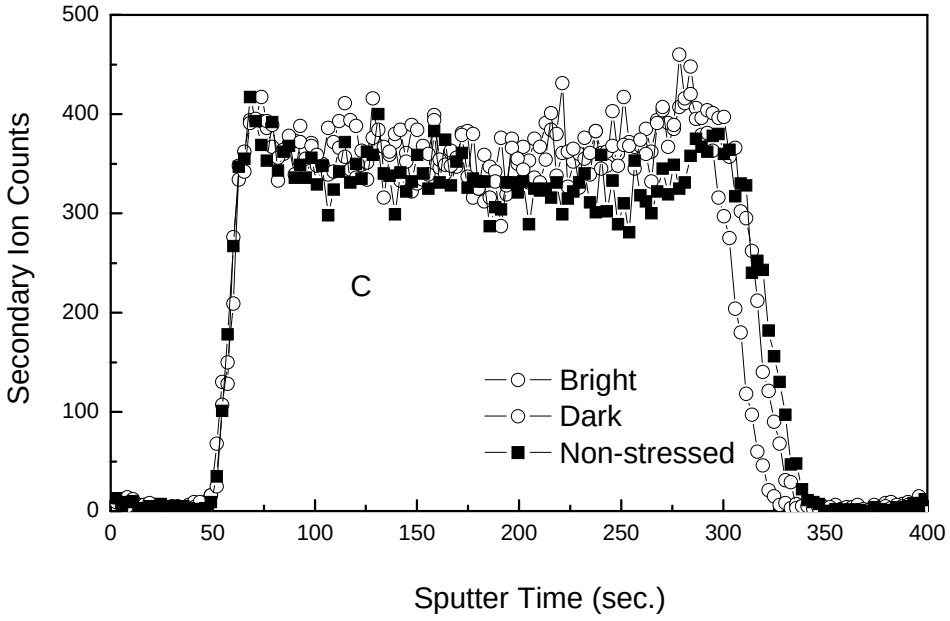

Figure 7.18: SIMS profile of C in device structure of: ITO/3nm parylene/HTL/EL/3nm parylene/Ca/Ag.

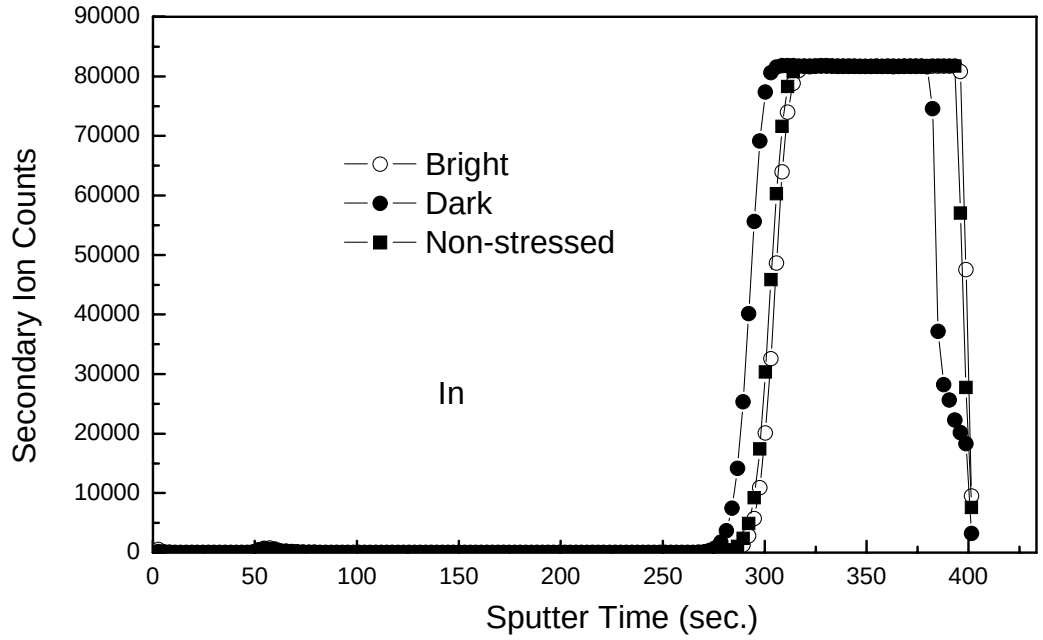

Figure 7.19: SIMS profile of In in device structure of: ITO/3nm parylene/HTL/EL/3nm parylene/Ca/Ag.

Figure 20 shows the lifetime curves for device structure ITO/parylene/HTL/EL/parylene/Ca/Ag operating at constant current 0.5mA in ambient condition and device structure ITO/HTL/EL/Ca/Ag operating at constant current 0.28mA in ambient condition. It shows that the new structure device has much longer lifetime and during lifetime period, the luminescence output is stable.

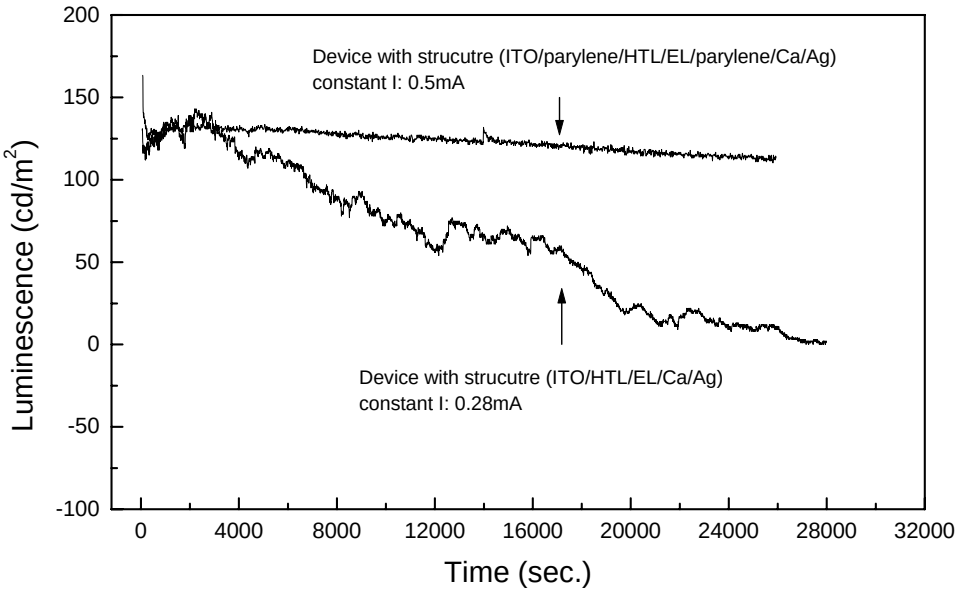

Figure 7.20: Device lifetime curve for structure of:
ITO/parylene/HTL/EL/parylene/Ca/Ag and ITO/HTL/EL/Ca/Ag

7.3.4 Device with organic interlayer III

Finally a new pinhole free parylene film introduced to cover the whole device to form device structure of ITO/HTL/EL/Ca/Ag/20nm parylene. Figure 7.21 is the lifetime curves for device structure of: ITO/ HTL/EL/Ca/Ag/parylene and ITO/HTL/EL/Ca/Ag. It shows that the structure

ITO/ HTL/EL/Ca/Ag/parylene has obvious better lifetime performance reaching about 16 hours in air without much deteriorate compared with the structure without the parylene protective layer.

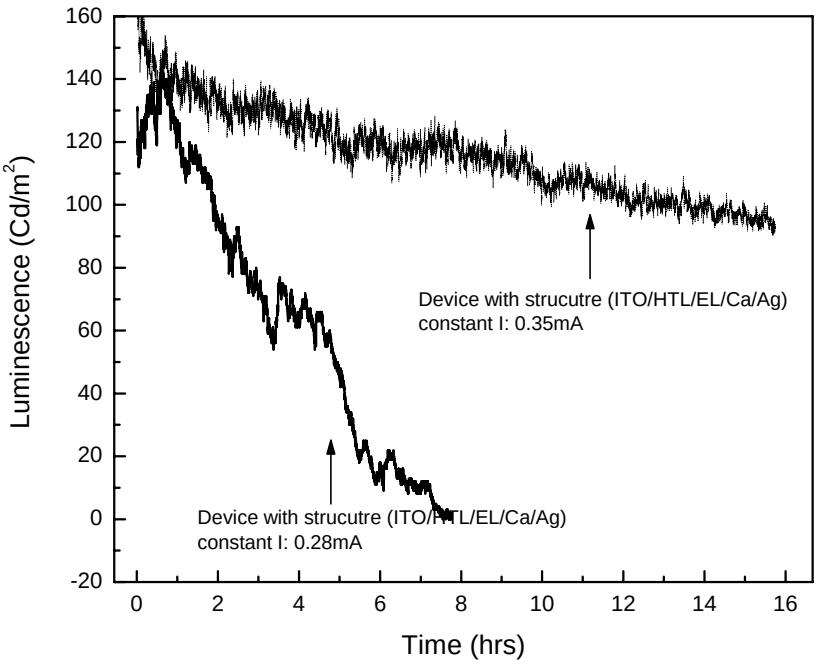

Figure 7.21: Lifetime curves for device structure of: ITO/ HTL/EL/Ca/Ag/parylene and ITO/HTL/EL/Ca/Ag.

7.4 Significance of this work

The number of dark spots would be reduced significantly using the above new device structure. The dark spot and defect growth are due to metal migration during electrical stress resulting in sharp points. Such sharp points cause a high current density to flow deteriorating the polymer and may even cause short circuit. Another problem of the organic light emitting device is due to the oxygen and moisture reacting with the OLED materials. The dark spot and defects growth is due to the oxygen and moisture reacting with the electrode and metal migration within the OLED

materials. Permeation & diffusion or oxygen and moisture may take place through the substrates and the type of encapsulation technique. Pinholes are also formed when magnesium or calcium are deposited by the resistive evaporation process.

The permeation of oxygen and moisture into the device has been controlled by the introduction of the organic inter layer I in between the transparent conductive oxide and the hole transport layer or in between the hole transport layer and the EL polymer or be introduced directly in between transparent conductive oxide and EL polymer. The organic interlayer I can also smooth the ITO surface and reduce the spikes, furthermore, reduce the device shorting. By introducing an organic thin film inter layer II with high barrier property to moisture and oxygen permeation on the top of EL layer in the order of 2 nm to 20 nm thick, it would act as a barrier layer and prevent oxygen diffusion from the EL polymer. Also it would act as a protective layer for sputter deposition of the calcium electrode. Using this method, the number of pinholes would be reduced by a few orders of magnitude. In the traditional structure, this protective layer has not so far been used and hence, resistive evaporation method was chosen where ion bombardment by sputter deposition can not be tolerated. The contamination issue is also solved by the sputter deposition method. It is claimed that CVD or spin coating or other vacuum deposition techniques could be used to deposit parylene or other suitable organic barrier layers as a protective layer for the sputter deposition of cathode materials. With these inter-layers, the oxygen and moisture diffusions into the device are well controlled. Hence gaseous evolution caused by moisture reacting with the Ca electrode controlled. The inter-layers also resist metal migration. The like hood of formation of sharp spikes is reduced and short circuit is suppressed. Finally with organic encapsulation layer III, the device can be protected both from intrinsic and external attack.

7.5 Summary

In this chapter, novel device structures were fabricated and demonstrated. It is proved to be able to reduce the number of pinholes in cathode, control the device interface, uniform the current and heat distribution and exercise effective control over growth of the non-luminescent areas in the EL polymer and cathode surfaces. The incorporated interlayers, which also have high barrier properties, can resist oxygen and water vapor diffusion and also metal migration. The organic layer I can also increase the quantum efficiency of the device through better matching of energy work function of metal and LUMO or HOMO of the polymer. The organic inter layer II acts as a protective layer and therefore, sputtering of cathode materials is possible. This technique reduces the number of pinholes as opposed to resistive heating evaporation. The suitable conformal coating has been designed on top of the entire Organic Light Emitting Devices and hence, moisture permeation after the encapsulation with glass is well controlled.

CHAPTER 8 CONCLUSIONS AND SUGGESTIONS FOR FURTHER INVESTIGATIONS

It has been demonstrated in this thesis that various complicated reasons contribute to the failure of the organic light emitting device (OLED). A systematic study of the dark non-emissive area formation and growth has been carried out and it has shown that electrode pinholes and defects, interface roughness and material quality are the major reasons for dark non-emissive area formation. A novel device structure and process technique has shown improvements in reducing the dark non-emissive area formation and prolonging device lifetime.

8.1 Contributions of PhD project

Specific major contributions of this thesis study:

1. It is crucial to understand the operation and degradation mechanism of OLED. This facilitates a deeper understanding on the type of mechanism that controls the current flow *I* and at a given applied bias *V*, and the relationship between the current flow *I* at a given applied bias *V* and the intensity of the emitted light. In this work, typical OLED device electric field, carrier concentration, current density and recombination rates have been calculated and simulated.

2. In this work, photoluminescence degradation organic light emitting devices has been investigated, which shows that electrical stress on the device followed by UV and oxygen can degrade the polymer extensively.

3. Dark non-emissive area formation and growth of Organic light emitting devices have been extensively studied and possible mechanism causing it has thus been proposed.

4. Bubble formation in organic light emitting devices has been elaborated.

5. A new device structure and process technique has adopted. Comparing with the traditional device structure, it shows optimised device structure, uniformed device current density and luminescence. Hence the new structure has proven to be effective in reducing the dark non-emissive area formation possibilities and prolonging the device lifetime.

8.2 Future work for organic LED technology

The entire OLED market today is divided between two competing technologies – the small molecule OLED (SMOLED) and the polymer OLED. Polymer OLED is still in the infancy stage and the first prototypes of commercial products have just emerged in the market place, whereas, small molecule OLEDs have a well-established base in the market. It is predicted that polymer OLED~~s~~ will eventually emerge the winner~~s~~ in the OLED display~~s~~ market due to its low-cost fabrication techniques.

Currently, OLED technology is challenging LCD's position in the market. However, some serious path breaking work in material stability and lifetimes has to be done for polymer OLED~~s~~ in order to overtake small molecule technology and LCD technology. Some of the challenges are:

1. Competition with the more mature LCD technology.

LCD~~s~~ today occupy almost 95% of the flat panel market share. No other technology is as popular as the LCD. The OLED technology is about two decades behind the LCD technology. As a result, the LCD technology is more mature in terms of technology as well as market share. There are also significant investments into improving the LCD technology. Furthermore, LCD has a proven track record of successful displays and more mature processing lines and materials.

2. Material lifetime~~s~~

One major concern for all OLED manufacturers is material lifetime~~s~~ and efficiency. Experts have concluded that for OLEDs to be fully marketable, they have to be three times better than what they are today, in terms of lifetimes and efficiencies.

3. Color

Many manufacturers are concerned about the colors produced by an OLED display. Traditionally, blue color has posed a problem for OLEDs. The perceptibility of this color is less for the human eye as compared to other colors, hence manufacturers adopted the blue-green color. With new material research, color should be a temporary challenge.

4. Substrates

Substrate, however, is still an issue for OLED displays compared to LCD displays. The use of thin flexible substrates provides the ability to conform, bend or roll a display into any shape, which cannot be realized by other display technology. The flexible substrates should have a high thermal stability, a uniformly coated ITO with a low surface resistance, and a low water and gas permeability. A new type of encapsulation is also needed to protect the PLEDs, All above still remains major hurdles.

5. Infancy of current manufacturing techniques

OLEDs are currently manufactured only by vacuum deposition technique. This is also a challenge because it limits the size of the OLED being manufactured. New manufacturing techniques such as roll-to-roll processing, in which large-sized displays can be manufactured, have yet to take firm roots in the display industry. Even if roll-to-roll processing becomes popular, it is more suitable for light-emitting polymers than for SMOLEDs. The yield of OLEDs manufactured by the vacuum deposition technique too is not high enough for profitable production, and there is a lot of material wastage.

Author hopes this PhD research results would contribute to Organic Light Emitting Display industry.

Reference

[1] C. Tang, US Patent 4 164 431, 1979.

[2] C. Tang, US Patent 4 356 429, 1982.

[3] C. Tang, S. VanSlyke, Appl. Phys. Lett. 1987, 51, 913.

[4] J. Burroughes, D. Bradley, A. Brown, R. Marks, K. Mackay, R. Friend, P. Burn, A. Holmes, Nature 1990, 347, 539.

[5] R. Wessling, R. Zimmerman, US Patent 3 401 152, 1968.

[6] R. Wessling, R. Zimmerman, US Patent 3 706 677, 1972.

[7] R. Wessling, J. Polym. Sci. Polym. Symp. 1985, 72, 55.

[8] R. Friend, J. Burroughes, D. Bradley, WO Patent 90/13 148, 1990. R. Friend, J. Burroughes, D. Bradley, US Patent 5 247 190, 1993.

[9] D. Braun, A. Heeger, Appl. Phys. Lett. 1991, 58, 1982.

[10] H. Radousky, A. Madden, K. Pakbaz, T. Hagler, H. Lee, H. Lorenzana, G. Fox, P. Elliker, Int. SAMPE Tech. Conf. 1995, 27, 1143.

[11] J. Scott, J. Kaufman, P. Brock, R. DiPietro, J. Salem, J. Goitia, J. Appl. Phys. 1996, 79, 2745.

[12] S. Janietz, D. Bradley, M. Grell, M. Inbasekaran, E. Woo, Appl. Phys. Lett. 1998, 73, 2453.

[13] M. Bernius, M. Inbasekaran, E. Woo, W. Wu, L. Wujkowski, Thin Solid Films 2000, 363, 55.

[14] A. Bemtsen, P. van de Weijer, Y. Croonen, C. Liedenbaum, J. Vleg-gaar, Sot. Inform. Display Conf. Proc., Int. Display Res. Conf., Toronto, Canada, 15-19 Sept. 1997, p. F28.

[15] K. Pichler, S.K. Heeks, CR. Towns, N.T. Harrison, N. Tessler, R.H. Friend, Sot. Inform. Display Conf. Proc., Int. Display Res. Conf., Toronto, Canada, 15-19 Sept. 1997, p. F19.

[l6] J. C. Carter, I. Grizzi, S. K. Heeks, D. J. Lacey, S. G. Latham, P. G. May, R. Pahos, K. Pichler, C. R. Towns, H.F. Wittman, Appl. Phys. Lett. 71 (1997) 34.

[17] Y. Cao, G. Yu, C. Zhang, R. Menon, A.J. Heeger, Synth. Met. 87 (1997) 171.

[18] A. Benninghoven, B. Hagenhoff, E. Niehuis, Anal. Chem. 65 (1993) 630A.

[19] F. Cacialli, R.H. Friend, S.C. Moratti, A.B. Holmes, Synth. Met, 67 (1994) 157.

[20] K. Pichler, Philos. Trans. R. Sot. London, Ser. A 355 (1997) 829. 1401 H. Nakada, T. Tohma, in R.H. Mauch, H.-E. Gumlich (eds.), Inorganicacd Organic Electroluminescence, Wissenschaft und Technik Verlag, .Berlin, 1996, pp. 385-390.

[21] R. D. Scurlock, B. J. Wang, P. R. Ogilby, J. R. Sheats, R. L. Clough, J. Am. Chem. Sot. 117 (1995) 10 194.

[22] M. Yan, L.J. Rothberg, F. Papadimitrakopoulos, M. E. Galvin, T. M. Miller, Phys. Rev. Lett. 73 (1994) 744.

[23] B. H. Cumpston, K. F. Jensen, Trends Polym. Sci. 4 (1996) 151.

[24] E. G. J. Staring, A. J. M. Berntsen, S. T. R. Romme, G. L. J. A. R&en. P. Urbach, Philos. Trans. R. Sot. London, Ser. A 355 (1997) 695.

[25] A. Lux, A. B. Holmes, R. Cervini, J. E. Davies, S. C. Moratti, J. Griiner, F. Cacialli, R. H. Friend, Synth. Met. 84-86 (1997) 293.

[26] Q. Pei, Y. Yang, J. Am. Chem. Sot. 118 (1996) 7416.

[27] H. H. Horhold, Proc. SPIE 1348 (1997) in press.

[28] T. Kouzeki, S. Tatezono, H. Yanagi, J. Phys. Chem. 100 (1996) 20 097.

[29] J. C. Scott, J. H. Kaufman, P. J. Brock, R. DiPietro, J. Salem, J. A.Goitia, J. Appl. Phys. 79 (1995) 2745.

[30] E. Gamier, A. Lorin, J. M. Nunzi, A. Schalchli, J. J. Benattar, D.Vital, Appl. Phys. Lett. 69 (1996) 1071.

[31] C. I. Chao, K. R. Chuang, S.A. Chen, Appl. Phys. Lett. 69 (1996) 2 8 9 4 .

[32] R. K. Kasim, Y. Cheng, M. Pomerantz, R. L. Elsenbaumer, Synth. Met. 84-86 (1997) 1213.

[33] H. Aziz, G. Xu, Synth. Met. 80 (1996) 7.

[34] D. B. Rcbitman, J. Shears, H. Antoniadis, M. Hueschen, Y. Yang, 27th SAMPE: Int. Conf., Vol. 681, 1995.

[35] S. Karg, J. C. Scott, J. R. Salem, M. Angelopoulos, Synth. Met. 80 (1996) 111.

[36] J. C. Scott, S. A. Carter, S. Karg, M. Angelopoulos, Synth. Met. 84-86 (1997) 1197.

[37] S.A. Carter, M. Angelopoulos. S. Karg, P.J. Brock, J.C. Scott, Appl. Phys. Len. 70 (1997) 2067.

[38] H. Antoniadis, M. Abkowitz, B.R. Hsieh, Appl. Phys. Lett. 65 (1994) 2030.

[39] G. Sauer, M. Kilo, M. Hund, A. Wokaun, S. Karg, M.Meier, W.Riess, M. Schwoerer, H. Suzuki, J. Simmerer, H. Meyer, D. Haarer, Fresenius Z. Anal. Chem. 353 (1996) 642.

[40] A.R. Schlatmann, D.W. Fleet, A. Hilberer, F. Garten, P.J.M. Smulders, T.M. Klapwijk, G. Hadziioannou, Appl. Phys. Lett. 69 (1996) 1764.

[41] S. F. Alvarado, W. Riess, P.F. Seidler, P. Strohriegl, Phys. Rev. B 56 (1997) 1269.

[42] J. R. Sheats, Y. L. Chang, D.R. Roitman, (1997) to be published.

[43] J. McElvain, H. Antoniadis, M.A. Hueschen, J.N. Miller, R.L. Moon, D.M. Roitman, J.R. Sheats, J. Appl. Phys. 80 (1996) 6002.

[44] B. H. Cumpston and K. F. Jensen. Appl. Phys. Lett. 69, 3941 (1996)

[45] H. Aziz, Z. D. Popovic, A. M. Hor, N. X. Hu and G. Xu, Science 283, 900 (1999).

[46] A. Giebeler, S. A. Whitelegg, D. G. Lidzey, P. A. Lane and D. D. C. Bradley, Appl. Phys. Lett. 75, 2144 (1999).

[47] P. E. Burrows, V. Bulovic, S. V. Forrest, L. S. Sapochak, D. M. McCarty, and M. E. Thompson, Appl. Phys. Lett. 65, 2922(1994)

[48] Vadim N. Savvate'ev, Aharon V. Yakimov, and Dan Davidov, Appl. Phys. Lett. 71, 3344 (1997)

[49] F. Papadimitrakopoulos, X. M. Zhang, D. L. Thomsen, and K. A. Higginson, Chem. Mater. 8, 1363 (1996)

[50] S. T. Lee and Z. Q. Gao, L. S. Hung, App. Phys. Letter 74,140 (1999)

[51] R. E. Gill, Van de P. Weijer, C. T. H. Liedenbaum, H. F. M. Schoo, A. Berntsen, J. J. M. Vleggaar, R. J. Visser, Opt. Mat 12, 183 (1999)

[52] M. Yan, L. J. Rothberg, F. Papadimitrakopoulos, M. E. Galvin and T. M. Miller, Phys. Rev. Lett. 73, 744 (1994).

[53] L. Ke, S. J. Chua, K.R. Zhang, N. Yakovlev, Appl. Phys. Lett., Vol.80, 2195 (2002)

[54] L. Ke, S. J. Chua, K. R. Zhang, P. Chen, Appl. Phys. Lett. 80, 171 (2001)

[55] R. N. Marks, D. D. C. Bradley, R. W. Jackson, P. L. Burn, and A. B. Holmes, Synth. Met. 55, 4128 (1993).

[56] I. D. Parker, J. Appl. Phys. 75, 1656 (1994).

[57] J. Gmeiner, S. Karg, M. Meier, W. Riess, P. Strohriegl, and M. Schwo-erer, Acta Polym. 44, 201 (1993).

[58] P. W. M. Blom, M. J. M. de Jong, and J. J. M. Vleggaar, Appl. Phys. Lett. 68, 3308 (1996).

[59] P. W. M. Blom, M. J. M. de Jong, and M. G. van Munster, Phys. Rev. B 55, R656 (1997).

[60] P. E. Burrows, Z. Shen, V. Bulovic, D. M. McCarty, S. R. Forrest, J. A. Cronin, and M. E. Thompson, J. Appl. Phys. 79, 7991 (1996).

[61] L. Ke, P. Chen, S. J. Chua. Appl. Phys. Lett., Vol 80. 697 (2002)

[62] L. Ke, S. J. Chua, W. Wang Asia Display/IDW'01 Proceedings of The 21st International Display Research Conference in conjunction with The 8th International Display Workshops. Nagoya, Japan

[63] Y. Yan, L. J. Rothberg, F. Papadimitrakopoulos, M. E. Galvin, T. M. Miller. Phys. Rev. Lett. 73 (1994) 744.

[64] J. H. F. Martens, D. D. C. Bradley, P. L. Burn, R. H. Friend, A .B. Holms, E. A. Marseglia, Syn. Met., 41 (1991) 301

[65] D. Chen, M. J. Winokur, M. A. Masset, Frank E. Karasz POLYMER, 33, (1992) 3116

[66] R.D. Scurlock, B.Wang, P.R. Ogilby, J.R. Sheats, R. L. Clough. J Am Chem Soc 117 (1995) 10194.

[67] E. G. J. Staring, A. J. M. Berntsen, S. T. R. Romme, G. L. J. A. Rikken, P. Urbach, Philos. Trans. R. Soc. London, Ser. A 355 (1997) 695.

[68] B. H. Cumpston, K. F. Jensen, Synth. Met. 73 (1995) 195.

[69] B. H. Cumpston, I. D. Parker, K. F. Jensen, J. Appl. Phys. 81 (1997) 3716.

[70] H. Wang, Master thesis, National University of Singapore 2000 "Photoluminescence and Degradation of Light emitting polymer"

[71] D. G. J. Sutherland, J. A. Carlisle, P. Elliker, G. Fox, T.W. Hagler, I. Jimenez, H.W. Lee, K. Pakbaz, L. J. Terminello, S. C. Williams, F. J. Himpsel, D.K. Shuh, W. M. Tong, J.J. Jia, T.A. Callcot, D.L. Ederer, Appl. Phys. Lett. 68 (1996) 2046.

[72] T. Zyung, J.J. Kim, Appl. Phys. Lett. 67 (1995) 3420.

[73] X. H. Zhang, S. J. Chua, H. Wang and W. Huang "Recovery Photo-degradation of Light Emitting Polymers" MRS Singapore

[74] L. Ke, S. J. Chua, K. R. Zhang, P. Chen Appl. Phys. Lett., Vol.80, 171 (2002)

[75] L. Ke, S. J. Chua, K. R. Zhang, N. Yakovlev, Appl. Phys. Lett., Vol.80, 2195 (2002)

[76] J. R. Rasmusson, P. Broms, J. Birgeson, R. Erlandsson, and W. R. Salanek, Synth. Met. 79,754 (1996)

[77] Vadim N. Savvate'ev, Aharon V. Yakimov, and Dan Davidov, Appl. Phys. Lett. 71, 3344 (1997)

[78] M. Fujihira, M. D. Lee, K. Amane and E. M. Han, Appl. Phys. Lett. 68, 1788 (1996)

[79] S. F. Lim, L. Ke, W. Wang, S. J. Chua. Appl. Phys. Lett. Vol. 78, (13) 2116 (2001)

[80] K. L. Ke, S. J. Chua, S. F. Lim, W. Wang J. of App. Phys. Vol. 90, (2) 976 (2001).

[81] L. Ke, S. F. Lim, S. J. Chua J. of Appl. Polymer Science, Part B (Polymer physics) Vol. 39, 1697, 2001

[82] S. J. Chua, L. Ke, R. S. Kumar, K. R. Zhang, Appl. Phys.Lett. Vol 81, 1119 (2002)

[83] L. Ke, R. S. Kumar, K. R. Zhang, S. J. Chua, A.T.S. Wee Syn. Met. Vol.140, 295 (2004)

[84] L. Ke, R. S. Kumar, S. J. Chua "Dark Spot Inhibition in Organic Light-Emitting Devices" PCT International Application No: PCT/SG02/00276 International Filing Date: 27 Nov 2002

[85] C. Tang, US Patent 4 164 431, 1979. C. Tang, US Patent 4 356 429, 1982.

[86] L. S. Hung, L.S. Liao, C. S. Lee, and S.T. Lee J. Appl. Phys. 86(8) pp.4607 (1999)

[87] R. Friend, J. Burroughes, D. Bradley, WO Patent 90/13 148 1990.

[88] R. Friend, J. Burroughes, D. Bradley, US Patent 5 247 190, 1993.

[89] Y. E. Kim, H. Park, and J. J. Kim Appl. Phys. Lett. 69(5) pp.599(1996)

[90] F. Li, J. Tang, J. Anderegg, J. Shinar Appl. Phys. Lett. 70(10) pp.1233 (1997)

[91] L.S. Hung, C. W. Tang, and M. G. Mason Appl. Phys. Lett. 70(2) pp.152 (1997)